KU LEUVEN

FACULTY OF SCIENCE

AN-OWL
Analytical Model for OWL Sensors
A look at the Strain-Mismatch interaction in DNA

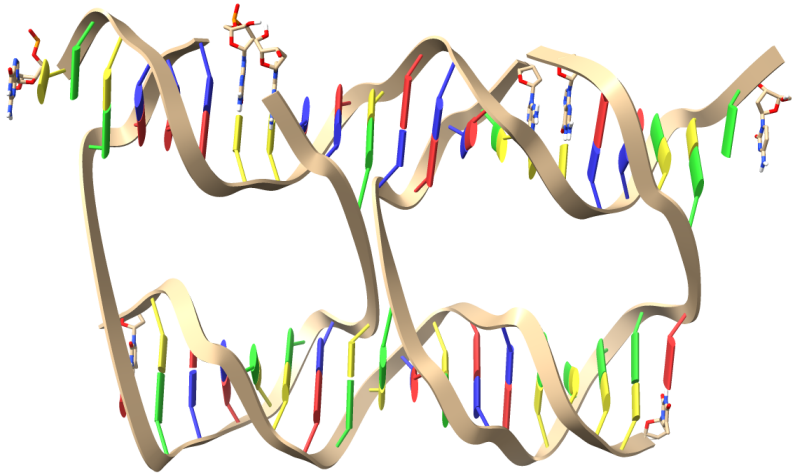

Thibau MANGELSCHOTS

Supervisor: Prof. J. Hooyberghs
UHasselt, Data Science Institute,
Theory Lab

Co-supervisor: Prof. E. Carlon
KU Leuven, Department of Physics and
Astronomy, Soft Matter and Biophysics

Master thesis presented in fulfillment
of the requirements for the degree of
Master of Science in Physics

Academic year 2025-2026

Preface

Acknowledgements

First of all, I sincerely thank Jef Hooyberghs for introducing me to the wonderful world of theoretical DNA physics, all the way back during my bachelor's thesis three years ago. He also gave me the fantastic opportunity to return to where I truly belong: the fifth floor of the Science Tower in Diepenbeek. I want to stress how great it is to work there and thank everyone for creating such a fun working environment. Special mention to Yannick for helping me with conceptual questions on my thesis, and to Wout and Giel for keeping me company and making my office time a good laugh. From the Leuven side, I'm grateful to Enrico Carlon for insightful discussions on how to improve our work and for being such an amazing teacher in many of the key subjects I learned. Arianna Fassino also deserves a mention for helping me set up the simulations. I would also like to acknowledge Dmitry Kolpashchikov from UCSF for the OWL collaboration and for calling in from Florida. My second readers, Patrick Wagner and Marco Baiesi, are thanked for taking the time to review the manuscript. Finally, I cannot thank my parents enough for giving me the opportunity to pursue my career in physics.

Contribution Statement

Thibau Mangelschots performed all derivations and simulations and produced all results. Jef Hooyberghs independently derived the free-energy-interaction term (2.52) for another purpose, using a different notation. Enrico Carlon suggested using oxDNA for simulations, and Arianna Fassino provided guidance on setting them up. Yannick Stulens provided the base OWL-like structure used for simulations. Thibau Mangelschots subsequently adapted it to stabilise the structure and create alternative versions. Yannick Stulens also provided results and figures from a yet-to-be-published manuscript. These are cited [1] where used.

Summary

DNA-hybridisation-based biosensing stands at the forefront of liquid biopsy development and, consequently, the next generation of non-invasive tumour detection. These biosensors are fundamentally limited by the thermodynamic challenge of discriminating trace single-nucleotide variants (SNVs) from the large excess of wild-type DNA background. Recent advances indicate that incorporating structural constraints in the design of molecular beacon-based OWL sensors can significantly enhance their selectivity. However, the underlying mechanism behind these constraints remains speculative. In this work, we test the hypothesis that these constraints induce torsional strain within these probes and seek to optimise their working regime by developing an analytically solvable coarse-grained model. The sensor is modelled as a one-dimensional lattice system in which nodes are coupled via harmonic interactions of exponentially decaying (Kac-Baker-like) strength. Through the Schur complement of the twist coordinate of the cgDNA+ stiffness matrix, the model effectively accounts for the higher-dimensional degrees of freedom in the DNA duplex. In a general framework, we aim to identify the non-additive free-energy interaction term $\Delta\Delta\mathcal{F}$ that arises between two perturbations in the system, and then analyse its application to the presence of a single-base mismatch and to global frustration in the system. This approach allows us to analyse regimes in which the mismatch destabilises the duplex. Specifically, we demonstrate that an optimisable destabilising regime exists for any softening mismatch within this framework, consistent with the expected mechanical effect of a mismatch.
To validate the hypothesis that these constraints induce torsional frustration in the sensor, we perform coarse-grained molecular dynamics simulations with the oxDNA LAMMPS module. We construct a closed-loop system resembling OWL sensors. This closed loop is expected to impose significant structural strain because the 9-base-pair hybridising region is incompatible with DNA's natural helical periodicity ($\sim$ 10.4 bp). This structure is subsequently compared with its helically compatible 10-base-pair counterpart and an open-loop variant. Using 3DNA analysis, we can extract physical degrees of freedom from the simulated duplexes and find that bending of the hybridised region, rather than twist, imposes the dominant contribution to strain.

Popularising Summary

We can imagine DNA as a long chain of two complementary pairs. The order of these pairs is incredibly important, as it contains all the information our cells need to work properly. These cells have a complex regulatory mechanism to check for errors in this ordering, they are very rare and often localised to one single pair. These are known as mutations. Some mutations can have severe consequences, including the development of tumours.
To find these tumours early, patients often have to undergo physically draining surgeries. An alternative to these surgeries is liquid biopsies, which require nothing more than some fluid from the patient, for instance, blood. These are based on sensors which create matching DNA pairs with mutated DNA. But since the mutations are particularly small and very rare, these might be incredibly difficult to find. The sensor might bind to lookalike healthy DNA strands. When this occurs, we get a mismatched pair that still looks a lot like a good binding, but it is slightly weaker. The best way to describe it is like looking for a needle in a haystack; We will not find the needle by just searching through the haystack. We need to use the one difference between the needle and the hay. It is magnetic so that we can get it out with a magnet.
The magnet to our needle is a strain in the sensors, which we can see as something literally pulling on or twisting the DNA in the sensors. If we pull on the DNA with the mutation, nothing happens because the pairs are strong enough to withstand it, and it will light up. But if we pull on a strand with a mismatched pair, the sensor will break, and we will not see any light.
Our goal is to understand why this happens and whether we can find ways to make this pulling even more effective at finding mutations. We also want to know what causes the pulling in the DNA sensors and whether this provides alternative techniques for making other sensors.
To start with, we use simple physical models based on a long series of coupled springs. This might seem too simple, but if we account correctly for the many complex interactions we see in real DNA, it turns out to be a quite accurate model for the strain-mismatch interaction in the sensor. The model proves that the interaction can optimise sensor design through an elastic optimum. We also simulate the DNA to catch the strain in action in the sensor. This allows us to identify what is causing this strain and the reason why. This could serve as an inspiration for future sensor design.

Acronyms

Abbreviation	Meaning
DNA	Deoxyribonucleic acid
ctDNA	Circulating tumour DNA
wtDNA	Wild-type DNA
SNV	Single-nucleotide variant
MM	Mismatch
LoD	Limit of detection
P	Probe
bp	Base pair
EGFR	Epidermal Growth Factor Receptor
MMP	Matched-Mode Perturbation
PBC	Periodic boundary conditions
TWLC	Twistable worm-like chain
MD	Molecular dynamics
TacoxDNA	Tools and Converters for oxDNA
PDB	Protein Data Bank
SEM	Standard error of the mean
LAMMPS	Large-scale Atomic/Molecular Massively Parallel Simulator

Symbols

Symbol	Meaning	Symbol	Meaning
S	Signal	c	Concentration
G	Gibbs free energy	LoD	Limit of detection
F	Helmholtz free energy	$\hat{K}_0$	Unperturbed stiffness matrix
S	Entropy	$\hat{K}_0^{-1}$	Structure matrix
E	Energy	$\hat{K}$	Full stiffness matrix
H	Hamiltonian	Z	Partition function
$\beta = 1/k_B T$	Inverse temperature	D	Perturbation determinant
$\mathcal{F}, \mathcal{S}, \mathcal{E}, \mathcal{H}$	Thermally normalised quantities	$\tilde{K}_q$	Eigenvalue of $\hat{K}_0$
$\Delta[\,]$	Penalty	$\|q\rangle$	Eigenvector of $\hat{K}_0$
$\Delta\Delta[\,]$	Interaction term	$\hat{S}$	Shift operator
N	Number of bonds	$\|1_N\rangle$	All-ones vector
u	Position coordinate	$\|n\rangle$	Unit vector
$\|u\rangle\langle v\|$	Outer product	δ_{mn}	Kronecker delta
a	Interaction rest length	δK	Mismatch stiffness perturbation
x	Displacement coordinate	δa	Local rest-length perturbation
$\|x\rangle$	Displacement vector	L	Base-system equilibrium length
K'	Closing stiffness	δL	Global rest-length perturbation
$[\,]_r$	Rigid-limit value	K_0	Fundamental self-coupling
λ	Characteristic coupling length	$\langle x_n x_m \rangle$	Displacement correlation
τ	Torque	$[\,]^*$	Extremal value

List of Figures

List of Tables

Contents

1 Introduction

1.1 Liquid Biopsies

Early tumour detection is pivotal for the prospects of cancer patients. Contemporary diagnostics relies on physical tissue biopsies. This involves removing tissue from patients and analysing it for possible tumours. While effective, it is also a very invasive procedure for the patient, making the search for a potentially life-changing condition even harder. It also makes these procedures inconvenient for continuous modelling of tumour development. A very promising alternative candidate is the liquid biopsy, which relies on the simple method of collecting bodily fluids and searching for circulating tumour DNA (ctDNA), for example [2]. The procedure is minimally invasive, as it requires only a small amount of the patient's fluid. This can even be performed at home, which is both more comfortable for the patient and useful if hospitals are already under pressure, as during a global pandemic [3].
CtDNA is characterised by mutations specific to the tumour, compared with wild-type DNA (wtDNA) found in the bloodstream. The majority of mutations are single-nucleotide variants (SNVs), which account for around 80% of differences in DNA between two individuals. They consist of the substitution of a single base pair in the DNA sequence and are thus relatively easy to form, occurring at a rate of $\sim 10^{-8}$ mutations per base pair per generation [4]. Nevertheless, ctDNA is often present in only small background amounts compared with wtDNA, ranging from $\mathcal{O}(10^{-3})\% \rightarrow 90\%$ depending on the tumour type [5]. This creates a unique challenge in detecting trace amounts of ctDNA whilst ignoring the excess of wtDNA.

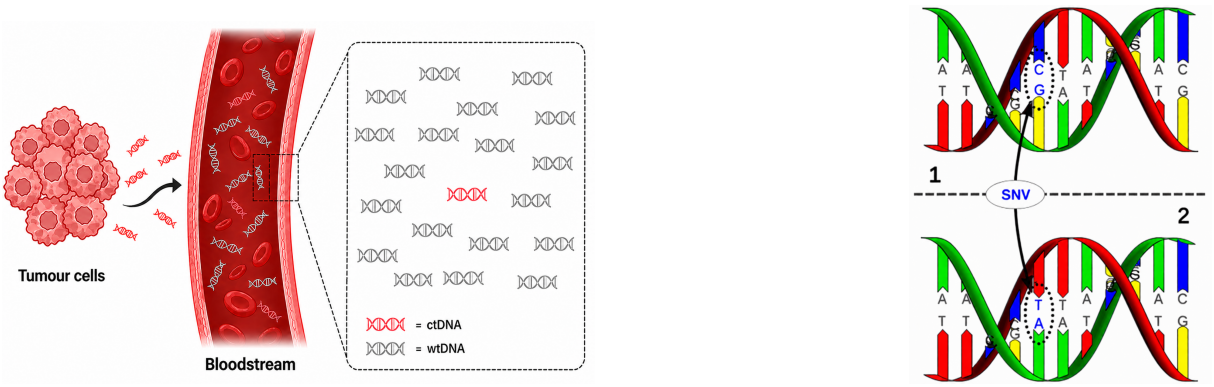

(a) (b)

Figure 1.1: (a) CtDNA is difficult to detect due to the excess of the wtDNA background in the bloodstream [6] (ChatGPT 2026). (b) Single-nucleotide variants consist of the replacement of a single base pair in the helix. (figure adapted from [7])

1.2 Hybridisation-Based Biosensors

Hybridisation-based biosensors are ideal for liquid biopsies. Their main working principle relies on hybridising single-stranded DNA probes complementary to known ctDNA strands. To detect SNVs, these sensors are immediately confronted with the previously described problem of selectivity between the ctDNA and the wtDNA. Hybridisation with wtDNA is not uncommon, even though it creates base mismatches (MMs). These do carry a different free-energy penalty when bound as shown in figure 1.2.

$$\Delta\Delta G_{\text{MM}} = \Delta G_{\text{MM,wtDNA}} - \Delta G_{\text{Match,ctDNA}} > 0 \tag{1.1}$$

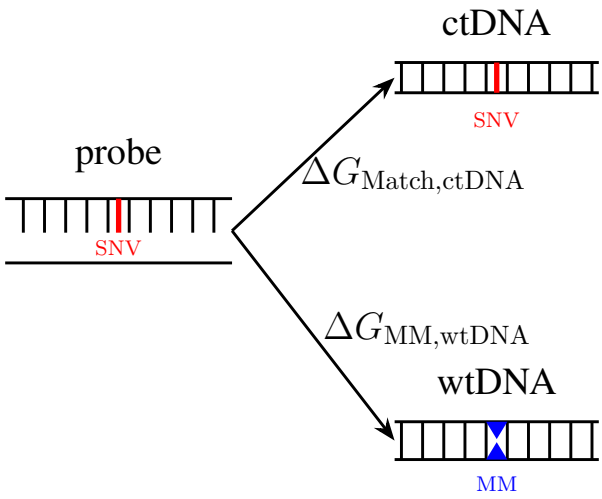

Figure 1.2: Probe hybridisation with a mismatch creates a different free-energy penalty than hybridisation with the complementary SNV.

For given concentrations c of wtDNA and ctDNA, we can directly relate the signal S a sensor will report to the Boltzmann weight of this free-energy penalty [1].

$$\text{S} = \log\left(1 + \frac{c_{\text{ctDNA}}}{c_{\text{wtDNA}} + c_{\text{ctDNA}}} e^{\Delta\Delta G_{\text{MM}}/RT}\right) \tag{1.2}$$

We can invert this relation to obtain the limit of detection (LoD), the smallest detectable fraction of mutants.

$$LoD \approx \text{S}_{\text{min}} e^{-\Delta\Delta G_{\text{MM}}/RT} \tag{1.3}$$

To decrease this LoD, i.e., make the sensor more selective, we must increase the free-energy penalty associated with a mismatch. There exist many ways to do this, including the introduction of blocker strands [1], depletion-based techniques [8, 9] and the focus of this thesis, the introduction of structural strain within the probe. A family of designs based on this principle is the OWL design shown schematically in figure 1.3a.
The sensors form a rigid, structurally imperfect structure when they bind to a complementary analyte. However, when they attempt to hybridise with the mismatched wild-type, the system is further perturbed, leading to the collapse of the entire complex and, consequently, quenching the fluorescent universal molecular beacon. This allows effective differentiation between fully complementary and mismatched analytes [10].

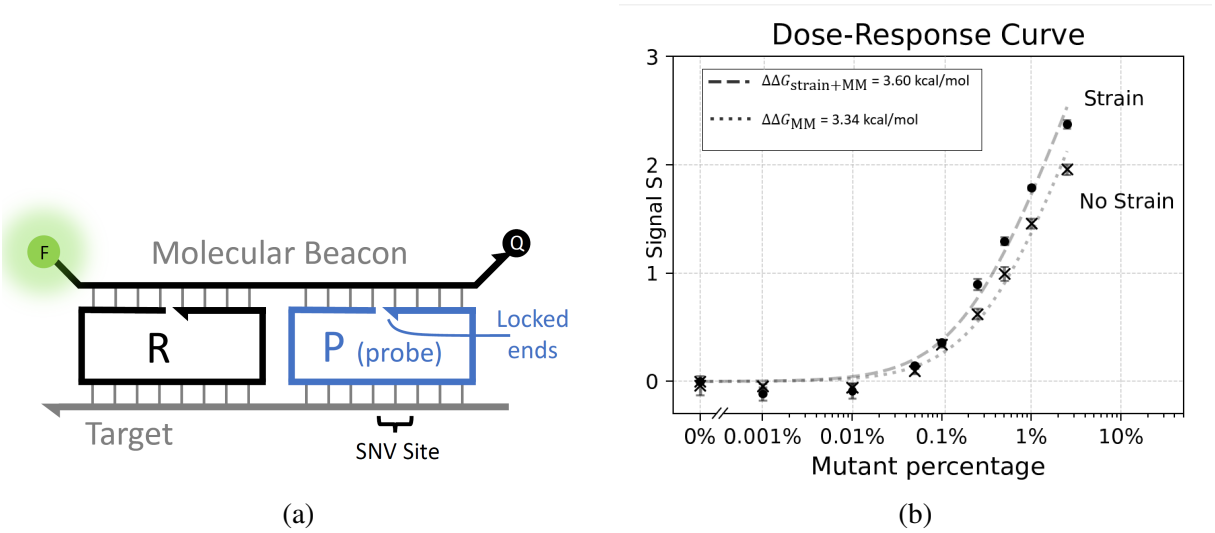

(a) (b)

Figure 1.3: (a) Schematic of the OWL design, the imperfectly locked end on the P strand applies strain interacting with the SNV site. (b) The contribution of strain leads to a 1.5-fold improvement in LoD. (Figures from [1])

The structural imperfection in the OWL design is based on the helical periodicity of 10.4 base pairs (bp) in DNA, the number of base pairs required for the helix to turn $360°$. The geometry of OWL sensors is such that the SNV-matching Probe (P) strand lacks a base pair when closed. It is expected that this exerts significant torque on the structure, overtwisting the helix along the entire P-strand. The circularised segment remains stable thanks to the stacking interactions at both ends. Effectively creating a rigid, 'locked ends' structure [11]. This places significant strain on the system, which interacts with the mismatch site and disrupts the structure. We expect this strain-mismatch interaction to be elastic, yielding an additive contribution to the overall free energy penalty. In this thesis, it is modelled by a quadratic chain model without volume/pressure dependence; we therefore denote it as $\Delta\Delta F_{\text{Strain-MM}}$.

$$\Delta\Delta G = \Delta\Delta G_{\text{MM}} + \Delta\Delta F_{\text{Strain-MM}} \tag{1.4}$$

Stulens *et al.* [1] observed the existence of this free-energy interaction term shown in figure 1.3b for the clinically relevant p.T790M mutation. Where an SNV is present in the epidermal growth factor receptor (EGFR) gene, it is known to increase drug resistance in lung cancer [12].

$$\Delta\Delta F_{\text{Strain-MM}} = 0.26 \pm 0.08 \text{kcal/mol} \tag{1.5}$$

This interaction term yields a 1.5-fold improvement in selectivity over the non-strained case, an OWL sensor with a flexible linker (see section 5.2), using equation (1.3).
The goal of this thesis is to provide a physical framework to model the strain-mismatch interaction and to describe its qualitative and quantitative features. An important aspect of this is the possible optimisation of the detection regime of strain-based sensors. We also perform molecular dynamics simulations in oxDNA to test the hypothesis that torque is indeed the primary source of strain in the system.

2 Mathematics of Chain Models

To model the free-energy interaction term for the strain-mismatch interaction, we first need to define what it entails. We define it by subtracting the combined free-energy penalty of the mismatch and the strain with their separate effects, as shown in figure 2.1.
To capture the interaction mathematically, we first develop a general formalism for one-dimensional quadratic chain-like systems and then perturb them in ways equivalent to applying strain or introducing a mismatch. The perturbations will consist of two parts: a quadratic part that fundamentally alters the underlying structure, and a linear part that acts as a force term on the chain. They will come with the special property of coupling to the same spatial region in the system and will be denoted as matched-mode perturbations (MMPs). We develop the free-energy interaction term for more general MMPs, making the formalism useful beyond its present purposes. It is then applied consistently in the following chapters to obtain qualitative and quantitative information about the interaction.

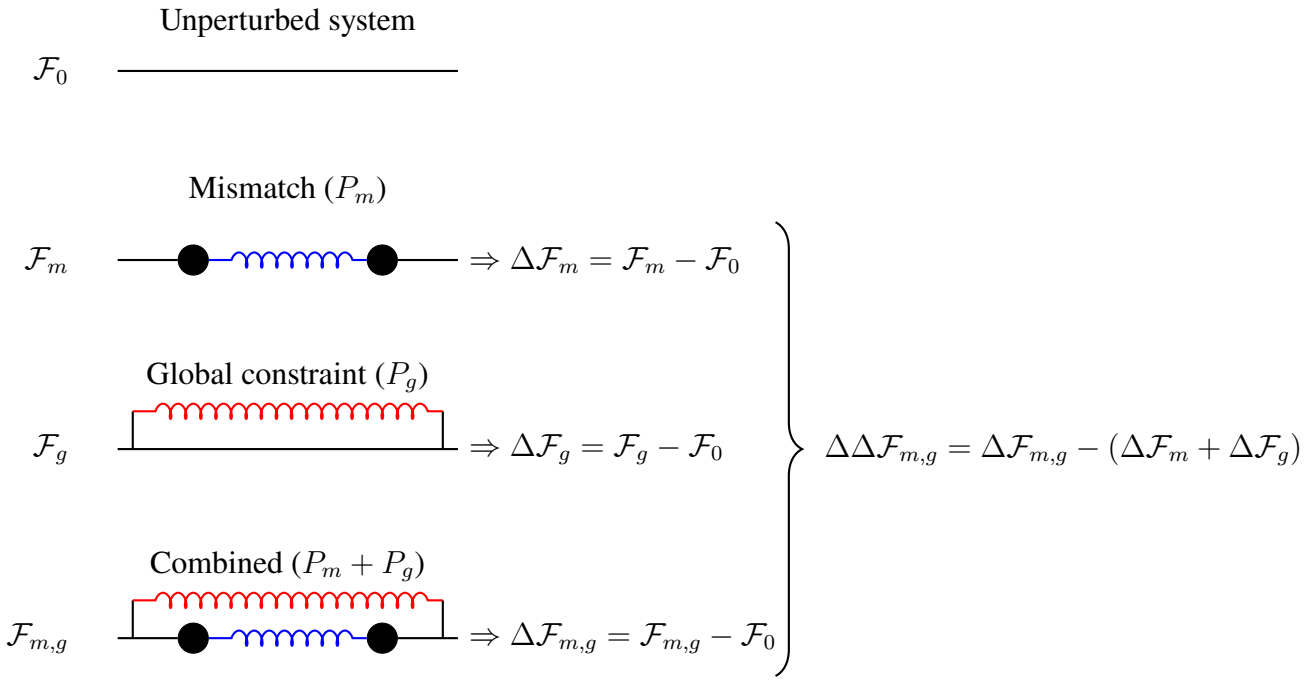

Figure 2.1: Definition of the strain-mismatch free-energy interaction term.

2.1 The Decoupled Chain

The simplest model of a polymer is a one-dimensional decoupled harmonic chain. This is a lattice of $N+1$ nodes at discrete positions, connected by N springs. We denote the position of the n-th node by u_n and its connection to the $n+1$-st node by a spring with spring constant K_n and rest length a.

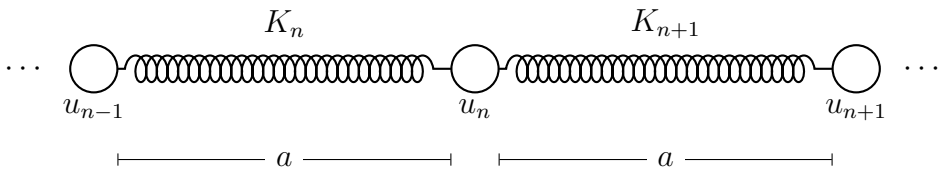

Figure 2.2: The decoupled chain

Since all these interactions are harmonic, we can easily write down a Hamiltonian consisting of N decoupled harmonic oscillators. For the purposes of this thesis, the kinetic energy of each node is treated as an additional decoupled degree of freedom only, contributing a normalisation constant. We therefore do not include it. We normalise the Hamiltonian by the inverse temperature $\beta \equiv 1/k_B T$.

$$\beta H \equiv \mathcal{H} = \frac{1}{2} \sum_{n=0}^{N-1} K_n [(u_{n+1} - u_n) - a]^2 \tag{2.1}$$

It is more convenient to work in displacement coordinates compared to the rest length.

$$x_n \equiv u_{n+1} - u_n - a \tag{2.2}$$

So that the Hamiltonian is a sum of the independent displacements.

$$\mathcal{H} = \frac{1}{2} \sum_{n=0}^{N-1} K_n x_n^2 \tag{2.3}$$

In the decoupled case, the sum notation is intuitive and easy to use. However, when we complicate the system by introducing couplings between oscillators or perturbations, the sum notation quickly becomes cumbersome. It is thus often easier and more intuitive to work in matrix notation.

We start by defining the n-th unit vector in the N-dimensional phase space.

$$|n\rangle = \begin{pmatrix} 0 \\ \vdots \\ 0 \\ 1 \\ 0 \\ \vdots \\ 0 \end{pmatrix} \leftrightarrow n\text{-th index} \tag{2.4}$$

The set of unit vectors constitutes $\{|0\rangle, \ldots, |N-1\rangle\}$ an orthonormal basis of the N-dimensional inner product space such that:

$$\langle m|n\rangle = \delta_{mn} = \begin{cases} 1 & \text{if } m = n \\ 0 & \text{if } m \neq n \end{cases} \tag{2.5}$$

From this, we can define the displacement vector $|x\rangle$ and its dual $\langle x|$ by summing over all unit vectors with distinct displacements x_n.

$$|x\rangle \equiv \sum_{n=0}^{N-1} x_n |n\rangle = \begin{pmatrix} x_0 \\ x_1 \\ \vdots \\ x_{N-1} \end{pmatrix}$$
$$\langle x| = \sum_{n=0}^{N-1} x_n \langle n| = \begin{pmatrix} x_0 & x_1 & \ldots & x_{N-1} \end{pmatrix}$$

We can couple each displacement via the stiffness matrix $\hat{K}$. In the decoupled chain, this is particularly easy because the displacements are independent, yielding a diagonal stiffness matrix.

$$\hat{K} \equiv \sum_{n=0}^{N-1} K_n |n\rangle\langle n| = \begin{pmatrix} K_0 & 0 & \ldots & 0 \\ 0 & K_1 & 0 & \vdots \\ \vdots & 0 & \ddots & \vdots \\ 0 & \ldots & \ldots & K_{N-1} \end{pmatrix} \tag{2.6}$$

We can now rewrite the decoupled chain (2.1) Hamiltonian in matrix notation.

$$\mathcal{H} = \frac{1}{2} \langle x|\hat{K}|x\rangle \tag{2.7}$$

2.2 The Stiffness Matrix

We can easily generalise this notation by allowing off-diagonal entries in the stiffness matrix; this corresponds to general quadratic systems.

$$\mathcal{H} = \frac{1}{2} \sum_{n=0}^{N-1} \sum_{m=0}^{N-1} K_{nm} x_n x_m = \frac{1}{2} \langle x|\hat{K}|x\rangle \tag{2.8}$$

The (m, n)-th entry of the stiffness matrix now represents the coupling between the displacements of the m-th and n-th oscillators.
As we are interested in the thermodynamic features of this system, we introduce the classical partition sum by integrating over the entire phase space, in which we denote the previously introduced vectors as $\mathbf{x}$.

$$Z = \int d\mathbf{x} e^{-\mathcal{H}(\mathbf{x})} = \int d\mathbf{x} e^{-\frac{1}{2}\langle x|\hat{K}|x\rangle} \tag{2.9}$$

By this definition, any physical stiffness matrix must satisfy two properties.

1. $\hat{K}$ must be real and symmetric such that $\hat{K}^T = \hat{K}$, such that all harmonic interactions are symmetric.

2. $\hat{K}$ must be positive definite for the convergence of the partition sum. We refer to this as the stability criterion, as any non-positive definite system is fundamentally unstable to the application of any perturbation.

If all these are met, we can apply the Gaussian integral theorem B.2 to evaluate the partition sum. This can be done using both the eigenvalues $\tilde{K}_q$ and the determinant of the stiffness matrix.

$$Z = \int d\mathbf{x} e^{-\frac{1}{2}\langle x|\hat{K}|x\rangle} = \sqrt{\frac{(2\pi)^N}{\det \hat{K}}} = (2\pi)^{N/2} \left(\prod_{q=0}^{N-1} \tilde{K}_q \right)^{-1/2} \tag{2.10}$$

For the decoupled chain, identifying the eigenvalues is particularly easy; these are exactly the spring constants of the individual springs, as can be identified from the diagonal stiffness matrix (2.6). This will generally be a non-trivial exercise, though; we take care of this in chapter 4. As we are interested in comparing systems, it is convenient to work with the system's free energy $F \equiv E - TS$ as it is an additive quantity. It also allows a clear distinction between entropic and energetic contributions. We normalise the free energy $\mathcal{F} \equiv \beta F$ with respect to thermal fluctuations via the inverse temperature $\beta = 1/k_B T$ and then relate it to the partition sum by:

$$\mathcal{F} = \beta F = -\log Z = \frac{1}{2}\left[\sum_{q=0}^{N-1} \log \tilde{K}_q - N \log(2\pi) \right] \tag{2.11}$$

This reveals the entropic nature of the unperturbed chain model. This is a general feature: any harmonic degree of freedom in Gaussian systems can be treated as entropic, as we will see for quadratic perturbations later.

2.3 Linear Terms

2.3.1 Force Application

Consider a local constant force application $f = -\frac{\Delta \mathcal{V}}{\Delta u}$ by some potential $\mathcal{V}$ on two adjacent nodes in the decoupled chain as shown in figure 2.3.

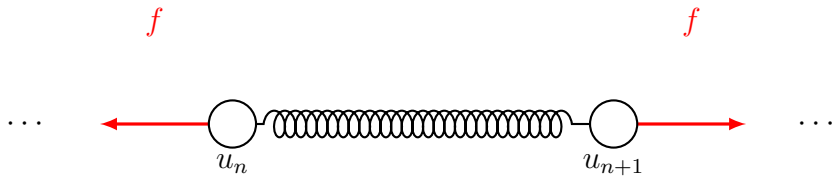

Figure 2.3: Local force application on the decoupled chain

The potential energy shifts based on the displacement of each node from its natural lattice site. We define the equilibrium position of the n-th node as na. The displacement from equilibrium is then:

$$\Delta u_n = u_n - na \tag{2.12}$$

There are two contributions to the potential energy, as the force acts on both the n-th and the $n+1$-st nodes.

$$\begin{cases} \mathcal{V}(u_n) = f(u_n - na) \\ \mathcal{V}(u_{n+1}) = -f(u_{n+1} - (n+1))a \end{cases} \Rightarrow \mathcal{V} = f(u_{n+1} - u_n - a) = fx_n \tag{2.13}$$

We thus observe a linear shift in the system relative to the base Hamiltonian H_0.

$$\mathcal{H} = \mathcal{H}_0 - f \langle n|x\rangle \tag{2.14}$$

Any linear term in the Hamiltonian can thus be associated with a constant force acting on the system. We will now develop the formalism for handling linear terms of this type in the Hamiltonian.

2.3.2 A General Linear Term

Suppose we have a Hamiltonian of the form:

$$\mathcal{H} = \frac{1}{2}\sum_n \sum_m K_{nm} x_n x_m + \sum_n b_n x_n + c \tag{2.15}$$

We handle the quadratic term as before by incorporating it into the stiffness matrix. The inclusion of a linear term complicates the evaluation of the partition sum. We use matrix notation again, defining $|b\rangle = \sum_n b_n |n\rangle$.

$$\mathcal{H} = \frac{1}{2}\langle x|\hat{K}|x\rangle + \langle b|x\rangle + c \tag{2.16}$$

The stability criterion ensures that the stiffness matrix is symmetric and positive definite. By the spectral theorem B.1, this also means it is invertible, and its inverse is symmetric and positive definite. We call this inverse $\hat{K}^{-1}$, the structure matrix of the system. To recover a quadratic Hamiltonian, we shift to normal coordinates $|y\rangle$.

$$|y\rangle \equiv |x\rangle + \hat{K}^{-1}|b\rangle \tag{2.17}$$

$$\langle y| = \langle x| + \langle b|\hat{K}^{-1} \tag{2.18}$$

The Hamiltonian in these normal coordinates is now given by:

$$\begin{aligned}\mathcal{H} &= \frac{1}{2}\langle x|\hat{K}|x\rangle + \langle b|x\rangle + c \\ &= \frac{1}{2}\Big(\langle y| - \langle b|\,\hat{K}^{-1}\Big)\hat{K}\Big(-\hat{K}^{-1}\,|b\rangle + |y\rangle\Big) + \langle b|\,\Big(|y\rangle - \hat{K}^{-1}\,|b\rangle\Big) + c \\ \mathcal{H} &= \frac{1}{2}\langle y|\hat{K}|y\rangle - \frac{1}{2}\langle b|\hat{K}^{-1}|b\rangle + c \end{aligned} \tag{2.19}$$

The only extra calculation required, then, is the construction of the structure matrix $\hat{K}^{-1}$. For the partition sum (2.9), this linear term leaves the Gaussian integral since $d\mathbf{x} = d\mathbf{y}$.

$$\begin{aligned} Z &= e^{\frac{1}{2}\langle b|\hat{K}^{-1}|b\rangle - c}\int d\mathbf{y} e^{-\frac{1}{2}\langle y|\hat{K}|y\rangle} \\ &= e^{\frac{1}{2}\langle b|\hat{K}^{-1}|b\rangle - c}(2\pi)^{N/2}\left(\prod_{q=0}^{N-1}\tilde{K}_q\right)^{-1/2} \end{aligned} \tag{2.20}$$

In the free energy, this term returns as an additive contribution, using equation (2.11) we find:

$$\mathcal{F}_l = \underbrace{\frac{1}{2}\left[\sum_{q=0}^{N-1}\log\tilde{K}_q - N\log(2\pi)\right]}_{\text{Entropic}} \underbrace{-\frac{1}{2}\langle b|\hat{K}^{-1}|b\rangle + c}_{\text{Energetic}} \tag{2.21}$$

The term has energetic units and consequently represents the energetic/enthalpic contribution to the free energy. We can interpret it as the work performed by the linear force term to shift the equilibrium coordinates $|x\rangle$ to the new coordinates $|y\rangle$. When comparing to the base system without the linear term, the free energy differences are purely this energetic term.

$$\Delta\mathcal{F}_l = \beta\Delta E_l \equiv \Delta\mathcal{E} = -\frac{1}{2}\langle b|\hat{K}^{-1}|b\rangle + c \tag{2.22}$$

2.3.3 Thermal Averages

For a general function $f(\mathbf{x})$ of the displacement coordinates $\mathbf{x}$, thermal averaging is performed using the partition sum as a probability density.

$$\langle f(\mathbf{x})\rangle = \frac{1}{Z_0}\int \mathrm{d}\mathbf{x} f(\mathbf{x}) e^{-\frac{1}{2}\langle x|\hat{K}|x\rangle} \tag{2.23}$$

Where Z_0 is the unperturbed partition sum given by equation (2.9), we can now manipulate the machinery we developed in the previous section to simplify this expression by the introduction of a vanishing linear term to shift the term within the function itself as performed by Osborn [13].

$$f(\mathbf{x}) = f(-\nabla_{\mathbf{b}})\; e^{\langle b|x\rangle}\Big|_{\mathbf{b}=0} \tag{2.24}$$

Where $\nabla_{\mathbf{b}}$ represents the gradient towards the components of the $|b\rangle$ vectors only. We fill this into equation (2.23).

$$\begin{aligned}\langle f(\mathbf{x})\rangle &= \frac{1}{Z_0}\int \mathrm{d}\mathbf{x}\; f(-\nabla_{\mathbf{b}})e^{-\frac{1}{2}\langle x|\hat{K}|x\rangle+\langle b|x\rangle}\Big|_{\mathbf{b}=0} \\ &= f(-\nabla_{\mathbf{b}})\frac{Z_b}{Z_0}\Big|_{\mathbf{b}=0}\end{aligned}$$

Comparing Z_b and Z_0, only the artificially introduced energetic term equation (2.20) survives, and all the $|b\rangle$ dependence will cancel as $|b\rangle \to 0$.

$$\langle f(\mathbf{x})\rangle = f(-\nabla_{\mathbf{b}})e^{-\frac{1}{2}\langle b|\hat{K}^{-1}|b\rangle}\Big|_{\mathbf{b}=0} \tag{2.25}$$

2.4 Single-Mode Perturbations

We now turn our attention to single-mode perturbations, i.e. perturbations to the system, which perturb the Hamiltonian in such a way that the stiffness matrix only changes through the addition of a single outer product term.

$$\mathcal{H}_0 \to \mathcal{H} \quad \text{such that} \quad \hat{K} = \hat{K}_0 + |u\rangle\langle v| \tag{2.26}$$

We must note that these are not, by definition, local, as they can couple to larger regions in the system and, consequently, to multiple entries of the stiffness matrix.

2.4.1 Quadratic Perturbations

Suppose we perturb the system quadratically:

$$\mathcal{H} = \frac{1}{2}\langle x|\hat{K}_0|x\rangle + \frac{1}{2}\langle x|u\rangle\langle v|x\rangle \tag{2.27}$$

As we saw in section 2.1, the entropic contribution to the system can be found through both the eigenvalues and the determinant of the stiffness matrix. To find the entropic differences present by these perturbations, we must thus find new expressions for these. For these single-mode perturbations, the most efficient way to do this is through the matrix-determinant lemma.

Lemma 2.1 (Matrix-determinant)**.** *For any square invertible matrix $\hat{K}_0$ and column vectors $|u\rangle, |v\rangle$ the determinant of the rank-one updated $\hat{K} = \hat{K}_0 + |u\rangle\langle v|$ is given by [14]:*

$$\det\hat{K} = \det\Big(\hat{K}_0 + |u\rangle\langle v|\Big) = \det\hat{K}_0\Big[1 + \langle v|\hat{K}_0^{-1}|u\rangle\Big] \tag{2.28}$$

The free energy difference conflicted by this quadratic perturbation can now be found through equation (2.11)

$$\begin{aligned}\Delta F_q &= -T\Delta S \\ &= -T(S - S_0) \\ &= \frac{k_B T}{2}\Big[\log\det\hat{K} - \log\det\hat{K}_0\Big] \\ &= \frac{k_B T}{2}\Big[\log\Big(\det\hat{K}_0(1 + \langle v|\hat{K}_0^{-1}|u\rangle)\Big) - \log\det\hat{K}_0\Big]\end{aligned}$$

Thanks to the explicit temperature dependence in this equation, the entropic nature of the free-energy difference becomes clear. Splitting the first logarithmic term, we find:

$$\Delta\mathcal{F} = -\Delta\mathcal{S} = \frac{1}{2}\log\Big(1 + \langle u|\hat{K}_0^{-1}|v\rangle\Big) \tag{2.29}$$

2.4.2 Quadratic and Linear Perturbations

By treating both the quadratic and linear terms in the Hamiltonian as simultaneous perturbations to the reference system, we reveal their coupled effects.

$$\mathcal{H} = \frac{1}{2}\langle x|\hat{K}_0|x\rangle + \underbrace{\frac{1}{2}\langle x|u\rangle\langle v|x\rangle}_{\text{Quadratic}} + \underbrace{\langle b|x\rangle}_{\text{Linear}} + c \tag{2.30}$$

The quadratic perturbation fundamentally modifies the system's stiffness matrix through a rank-one update:

$$\hat{K}_0 \to \hat{K} = \hat{K}_0 + |u\rangle\langle v| \tag{2.31}$$

This also alters the structure matrix of the system $\hat{K}_0^{-1} \to \hat{K}^{-1}$ and consequently the energetic contribution to the free energy. We handle this through the Sherman-Morrison formula.

Theorem 2.2 (Sherman-Morrison)**.** *For any square invertible matrix $\hat{K}_0$ and column vectors $|u\rangle, |v\rangle$ the inverse of the rank-one updated $\hat{K} = \hat{K}_0 + |u\rangle\langle v|$ is given by [15]:*

$$\Big(\hat{K}_0 + |u\rangle\langle v|\Big)^{-1} = \hat{K}_0^{-1} - \frac{\hat{K}_0^{-1}|u\rangle\langle v|\hat{K}_0^{-1}}{1 + \langle u|\hat{K}_0^{-1}|v\rangle} \tag{2.32}$$

Due to this alteration of the structure matrix, the linear perturbation now acts on a different background. This introduces new cross-terms in the total energy, extending beyond the linear effects seen in the previous section. By performing the appropriate coordinate transformation as discussed in section 2.3 and using our newly obtained form of the structure matrix, we find a new energetic shift in the system

$$\begin{aligned}\Delta\mathcal{E} &= -\frac{1}{2}\langle b|\hat{K}^{-1}|b\rangle + c \\ &= \underbrace{-\frac{1}{2}\langle b|\hat{K}_0^{-1}|b\rangle}_{\text{Linear shift}} + \underbrace{\frac{1}{2}\frac{\langle b|\hat{K}_0^{-1}|u\rangle\ \langle v|\hat{K}_0^{-1}|b\rangle}{1 + \langle u|\hat{K}_0^{-1}|v\rangle}}_{\text{Coupling shift}} + c\end{aligned} \tag{2.33}$$

Since linear perturbation leaves the entropic free energy invariant, we can combine this energetic shift with equation (2.29) to find the full expression of the free energy change for a single mode perturbation.

$$\Delta\mathcal{F}_{q,l} = \frac{1}{2}\log\Big(1 + \langle v|\hat{K}_0^{-1}|u\rangle\Big) - \frac{1}{2}\langle b|\hat{K}_0^{-1}|b\rangle + \frac{1}{2}\frac{\langle b|\hat{K}_0^{-1}|u\rangle\ \langle v|\hat{K}_0^{-1}|b\rangle}{1 + \langle v|\hat{K}_0^{-1}|u\rangle} + c \tag{2.34}$$

The cases of interest to us are single-mode perturbations in which the linear and quadratic terms perturb the same spatial mode; we refer to these as Matched-Mode Perturbations

(MMPs). To avoid mixing the structure of the mode with its physical magnitude, we separate its structure into a fixed vector $|\hat{s}\rangle$ and two scaling parameters $\sqrt{\kappa}$ and f.

$$\begin{cases} |u\rangle = |v\rangle \equiv \sqrt{\kappa}\,|\hat{s}\rangle \\ |b\rangle = f|\hat{s}\rangle \end{cases} \qquad \text{Matched-Mode-Perturbation (MMP)} \tag{2.35}$$

Here, κ represents the magnitude of the quadratic (stiffness) perturbation. We choose f to represent the magnitude of the linear perturbation, since these are linked to the application of forces in the system. Substituting these relations substantially simplifies the expression for the perturbed free energy, as the physical magnitudes factor cleanly out of the inner products:

$$\Delta\mathcal{F}_{q,l} = \frac{1}{2}\log\left(1+\kappa\langle\hat{s}|\hat{K}_0^{-1}|\hat{s}\rangle\right) - \frac{1}{2}f^2\langle\hat{s}|\hat{K}_0^{-1}|\hat{s}\rangle + \frac{1}{2}\frac{f^2\kappa\langle\hat{s}|\hat{K}_0^{-1}|\hat{s}\rangle^2}{1+\kappa\langle\hat{s}|\hat{K}_0^{-1}|\hat{s}\rangle} + \Delta c \tag{2.36}$$

A shortened expression may be suitable when focusing solely on simple free energy differences. However, it is not advisable to use it in the next section, where the focus shifts to interaction free energy, as it would make the expressions less explicit. By finding a common denominator, it neatly combines the first and second terms in the energy

$$\Delta\mathcal{F}_{q,l} = \frac{1}{2}\log\left(1+\kappa\langle\hat{s}|\hat{K}_0^{-1}|\hat{s}\rangle\right) - \frac{1}{2}\frac{f^2\langle\hat{s}|\hat{K}_0^{-1}|\hat{s}\rangle}{1+\kappa\langle\hat{s}|\hat{K}_0^{-1}|\hat{s}\rangle} + \Delta c \tag{2.37}$$

2.5 Interaction Terms

One of the primary objectives of this thesis is to develop a framework for comparing the relative impacts of perturbations on the system and assessing their interactions. The most obvious way to do so is to compare their respective free energies. These will include both additive and non-additive contributions arising from interactions between the perturbations. To formalise this, we introduce the free-energy interaction term $\Delta\Delta\mathcal{F}$ as outlined below.

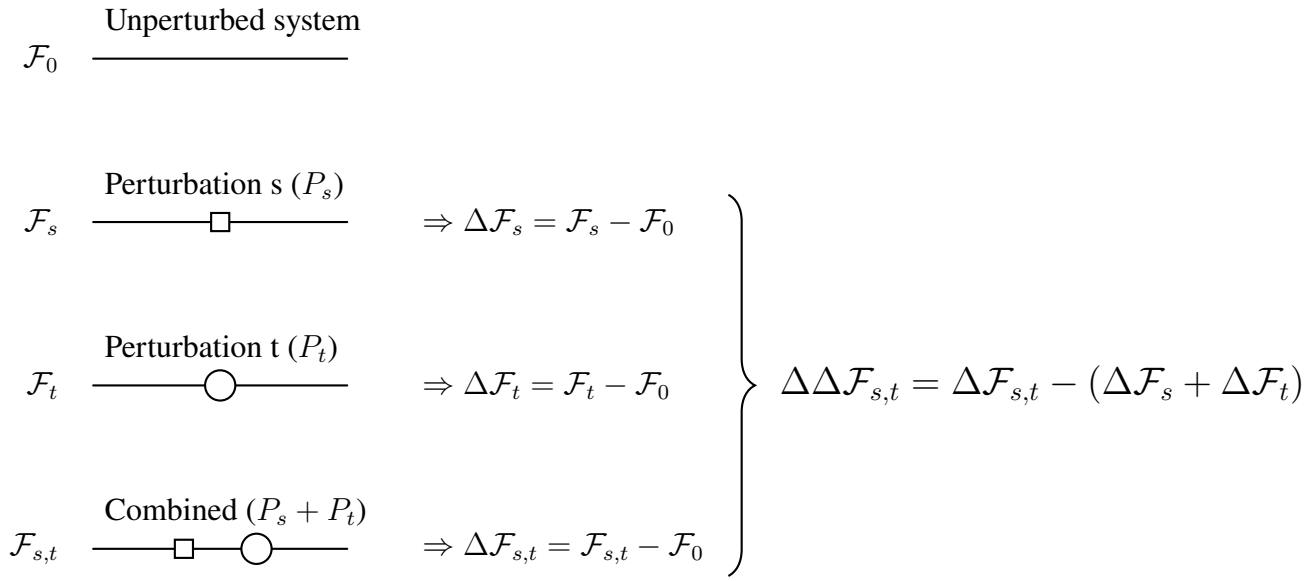

Figure 2.4: The definition of the free-energy interaction term

At this point, we make no assumptions about the perturbations to the system, other than that the individual perturbations are matched-mode. First, we must develop the mathematical formalism to model a double perturbation in the system. We do this more abstractly than before by applying a quadratic perturbation to the stiffness matrix again using MMPs.

$$\hat{K}_0 \to \hat{K} = \hat{K}_0 + \kappa \left|\hat{s}\right\rangle\!\left\langle\hat{s}\right| + \xi \left|\hat{t}\right\rangle\!\left\langle\hat{t}\right| \tag{2.38}$$

The perturbations are matched-mode, so they have an associated force term:

$$\sqrt{\kappa}\left|\hat{s}\right\rangle \leftrightarrow f_s \left|\hat{s}\right\rangle \tag{2.39}$$

$$\sqrt{\xi}\left|\hat{t}\right\rangle \leftrightarrow f_t \left|\hat{t}\right\rangle \tag{2.40}$$

This joint perturbation to the base stiffness matrix $\hat{K}_0$ is often referred to as a rank-2 update. The most efficient way to handle these is to apply a second-order Woodbury update. The Woodbury matrix identity generalises the Sherman-Morrison formula.

Theorem 2.3 (Woodbury matrix identity)**.** *Let $\hat{K}_0 \in \mathbb{R}^{n\times n}$, $U^t \in \mathbb{R}^{n\times k}$, $C \in \mathbb{R}^{k\times k}$, and $V \in \mathbb{R}^{k\times n}$ be matrices and $\hat{K} = \hat{K}_0 + U^t C V$ then the inverse of the rank-k updated $\hat{K}$ is given by[15]:*

$$\hat{K}^{-1} = \hat{K}_0^{-1} - \hat{K}_0^{-1}U^t(C^{-1} + V\hat{K}_0^{-1}U^t)^{-1}V\hat{K}_0^{-1} \tag{2.41}$$

and for the determinant:

$$\det \hat{K} = \det\left(\hat{K}_0\right)\det(C)\det\left(C^{-1} + U^t\hat{K}_0^{-1}V\right) \tag{2.42}$$

Even for the rank-two case, the calculations to implement the two MMPs in the system are quite involved and therefore restricted to appendix B.2. The resulting updated structure matrix is given by:

$$\begin{aligned}\hat{K}^{-1} = \hat{K}_0^{-1} - \frac{1}{D}\big[&\xi\left(1 + \kappa\left\langle\hat{s}\right|\hat{K}_0^{-1}\left|\hat{s}\right\rangle\right)\hat{K}_0^{-1}\left|\hat{t}\right\rangle\!\left\langle\hat{t}\right|\hat{K}_0^{-1} + \kappa\left(1 + \xi\left\langle\hat{t}\right|\hat{K}_0^{-1}\left|\hat{t}\right\rangle\right)\hat{K}_0^{-1}\left|\hat{s}\right\rangle\!\left\langle\hat{s}\right|\hat{K}_0^{-1} \\ &- \kappa\xi\left(\hat{K}_0^{-1}\left|\hat{s}\right\rangle\!\left\langle\hat{t}\right|\hat{K}_0^{-1} + \hat{K}_0^{-1}\left|\hat{t}\right\rangle\!\left\langle\hat{s}\right|\hat{K}_0^{-1}\right)\big]\end{aligned} \tag{2.43}$$

While the new determinant of the system is given by:

$$\det\left(\hat{K}\right) = \det\left(\hat{K}_0\right)\left[\left(1 + \kappa\left\langle\hat{s}\right|\hat{K}_0^{-1}\left|\hat{s}\right\rangle\right)\left(1 + \xi\left\langle\hat{t}\right|\hat{K}_0^{-1}\left|\hat{t}\right\rangle\right) - \kappa\xi\left\langle\hat{s}\right|\hat{K}_0^{-1}\left|\hat{t}\right\rangle^2\right] \tag{2.44}$$

We see the appearance of a new perturbed determinant D, which is not a determinant of an $N \times N$ system as before, but rather of the 2×2 perturbed subsystem.

$$D \equiv \left(1 + \kappa\left\langle\hat{s}\right|\hat{K}_0^{-1}\left|\hat{s}\right\rangle\right)\left(1 + \xi\left\langle\hat{t}\right|\hat{K}_0^{-1}\left|\hat{t}\right\rangle\right) - \kappa\xi\left\langle\hat{s}\right|\hat{K}_0^{-1}\left|\hat{t}\right\rangle^2 \tag{2.45}$$

Entropic Contribution

First, we look at the entropic contribution of the jointly perturbed system. For this, we require the new determinant given by equation (2.44). In the perturbed determinant D, we see the same terms as in equation (2.29) appearing separately (we refer to these as D_s and D_t),

as well as a mixing term. This is the first sign that additivity across joint perturbations will be broken. We use the entropic definition from before:

$$\begin{aligned}\Delta\mathcal{S}_{s,t} &= \mathcal{S}_{s,t} - \mathcal{S}_0 \\ &= -\frac{1}{2}\Big[\log\Big(\det \hat{K}\Big) - \log\Big(\det \hat{K}_0\Big)\Big] \\ &= -\frac{1}{2}\Big[\log\Big(D \det \hat{K}_0\Big) - \log\Big(\det \hat{K}_0\Big)\Big] \\ &= -\frac{1}{2}\log(D) \\ &= -\frac{1}{2}\log\Big(\Big(1+\kappa\,\langle\hat{s}|\hat{K}_0^{-1}|\hat{s}\rangle\Big)\Big(1+\xi\,\langle\hat{t}|\hat{K}_0^{-1}|\hat{t}\rangle\Big) - \kappa\xi\,\langle\hat{s}|\hat{K}_0^{-1}|\hat{t}\rangle^2\Big)\end{aligned} \tag{2.46}$$

We are, of course, interested in the entropic interaction term for these joint perturbations. Using the definition of the interaction term, this requires evaluating the quadratic perturbations $\kappa\,|\hat{s}\rangle\langle\hat{s}|$ and $\xi\,|\hat{t}\rangle\langle\hat{t}|$ separately and comparing their sum with the simultaneous application of these perturbations via the rank-2 update.
We denote this as the interaction entropy $\Delta\Delta\mathcal{S}_{st}$:

$$\begin{aligned}\Delta\Delta\mathcal{S}_{s,t} &= \Delta\mathcal{S}_{s,t} - (\Delta\mathcal{S}_s + \mathcal{S}_t) \\ &= -\frac{1}{2}\log\Big(\Big(1+\kappa\,\langle\hat{s}|\hat{K}_0^{-1}|\hat{s}\rangle\Big)\Big(1+\xi\,\langle\hat{t}|\hat{K}_0^{-1}|\hat{t}\rangle\Big) - \kappa\xi\,\langle\hat{s}|\hat{K}_0^{-1}|\hat{t}\rangle^2\Big) \\ &+ \frac{1}{2}\log\Big(1+\kappa\,\langle\hat{s}|\hat{K}_0^{-1}|\hat{s}\rangle\Big) + \frac{1}{2}\log\Big(1+\xi\,\langle\hat{t}|\hat{K}_0^{-1}|\hat{t}\rangle\Big) \\ &= -\frac{1}{2}\log\left(1 - \frac{\kappa\xi\,\langle\hat{s}|\hat{K}_0^{-1}|\hat{t}\rangle^2}{\Big(1+\kappa\,\langle\hat{s}|\hat{K}_0^{-1}|\hat{s}\rangle\Big)\Big(1+\xi\,\langle\hat{t}|\hat{K}_0^{-1}|\hat{t}\rangle\Big)}\right)\end{aligned} \tag{2.47}$$

This exact formula analytically captures the coupling between the two quadratic perturbations, allowing us to compute the interaction directly rather than evaluating the systems completely separately. This is useful for the coming sections.

Energetic Contribution

The energetic contribution applied by the joint application of the MMPs is given by:

$$\Delta\mathcal{E}_{s,t} = -\frac{1}{2}\big(f_s\,\langle\hat{s}| + f_t\,\langle\hat{t}|\big)\hat{K}^{-1}\big(f_s\,|\hat{s}\rangle + f_t\,|\hat{t}\rangle\big) \tag{2.48}$$

We can find the inverse of the rank-2 updated matrix using the Woodbury matrix identity B.5, as shown in appendix B.2.

$$\begin{aligned}\hat{K}^{-1} = \hat{K}_0^{-1} - \frac{1}{D}\big[&\xi\Big(1+\kappa\,\langle\hat{s}|\hat{K}_0^{-1}|\hat{s}\rangle\Big)\hat{K}_0^{-1}\,|\hat{t}\rangle\langle\hat{t}|\,\hat{K}_0^{-1} + \kappa\Big(1+\xi\,\langle\hat{t}|\hat{K}_0^{-1}|\hat{t}\rangle\Big)\hat{K}_0^{-1}\,|\hat{s}\rangle\langle\hat{s}|\,\hat{K}_0^{-1} \\ &- \kappa\xi\Big(\hat{K}_0^{-1}\,|\hat{s}\rangle\langle\hat{t}|\,\hat{K}_0^{-1} + \hat{K}_0^{-1}\,|\hat{t}\rangle\langle\hat{s}|\,\hat{K}_0^{-1}\Big)\big]\end{aligned} \tag{2.49}$$

It is quite clear that this will initially lead to a very large term, particularly when we look at the interaction energy:

$$\Delta\Delta\mathcal{E}_{s,t} = \Delta\mathcal{E}_{s,t} - (\Delta\mathcal{E}_s + \Delta\mathcal{E}_t) \tag{2.50}$$

The calculation of this interaction energy is quite involved, due to the multitude of terms; it is therefore presented in appendix B.2.2. The final resulting interaction energy is given by:

$$\Delta\Delta\mathcal{E}_{st} = \frac{1}{D}\left[\frac{f_s^2}{2}\frac{\xi\left\langle\hat{s}\middle|\hat{K}_0^{-1}\middle|\hat{t}\right\rangle^2}{1+\kappa\left\langle\hat{s}\middle|\hat{K}_0^{-1}\middle|\hat{s}\right\rangle} + \frac{f_t^2}{2}\frac{\kappa\left\langle\hat{s}\middle|\hat{K}_0^{-1}\middle|\hat{t}\right\rangle^2}{1+\xi\left\langle\hat{t}\middle|\hat{K}_0^{-1}\middle|\hat{t}\right\rangle} - f_s f_t\left\langle\hat{s}\middle|\hat{K}_0^{-1}\middle|\hat{t}\right\rangle\right] \tag{2.51}$$

Combining with the interaction entropy (2.47), this gives us the free-energy interaction term between the application of both Matched-Mode-Perturbations separately and their joint application.

$$\begin{aligned}\Delta\Delta\mathcal{F}_{s,t} = &\frac{1}{2}\log\left(1 - \frac{\kappa\xi\left\langle\hat{s}\middle|\hat{K}_0^{-1}\middle|\hat{t}\right\rangle^2}{\left(1+\kappa\left\langle\hat{s}\middle|\hat{K}_0^{-1}\middle|\hat{s}\right\rangle\right)\left(1+\xi\left\langle\hat{t}\middle|\hat{K}_0^{-1}\middle|\hat{t}\right\rangle\right)}\right)\\ &+\frac{1}{D}\left[\frac{f_s^2}{2}\frac{\xi\left\langle\hat{s}\middle|\hat{K}_0^{-1}\middle|\hat{t}\right\rangle^2}{1+\kappa\left\langle\hat{s}\middle|\hat{K}_0^{-1}\middle|\hat{s}\right\rangle} + \frac{f_t^2}{2}\frac{\kappa\left\langle\hat{s}\middle|\hat{K}_0^{-1}\middle|\hat{t}\right\rangle^2}{1+\xi\left\langle\hat{t}\middle|\hat{K}_0^{-1}\middle|\hat{t}\right\rangle} - f_s f_t\left\langle\hat{s}\middle|\hat{K}_0^{-1}\middle|\hat{t}\right\rangle\right]\end{aligned} \tag{2.52}$$

The analytical form of the free-energy interaction term is the most important result of the MMP formalism, as it is a closed-form equation for a relatively complex manipulation of the stiffness matrix.

In both the entropic and energetic interaction terms, we observe the emergence of the individual MMP determinants, $D_s = 1+\kappa\left\langle\hat{s}\middle|\hat{K}_0^{-1}\middle|\hat{s}\right\rangle$ and $D_t = 1+\xi\left\langle\hat{t}\middle|\hat{K}_0^{-1}\middle|\hat{t}\right\rangle$. These factors effectively represent the local compliance changes introduced by the individual MMPs into the system, fundamentally modulating the interaction between the modes. Furthermore, we note that these determinants are intimately linked to the propagators of the MMPs in a continuous system [13].

The mathematical structure shows that, without a non-zero $\left\langle\hat{s}\middle|\hat{K}_0^{-1}\middle|\hat{t}\right\rangle$, the free-energy interaction term vanishes entirely, providing a mathematical counterpart to the idea of perturbation interaction. The matrix element thus serves as the interaction propagator and can therefore be regarded as the decisive variable of this framework.

The perfect symmetry between the MMPs in this expression is a natural consequence of keeping the formalism entirely general. However, while it is mathematically convenient to conceptualise them as local alterations, the matched-mode-perturbations we denote can represent vastly different physical phenomena and are not necessarily localised. We will see this principle in action later, when an MMP is shown to emerge directly from a system-wide constraint and turns out to be a global rather than a local perturbation.

2.6 Periodic Systems

2.6.1 Translational Invariance

In any finite system, the boundary nodes at sites u_0 and u_{N-1} are special cases. They are only coupled to the nodes farther inside the bulk system and thus experience boundary effects, whereas the other nodes are generally less influenced. In particularly small systems, these boundary effects are significant compared to the matched-mode perturbations and must be included. However, this makes calculations much more cumbersome, as translational invariance along the lattice is broken, complicating the calculation of the structure matrix $\hat{K}_0^{-1}$ and the eigenvalues.
We can circumvent these problems while preserving most of the underlying physics by using periodic boundary conditions (PBCs) in the system, as shown in figure 2.5. These connect the first and last node in the system by imposing:

$$u_N = u_0 \tag{2.53}$$

So that the N-th displacement extends beyond the boundary of a bounded system:

$$x_{N-1} \equiv u_0 - u_{N-1} - a \tag{2.54}$$

This construction restores translational invariance in the system: all nodes become equivalent under a discrete lattice translation.

$$n \to n + 1 \mod N \tag{2.55}$$

Boundary effects in the unperturbed system disappear as the physical boundary simply no longer exists. This still allows the formalism to capture the actual interaction effects of interest while removing any finite-size corrections.

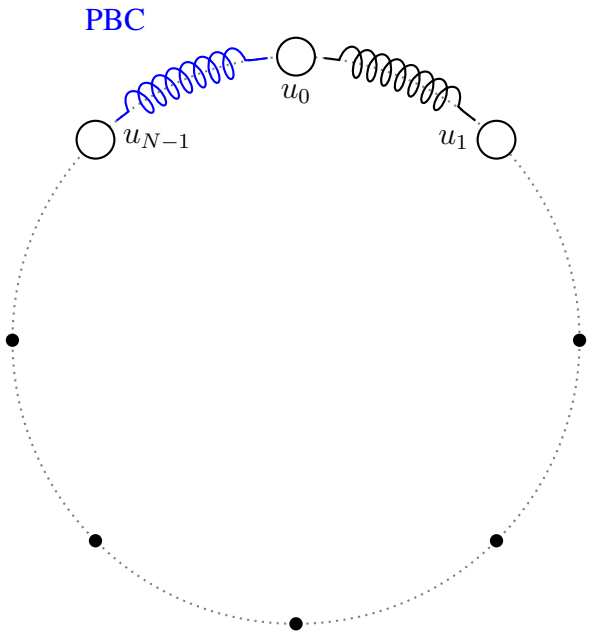

Figure 2.5: Periodic boundary conditions connect the final and first node of the system; this effectively circularises the system to restore translational invariance

To make this symmetry more formal, we introduce the lattice shift operators.

$$\hat{S} \equiv \sum_{n=0}^{N-1} |n-1\rangle\langle n| \tag{2.56}$$

$$\hat{S}^t \equiv \sum_{n=0}^{N-1} |n\rangle\langle n-1| \tag{2.57}$$

Such that they have the following effect on the basis vectors:

$$\hat{S}^k |n\rangle = |n-k \mod (N)\rangle \tag{2.58}$$

$$\hat{S}^{tk} |n\rangle = |n+k \mod (N)\rangle \tag{2.59}$$

As matrices:

$$\hat{S} = \begin{pmatrix} 0 & 0 & \cdots & 0 & 1 \\ 1 & 0 & \cdots & 0 & 0 \\ 0 & 1 & \ddots & \vdots & \vdots \\ \vdots & \ddots & \ddots & 0 & 0 \\ 0 & \cdots & 0 & 1 & 0 \end{pmatrix} \quad \hat{S}^t = \begin{pmatrix} 0 & 1 & 0 & \cdots & 0 \\ 0 & 0 & 1 & \cdots & 0 \\ \vdots & \ddots & \ddots & \ddots & \vdots \\ 0 & \cdots & 0 & 0 & 1 \\ 1 & 0 & \cdots & 0 & 0 \end{pmatrix} \tag{2.60}$$

The corner terms arise due to the periodic boundary conditions applied to the system. We know that these matrices shift each term so that a product of k shift matrices moves the elements of the matrix k times away from the diagonal. The same holds for the periodic terms in the corners of the shift matrices; they fill up the terms k times away from the corners. The set of all shift matrices $\left\{\mathbb{1}, \hat{S}, \hat{S}^2, \ldots, \hat{S}^{N-1}\right\}$, therefore, forms a basis for a more general set of matrices, the circulant matrices [16, 17]. Such that each circulant matrix can be written as a linear combination of the shift operator:

$$\hat{C} = \sum_{k=0}^{N-1} c_k \hat{S}^k \tag{2.61}$$

This gives a new meaning to the translational invariance in the system. Since every node is now physically equivalent, the base stiffness matrix $\hat{K}_0$ must be invariant under a cyclic shift of indices and therefore commute with the shift operators:

$$\left[\hat{K}_0, \hat{S}\right] = 0 \tag{2.62}$$

This consequently implies that $\hat{K}_0$ is a circulant matrix, i.e. it can be written as a linear combination of powers of the shift operator:

$$\hat{K}_0 = \sum_{k=0}^{N-1} c_k \hat{S}^k \tag{2.63}$$

We now briefly review the main properties of circulant matrices, which will play a central role in the analysis that follows. We base this analysis on the standard work of Gray [18].

2.6.2 Circulant Matrices

A symmetric circulant matrix $\hat{C}$ is generally defined by:

$$\hat{C} = \begin{pmatrix} c_0 & c_1 & c_2 & \cdots & c_2 & c_1 \\ c_1 & c_0 & c_1 & \cdots & c_3 & c_2 \\ \vdots & \ddots & \ddots & \ddots & \ddots & \vdots \\ \vdots & \ddots & \ddots & \ddots & \ddots & \vdots \\ c_2 & c_3 & \cdots & \cdots & c_0 & c_1 \\ c_1 & c_2 & \cdots & \cdots & c_1 & c_0 \end{pmatrix} \tag{2.64}$$

With the elements:

$$\hat{C}_{k,j} = c_{(j-k) \mod N} = \hat{C}_{j,k} \tag{2.65}$$

Note that these elements c_{j-k} are exactly the coefficients required in the linear combination of shift matrices to construct a given circulant matrix. It is therefore extremely convenient to express any circulant matrix using this notation. An important feature of circulant matrices is that they diagonalise in Fourier space. We use the convention:

$$|q\rangle = \frac{1}{\sqrt{N}} \sum_{n=0}^{N-1} |n\rangle \, e^{\frac{2\pi i}{N} nq} \tag{2.66}$$

where $q = 0, 1, \ldots, N-1$, these eigenvectors form a complete orthonormal basis.

$$\sum_{q=0}^{N-1} |q\rangle\langle q| = \mathbb{1} \tag{2.67}$$

With the corresponding eigenvalues being discrete Fourier transformations of the shift-coefficients c_k:

$$\tilde{C}_q = \sum_{n=0}^{N-1} c_n e^{-\frac{2\pi i}{N} nq} \tag{2.68}$$

The circulant matrix thus admits the spectral decomposition:

$$\hat{C} = \sum_{q=0}^{N-1} \tilde{C}_q \, |q\rangle\langle q| \tag{2.69}$$

Equivalently, in matrix notation:

$$\hat{C} = \hat{U} \hat{\Psi} \hat{U}^\dagger \tag{2.70}$$

Where $\hat{\Psi} \equiv \mathrm{diag}(\tilde{C}_q)$, and the unitary matrix $\hat{U}$ has the Fourier eigenvectors as its columns.

$$U_{nq} = \frac{1}{\sqrt{N}} e^{-\frac{2\pi i}{N} nq} \tag{2.71}$$

The matrix $\hat{U}$ is universal: it does not depend on the particular circulant matrix $\hat{C}$, but only on the system size N. Different circulant matrices are distinguished solely by their eigenvalues $\tilde{C}_q$.

Theorem 2.4. *If $\hat{C}$ is symmetric, positive definite and circulant, then $\hat{C}^{-1}$ is also symmetric, positive definite and circulant. The inverse matrix satisfies:*

$$\hat{C}^{-1} = \hat{U}\hat{\Psi}^{-1}\hat{U}^{\dagger} \tag{2.72}$$

Proofs for all three statements follow directly from the Fourier diagonalisation of circulant matrices and are given in appendix B.1. The spectral decomposition has another consequence that is especially useful in this work. Any perturbation coupling uniformly to the entire system can be written in terms of the all-ones vector

$$|1_N\rangle \equiv \sum_{n=0}^{N-1} |n\rangle = \begin{pmatrix} 1 \\ 1 \\ \vdots \\ 1 \end{pmatrix}. \tag{2.73}$$

This vector is proportional to the zero-mode Fourier-space eigenvector:

$$|1_N\rangle = \sqrt{N}\,|q=0\rangle\,. \tag{2.74}$$

The special role of $|1_N\rangle$ can be understood from what it measures. If we look specifically at the displacement coordinates applied by this all-ones vector, we get:

$$\langle 1_N|x\rangle = \sum_{n=0}^{N-1} x_n \tag{2.75}$$

It thus captures the global response of the system, whereas other Fourier modes describe more localised variations in the lattice. Translational invariance averages out these localised variations, so they cancel each other out.

$$\langle 1_N|q\rangle = \sum_{n=0}^{N-1} e^{\frac{2\pi i}{N}nq} = 0 \qquad \text{for } q \neq 0 \tag{2.76}$$

Any global perturbation will therefore only couple to this $q = 0$ mode. Consequently, for any circulant matrix $\hat{C}$:

$$\hat{C}\,|1_N\rangle = \tilde{C}_0\,|1_N\rangle \tag{2.77}$$

Where:

$$\tilde{C}_0 = \sum_{n=0}^{N-1} c_n \tag{2.78}$$

The sum of the shift coefficients used to construct this circulant matrix. Comparing with the matrix representation in equation (2.64), we see that this is exactly the row sum of $\hat{C}$. This leads us to a nice corollary.

Corollary 2.4.1. *Let $\hat{C}$ be an invertible circulant matrix. Then the row sum of $\hat{C}^{-1}$ is the inverse of the row sum of $\hat{C}$. Equivalently, using the all-ones vector notation.*

$$\frac{\langle 1_N|\hat{C}^{-1}|1_N\rangle}{N} = \frac{N}{\langle 1_N|\hat{C}|1_N\rangle} \tag{2.79}$$

Proof. Since $|1_N\rangle$ is proportional to the zero-mode Fourier eigenvector, it is an eigenvector of any circulant matrix:

$$\hat{C}\,|1_N\rangle = \tilde{C}_0\,|1_N\rangle \tag{2.80}$$

The corresponding eigenvalue is:

$$\tilde{C}_0 = \sum_{n=0}^{N-1} c_n \tag{2.81}$$

which is the row sum of $\hat{C}$. The eigenvalues of the inverse matrix $\hat{C}^{-1}$ are given by $1/\tilde{C}_q$, also in Fourier space.

$$\hat{C}^{-1}\,|1_N\rangle = \frac{1}{\tilde{C}_0}\,|1_N\rangle \tag{2.82}$$

Therefore, the row sum of $\hat{C}^{-1}$ is $1/\tilde{C}_0$, the inverse of the row sum of $\hat{C}$. Finally, using $\langle 1_N|1_N\rangle = N$, we get:

$$\langle 1_N|\hat{C}^{-1}|1_N\rangle = \frac{N}{\tilde{C}_0} \tag{2.83}$$

$$\langle 1_N|\hat{C}|1_N\rangle = N\tilde{C}_0 \tag{2.84}$$

Such that:

$$\frac{\langle 1_N|\hat{C}^{-1}|1_N\rangle}{N} = \frac{N}{\langle 1_N|\hat{C}|1_N\rangle} \tag{2.85}$$

□

An alternative proof based on algebraic manipulation of the indices is presented in section B.1.

3 Mismatches and Strain

In the previous chapter, we developed the MMP formalism for the general introduction to matched-mode perturbations. But we have not yet specified what these MMPs might be or how we can relate them to the physical alterations we observe in DNA or in strain-based sensors in general. We develop their intuition by introducing them to the decoupled chain before applying them to more general models later.

3.1 Mismatches as Localised Perturbations

As described in the introduction, hybridisation-based DNA probes are designed to match circulating tumour DNA, particularly single-nucleotide variants. This produces single-base-pair mismatches when the probes bind to the excess wild-type DNA background, resulting in a free-energy penalty. The structural defect caused by these mismatches is highly localised [19, 20] even if the elastic response in the system can yield long-distance interactions.
To describe this process, we turn to the formalism of the previous chapter and introduce the mismatch as a matched-mode perturbation. To do this, we first consider these local perturbations in the decoupled chain. We then generalise them as local MMPs in the formalism.
We propose two local alterations to a single spring in the decoupled chain model.

- A local perturbation in stiffness: In principle, this can be either a stiffening or a softening of the local MM site. We expect this to be a weakening in the local stability of the helix and therefore model it as a softening of the system.

$$K \to K + \delta K \tag{3.1}$$

- A local perturbation in rest length: The structural distortion of the local equilibrium geometry caused by the presence of the MM is represented by this parameter.

$$a \to a + \delta a \tag{3.2}$$

In the decoupled chain, the effect of these perturbations is intuitive. One spring in the system is replaced by another spring with an altered coupling constant and rest length.

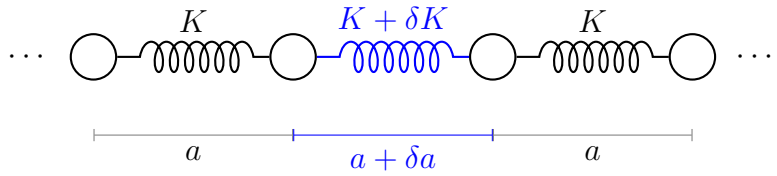

Figure 3.1: A mismatch in the decoupled chain is modelled by replacing a spring in the system with another with a perturbed coupling constant and perturbed rest length.

This is reflected in the perturbed Hamiltonian of the system as well:

$$\mathcal{H} = \mathcal{H}_0 - \frac{K}{2}(u_{n+1} - u_n - a)^2 + \frac{K+\delta K}{2}(u_{n+1} - u_n - (a+\delta a))^2 \tag{3.3}$$

We immediately recognise the displacement variables again.

$$\begin{aligned}\mathcal{H} &= \mathcal{H}_0 - \frac{K}{2}x_n^2 + \frac{K+\delta K}{2}(x_n - \delta a)^2 \\ &= \mathcal{H}_0 + \frac{\delta K}{2}x_n^2 - (K+\delta K)x_n\delta a + \frac{K+\delta K}{2}\delta a^2\end{aligned} \tag{3.4}$$

To generalise from the decoupled chain to a general model, we now shift to the vector notation.

$$\mathcal{H} = \frac{1}{2}\langle x|\Big(\hat{K}_0 + \delta K\,|n\rangle\langle n|\Big)|x\rangle - (K+\delta K)\delta a\,\langle n|x\rangle + \frac{K+\delta K}{2}\delta a^2 \tag{3.5}$$

Indeed, we see the mismatch return as a matched-mode perturbation, allowing us to introduce the general formalism we used before. The quadratic part is given through comparison with equation (2.35):

$$\hat{K}_0 \to \hat{K} = \hat{K}_0 + \delta K\,|n\rangle\langle n| \tag{3.6}$$

Where $|n\rangle$ denotes a localised mode acting on the n-th displacement in the system. The local softening of the system thus appears as a rank-one update to the system's stiffness matrix. It modifies the self-coupling diagonal element as an entirely local effect. Meanwhile, the force term returns linearly in the Hamiltonian such that:

$$f_m\,|n\rangle = -(K+\delta K)\delta a\,|n\rangle \tag{3.7}$$

This immediately allows us to write down the free energy contribution of a mismatch in the system using equation (2.34). Since we have both a quadratic and a linear perturbation, the result includes both an energetic and an entropic component.

$$\Delta\mathcal{F}_m = \frac{1}{2}\log\Big(1 + \delta K\,\langle n|\hat{K}_0^{-1}|n\rangle\Big) - \frac{(K+\delta K)^2\delta a^2}{2}\frac{\langle n|\hat{K}_0^{-1}|n\rangle}{1+\delta K\,\langle n|\hat{K}_0^{-1}|n\rangle} + \frac{K+\delta K}{2}\delta a^2 \tag{3.8}$$

This allows for a further simplification by combining the two energetic terms:

$$\begin{aligned}\Delta\mathcal{E}_m &= -\frac{(K+\delta K)^2\delta a^2}{2}\frac{\langle n|\hat{K}_0^{-1}|n\rangle}{1+\delta K\,\langle n|\hat{K}_0^{-1}|n\rangle} + \frac{K+\delta K}{2}\delta a^2 \\ &= \frac{K+\delta K}{2(1+\delta K\,\langle n|\hat{K}_0^{-1}|n\rangle)}\delta a^2\Big[-(K+\delta K)\,\langle n|\hat{K}_0^{-1}|n\rangle + 1 + \delta K\,\langle n|\hat{K}_0^{-1}|n\rangle\Big] \\ &= \frac{K+\delta K}{2}\delta a^2\left(\frac{1 - K\,\langle n|\hat{K}_0^{-1}|n\rangle}{1+\delta K\,\langle n|\hat{K}_0^{-1}|n\rangle}\right)\end{aligned} \tag{3.9}$$

We note that for the decoupled chain, the energetic contribution to the free energy cancels exactly because the structure matrix $\hat{K}_0^{-1}$ is diagonal with the elements of the inverse base stiffness.

$$\hat{K}_0^{-1} = \mathrm{diag}\left(\frac{1}{K}\right) \qquad \text{(decoupled chain only)} \tag{3.10}$$

Such that:

$$1 - K \langle n|\hat{K}_0^{-1}|n\rangle = 0 \qquad \text{(decoupled chain only)} \tag{3.11}$$

So that the bracketed energetic term vanishes, the absence of longer-range interactions therefore allows the rest-length perturbation to be fully relaxed, eliminating the energetic contribution associated with the mismatch geometry.
For the general model, the free energy penalty by a mismatch is then given by:

$$\Delta\mathcal{F}_m = \frac{1}{2}\log\Big(1 + \delta K \langle n|\hat{K}_0^{-1}|n\rangle\Big) + \frac{K+\delta K}{2}\delta a^2 \left(\frac{1 - K\langle n|\hat{K}_0^{-1}|n\rangle}{1+\delta K\langle n|\hat{K}_0^{-1}|n\rangle}\right) \tag{3.12}$$

The effect of the mismatch depends on a single matrix element of the base system's structure matrix: the n-th diagonal element. To evaluate the element, we make use of the completeness of the system's Fourier basis (2.67) and expand in terms of the momentum eigenvectors.

$$\begin{aligned}
\langle n|\hat{K}_0^{-1}|n\rangle &= \sum_q \sum_{q'} \langle n|q\rangle \ \langle q|\hat{K}_0^{-1}|q'\rangle \ \langle q'|n\rangle \\
&= \sum_q \sum_{q'} \frac{1}{\tilde{K}_q} \langle n|q\rangle \ \langle q|q'\rangle \ \langle q'|n\rangle \\
&= \sum_q \frac{|\langle n|q\rangle|^2}{\tilde{K}_q}
\end{aligned} \tag{3.13}$$

Expanding the eigenvectors as the discrete Fourier transform of the real space unit vectors, we get:

$$\langle n|q\rangle = \frac{1}{\sqrt{N}} \sum_{m=0}^{N-1} e^{qm\frac{2\pi i}{N}} \ \langle n|m\rangle = \frac{1}{\sqrt{N}} e^{\frac{2\pi i}{N}qn} \tag{3.14}$$

Such that any phase dependence vanishes in the local term, eliminating any dependence on the position of the site.

$$\langle n|\hat{K}_0^{-1}|n\rangle = \sum_{q=0}^{N-1} \frac{1}{N\tilde{K}_q} \tag{3.15}$$

The absence of site dependence has a deeper origin than the explicit cancellation of the Fourier phases. It follows from the translational symmetry of the base system. Since $\hat{K}_0$ is circulant, it commutes with the lattice shift operator $\hat{S}$; therefore, its inverse has the same symmetry.

$$\left[\hat{K}_0^{-1}, \hat{S}\right] = 0 \tag{3.16}$$

This means that translating the perturbation from site n to site $n+1$ cannot change this response, because the underlying system is unchanged under such translations. Explicitly,

$$\langle n+1|\hat{K}_0^{-1}|n+1\rangle \ \langle n|\hat{S}^t\hat{K}_0^{-1}\hat{S}|n\rangle = \ \langle n|\hat{K}_0^{-1}|n\rangle \, . \tag{3.17}$$

All diagonal elements of the structure matrix $\hat{K}_0^{-1}$ are therefore identical. Equation (3.15) is a manifestation of this symmetry as all modes are delocalised over the entire system and weigh equally on all sites.

3.2 Strain as a Global Perturbation

To capture the global strain imposed on the P strand in OWL sensors, we must translate this effect into a chain model. We have already seen such global coupling in section 2.6. Indeed, this means that such couplings will have the special property of being described by the $|1_N\rangle = \sqrt{N}\,|q=0\rangle$ eigenvector of the system. This simplifies calculations considerably. Intuitively, it is straightforward to impose a global strain on a chain system. We physically couple the first and last nodes in the system with a new spring spanning the full chain length. We do so in such a way that the system's equilibrium length:

$$L_0 = Na \tag{3.18}$$

does not match the spring's equilibrium length by an extra extension or shortening δL.

$$L = L_0 + \delta L \tag{3.19}$$

For reasons we discuss later, we expect the stiffness K' of this closing spring to be an order of magnitude greater than that of the couplings in the main chain.

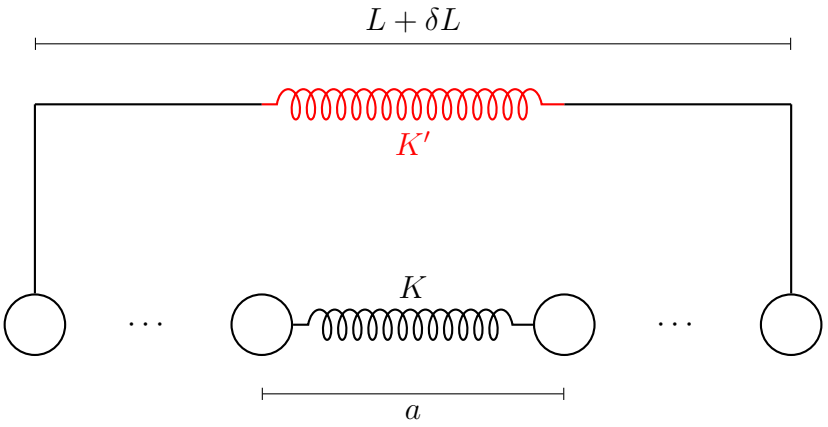

Figure 3.2: Global strain is introduced by adding a closing spring with equilibrium length $Na + \delta L$. This spring couples to the entire system, introducing a uniform shift across all bonds.

It must be noted that this closing spring works differently from the periodic boundary conditions we introduced before, as is evident from figures 2.5 and 3.2. The PBCs close the system onto itself, enforcing translational invariance without imposing any other constraint. The closing spring, on the contrary, does exert an influence over the entire system as we as will be evident in the Hamiltonian.
We introduce the perturbation in the same way as we did for the mismatch: we apply the closing spring to the decoupled chain, then generalise. The Hamiltonian for the closing chain in the decoupled chain is given by:

$$\mathcal{H} = \frac{K}{2}\sum_{n=0}^{N-1}(u_{n+1} - u_n - a)^2 + \frac{K'}{2}(u_N - u_0 - (Na + \delta L))^2 \tag{3.20}$$

Switching to displacement coordinates, we find:

$$u_N = u_0 + \sum_{n=0}^{N-1} x_n + Na \tag{3.21}$$

So that the Hamiltonian in displacement coordinates is given by:

$$\begin{aligned}\mathcal{H} &= \frac{K}{2}\sum_{n=0}^{N-1} x_n^2 + \frac{K'}{2}\left(\sum_{n=0}^{N-1} x_n - \delta L\right)^2 \\ &= \frac{K}{2}\sum_{n=0}^{N-1} x_n^2 + \frac{K'}{2}\left[\left(\sum_{n=0}^{N-1} x_n\right)^2 - 2\delta L\sum_{n=0}^{N-1} x_n + \delta L^2\right]\end{aligned} \tag{3.22}$$

As before, the base Hamiltonian is still evident in the first term, and we see quadratic and linear terms appear as expected for a matched-mode perturbation. The quadratic term includes both diagonal and correlation terms.

$$\left(\sum_{n=0}^{N-1} x_n\right)^2 = \sum_{n=0}^{N-1} x_n^2 + \sum_{n=0}^{N-1}\sum_{m\neq n}^{N-1} x_n x_m \tag{3.23}$$

In vector notation, this becomes:

$$\begin{aligned}\left(\sum_{n=0}^{N-1} x_n\right)^2 &= \langle x|x\rangle + \sum_{n=0}^{N-1}\sum_{m\neq n}^{N-1}\langle x|n\rangle\langle m|x\rangle \\ &= \langle x|\left(\sum_{n=0}^{N-1}|n\rangle\langle n| + \sum_{n=0}^{N-1}\sum_{m\neq n}^{N-1}|n\rangle\langle m|\right)|x\rangle\end{aligned} \tag{3.24}$$

Such that the new Hamiltonian in vector notation is given by:

$$\mathcal{H} = \mathcal{H}_0 + \frac{K'}{2}\langle x|\left[\sum_{n=0}^{N-1}|n\rangle\langle n| + \sum_{n=0}^{N-1}\sum_{m\neq n}^{N-1}|n\rangle\langle m|\right]|x\rangle + K'\delta L\sum_{n=0}^{N-1}\langle n|x\rangle + \frac{K'}{2}\delta L^2 \tag{3.25}$$

The perturbation takes the form of a matched-mode perturbation; to emphasise this point, we write down the rank-one update in matrix notation.

$$\sum_{n=0}^{N-1}|n\rangle\langle n| + \sum_{n=0}^{N-1}\sum_{m\neq n}^{N-1}|n\rangle\langle m| \equiv \begin{pmatrix} 1 & 1 & 1 & \cdots & 1 \\ 1 & 1 & 1 & \cdots & 1 \\ 1 & 1 & 1 & \cdots & 1 \\ \vdots & \vdots & \vdots & \ddots & \vdots \\ 1 & 1 & 1 & \cdots & 1 \end{pmatrix} \tag{3.26}$$

Which is the outer product $|1_N\rangle\langle 1_N|$ of the all-ones vector. Using equation (2.73), we see that the linear term can be written using $|1_N\rangle$ too.

$$\mathcal{H} = \mathcal{H}_0 + \frac{K'}{2}\langle x|1_N\rangle\langle 1_N|x\rangle - K'\delta L\langle 1_N|x\rangle + \frac{K'}{2}\delta L^2 \tag{3.27}$$

This allows us to identify the MMP components by comparing to equation (2.35), the quadratic update is given by:

$$\hat{K}_0 \to \hat{K} = \hat{K}_0 + K'|1_N\rangle\langle 1_N| \tag{3.28}$$

While the force term is:

$$f_g \left|1_N\right\rangle = -K'\delta L \left|1_N\right\rangle \tag{3.29}$$

This indeed shows that we have found the correct matched-mode perturbation to describe a frustration applied to the entire system. The formalism we developed earlier will now do the heavy lifting again to find the free energy penalty.

$$\Delta\mathcal{F}_g = \frac{1}{2}\log\Big(1 + K'\left\langle 1_N|\hat{K}_0^{-1}|1_N\right\rangle\Big) - \frac{(K'\delta L)^2}{2}\frac{\left\langle 1_N|\hat{K}_0^{-1}|1_N\right\rangle}{1 + K'\left\langle 1_N|\hat{K}_0^{-1}|1_N\right\rangle} + \frac{K'}{2}\delta L^2 \tag{3.30}$$

Again, we can simplify this by combining the energetic terms:

$$\begin{aligned}
\Delta\mathcal{E}_g &= -\frac{(K'\delta L)^2}{2}\frac{\left\langle 1_N|\hat{K}_0^{-1}|1_N\right\rangle}{1 + K'\left\langle 1_N|\hat{K}_0^{-1}|1_N\right\rangle} + \frac{K'}{2}\delta L^2 \\
&= \frac{K'}{2(1 + K'\left\langle 1_N|\hat{K}_0^{-1}|1_N\right\rangle)}\delta L^2\Big(-K'\left\langle 1_N|\hat{K}_0^{-1}|1_N\right\rangle + 1 + K'\left\langle 1_N|\hat{K}_0^{-1}|1_N\right\rangle\Big) \\
&= \frac{K'}{2(1 + K'\left\langle 1_N|\hat{K}_0^{-1}|1_N\right\rangle)}\delta L^2
\end{aligned} \tag{3.31}$$

The free energy penalty then yields:

$$\Delta\mathcal{F}_g = \frac{1}{2}\log\Big(1 + K'\left\langle 1_N|\hat{K}_0^{-1}|1_N\right\rangle\Big) + \frac{K'}{2(1 + K'\left\langle 1_N|\hat{K}_0^{-1}|1_N\right\rangle)}\delta L^2 \tag{3.32}$$

This is a nice result, as we see that the determinant of the rank-one update applied by the MMP appears twice: once in the logarithm and once as a normalisation of the energetic term. The simplest closing spring has the same quadratic form:

$$\mathcal{E}_{\text{Closing spring}} = \frac{K'}{2}\delta L^2 \tag{3.33}$$

The internal structure of the chain now distributes this energy over the chain, effectively altering the effective stiffness of the closing spring by the MMP determinant. This is the same suppression seen in the entropic part. The result closely resembles the global response observed in the general free-energy interaction term (2.52), in which both the rank-one and rank-two determinants appear. This further supports the interpretation of the determinant factor as a measure of the system's effective stiffness response.

The advantage of introducing periodic boundary conditions into the system becomes clear here, as the $|1_N\rangle$ vector is an eigenvector of the stiffness matrix $\hat{K}_0$ and consequently of its inverse $\hat{K}_0^{-1}$ as covered in section 2.6. It concerns the $q = 0$ eigenvalue in Fourier space, which is exactly the global mode of the system.

$$\hat{K}_0^{-1}\left|1_N\right\rangle = \frac{1}{\tilde{K}_0}\left|1_N\right\rangle \tag{3.34}$$

The norm of $|1_N\rangle$ is given by:

$$\left\langle 1_N|1_N\right\rangle = \sum_{n=0}^{N-1}\sum_{m=0}^{N-1}\langle n|m\rangle = N \tag{3.35}$$

Such that the free energy penalty from the global constraint in a circulant system depends both on the size of the system N and the ratio of the stiffness of the closing spring and the global stiffness.

$$\Delta\mathcal{F}_g = \frac{1}{2}\log\left(1 + N\frac{K'}{\tilde{K}_0}\right) + \frac{K'}{2\left(1 + N\frac{K'}{\tilde{K}_0}\right)}\delta L^2 \tag{3.36}$$

3.2.1 Rigid limit

As will become evident later, it is worth it to consider the limit of an infinitely strong closing spring.

$$K' \to \infty \tag{3.37}$$

The closing spring now no longer acts as a spring; instead, it fixes the end-to-end extension of the system to $L + \delta L$.

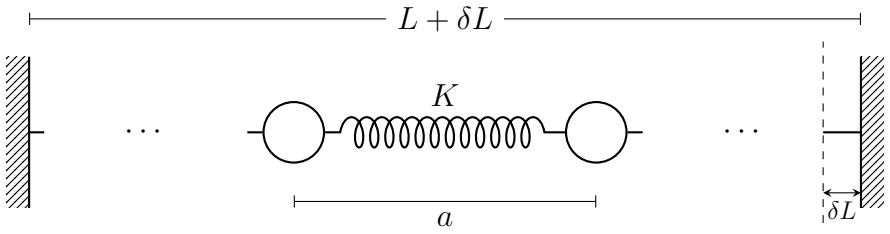

Figure 3.3: The rigid limit of the system fixes the ends of the system while applying strain by extending the system by δL. This places a holonomic constraint on the system, which requires extra consideration.

The energetic response of the system reduces simply to:

$$\Delta\mathcal{E}_g = \frac{\tilde{K}_0}{2N}\delta L^2 \tag{3.38}$$

But the entropic response in equation (3.36) seems to diverge when naively applying the rigid limit $K' \to \infty$. Because the formalism relies on Hamiltonian mechanics, we must carefully consider the rigid limit as a holonomic constraint [21]. We consider this again for the decoupled chain:

$$\sum_{n=0}^{N-1} x_n = \langle 1_N | x \rangle = \delta L \tag{3.39}$$

This alters the partition sum, as the Gaussian generated by this constraint approaches a Dirac-δ function as $K' \to \infty$. This eliminates a degree of freedom when integrating over phase space, defining the partition sum.

$$\begin{aligned} Z &= \int d^N\mathbf{x} \exp(-\mathcal{H}(x_0, \ldots, x_{N-1}))\delta(\langle 1_N | x \rangle - \delta L) \\ &= \int d^{N-1}\mathbf{y} \exp(-\mathcal{H}_{\text{constrained}}(\mathbf{y})) \end{aligned} \tag{3.40}$$

Using the Fourier basis of the circulant stiffness matrix, it becomes clear that the $|q = 0\rangle$ mode is constrained. This removes the zero mode from the partition sum, leaving the

system diagonal in the remaining $N-1$ unconstrained modes. These describe internal fluctuations within the chain and, consequently, do not influence the overall deformation of the system. For the details of this calculation, we refer the reader to appendix B.3. We note the finite result.

$$\Delta\mathcal{F}_r = -\frac{1}{2}\log\left(\tilde{K}_0\right) + \frac{\tilde{K}_0}{2N}\delta L^2 \tag{3.41}$$

The system's zero mode is naturally linked to its collective deformation imposed by the global constraint. Over sufficiently long length scales, the effective stiffness approaches the eigenvalue $\tilde{K}_0$, as shown by Skoruppa *et al.* [22] in a circulant model with next-nearest-neighbour couplings.

3.3 The Strain-Mismatch Interaction

As we have established, both strain and mismatch in strain-based sensors can be described using the matched-mode perturbation formalism. Thanks to the formalism developed in chapter 2, we can therefore conclude that, given a suitable choice of base, i.e. the stiffness matrix $\hat{K}_0$, an interaction between the two perturbations exists. We recall the definition of the interaction free energy:

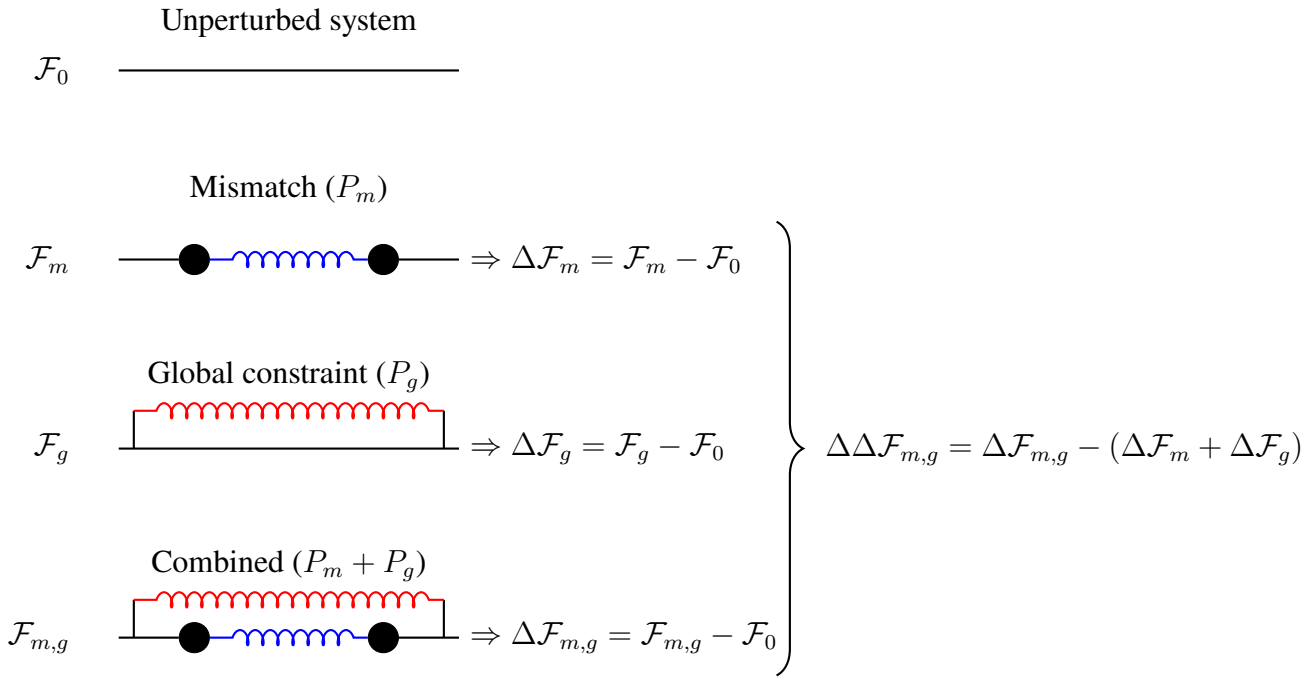

Figure 3.4: Definition of the free-energy interaction term for the strain-mismatch interaction.

The MMP formalism compares the perturbations separately before combining them using a rank-two update. Using the notation of equation (2.38), the rank-two update is given by:

$$\hat{K}_0 \to \hat{K} = \hat{K}_0 + \delta K\,|n\rangle\langle n| + K'\,|1_N\rangle\langle 1_N| \tag{3.42}$$

The MMP formalism now provides us with the new structure matrix of the doubly perturbed system (2.43):

$$\begin{aligned}\hat{K}^{-1} = \hat{K}_0^{-1} - \frac{1}{D}\Big[&K'\Big(1+\delta K\,\langle n|\hat{K}_0^{-1}|n\rangle\Big)\hat{K}_0^{-1}\,|1_N\rangle\langle 1_N|\,\hat{K}_0^{-1} \\ &+\delta K\Big(1+K'\,\langle 1_N|\hat{K}_0^{-1}|1_N\rangle\Big)\hat{K}_0^{-1}\,|n\rangle\langle n|\,\hat{K}_0^{-1} \\ &-2K'\delta K\Big(\hat{K}_0^{-1}\,|n\rangle\langle 1_N|\,\hat{K}_0^{-1}\Big)\Big]\end{aligned} \tag{3.43}$$

The last term picks up a factor of 2 because the structure matrix is symmetric. The determinant of the 2×2 update matrix is an important quantity, as it appears in both the entropic and energetic contributions.

$$D = \Big(1+\delta K\,\langle n|\hat{K}_0^{-1}|n\rangle\Big)\Big(1+K'\,\langle 1_N|\hat{K}_0^{-1}|1_N\rangle\Big) - K'\delta K\,\langle n|\hat{K}_0^{-1}|1_N\rangle^2 \tag{3.44}$$

We also see the rank-one update matrices appear.

$$D_m = 1+\delta K\,\langle n|\hat{K}_0^{-1}|n\rangle \tag{3.45}$$

$$D_g = 1+K'\,\langle 1_N|\hat{K}_0^{-1}|1_N\rangle \tag{3.46}$$

3.3.1 Stability

Before analysing the explicit form of the interaction free energy, several important properties of the system follow straight from the requirement of mechanical stability. These can be used to make qualitative remarks about the system independent of the base system, i.e. choice of $\hat{K}_0$.

The interaction free energy in the system is only defined if all systems we compare are stable. This implies that the corresponding stiffness matrices are positive definite and that all determinant factors appearing in the formalism are strictly positive. We start by demanding a positive-definite base system.

$$\det\Big(\hat{K}_0\Big) > 0 \qquad \text{and } \tilde{K}_q > 0 \quad \forall q \tag{3.47}$$

This consequently means that the matrix elements we construct are all positive, since they depend only on the system's eigenvalues.

$$\langle n|\hat{K}_0^{-1}|n\rangle = \sum_{q=0}^{N-1}\frac{1}{N\tilde{K}_q} > 0 \tag{3.48}$$

$$\langle 1_N|\hat{K}_0^{-1}|1_N\rangle = N\,\langle n|\hat{K}_0^{-1}|1_N\rangle = \frac{N}{\tilde{K}_0} > 0 \tag{3.49}$$

The determinants of the perturbed systems consist of the determinant of the base system multiplied by their perturbing determinants; this means all these must also be positive.

$$D > 0 \tag{3.50}$$

$$D_m > 0 \tag{3.51}$$

$$D_g > 0 \tag{3.52}$$

The main restriction from this requirement arises from the introduction of the mismatch, as mismatches generally soften the system ($\delta K < 0$), restricting the choice of circulant $\hat{K}_0$ in the later sections.

3.3.2 Entropic contribution

Since we have the determinant of the system, we can write down the entropic interaction term using equation (2.47):

$$\Delta\Delta\mathcal{S} = -\frac{1}{2}\log\left(1 - \frac{K'\delta K \langle n|\hat{K}_0^{-1}|1_N\rangle^2}{(1+\delta K\langle n|\hat{K}_0^{-1}|n\rangle)(1+K'\langle 1_N|\hat{K}_0^{-1}|1_N\rangle)}\right) \tag{3.53}$$

A first qualitative look at the most general system will consist of determining the signs of the contributions. This is particularly easy to do for the entropic interaction term, since the terms in the denominator are the determinants of the mismatch and global perturbation, respectively, and inequality (3.49), its sign only depends on the relative sign of K' and δK.

$$\text{sign}(\Delta\Delta\mathcal{S}) = \text{sign}(K'\delta K) \tag{3.54}$$

$\Delta\Delta\mathcal{S}$	$\delta K > 0$	$\delta K < 0$
$K' > 0$	$+$	$-$
$K' < 0$	$-$	$+$

Table 3.1: Sign structure of the entropic interaction term $\Delta\Delta S$.

As the free energy increases with decreasing entropy, a positive relative sign indicates entropic stabilisation of the system. In contrast, a negative relative sign destabilises the system. We expect a mismatch in the system to be softening and therefore a negative δK. While a positive K' seems like the only physically relevant case for the global constraint if it is to be modelled by a closing spring. We thus expect strain-based sensors to be further entropically destabilised by the interaction of the mismatch and the global constraint.

3.3.3 Energetic interaction term

For the energetic interaction term, we also require the force terms from the MMPs.

$$\sqrt{\delta K}\,|n\rangle \leftrightarrow (K+\delta K)\delta a\,|n\rangle \tag{3.55}$$

$$\sqrt{K'}\,|1_N\rangle \leftrightarrow K'\delta L\,|1_N\rangle \tag{3.56}$$

Equation (2.51) now gives the energetic interaction term:

$$\begin{aligned}\Delta\Delta\mathcal{E} = \frac{1}{D}\Bigg[&\frac{K'\delta L^2}{2}\frac{K'\delta K\langle n|\hat{K}_0^{-1}|1_N\rangle^2}{1+K'\langle 1_N|\hat{K}_0^{-1}|1_N\rangle} + \frac{(K+\delta K)^2\delta a^2}{2}\frac{K'\langle n|\hat{K}_0^{-1}|1_N\rangle^2}{1+\delta K\langle n|\hat{K}_0^{-1}|n\rangle} \\ &- K'\delta L(K+\delta K)\delta a\langle n|\hat{K}_0^{-1}|1_N\rangle\Bigg]\end{aligned} \tag{3.57}$$

As before, we see all the determinants appear as normalising factors for the relevant perturbations. The relative strength of each term consequently depends on how close each determinant is to zero. We expect a relatively large global update determinant due to its size dependence, while the normalisation of the mismatch $\mathcal{O}(\delta a^2)$ term will generally be between zero and one, owing to the relative softening of the local stiffness ($\delta K < 0$). This

leads to a significant amplification of the mismatch-related term compared with the impact of the global constraint.
All terms are multiplied by the matrix element $\langle n|\hat{K}_0^{-1}|1_N\rangle$, so the interaction term is relevant only if this is sufficiently large. Using equation (3.49), we know this is exactly the inverse of the system's zero-stiffness mode $\tilde{K}_0^{-1}$. Physically, this means that local mismatches interact most strongly with the global constraint when the underlying system is easily deformed over long length scales, as we would intuitively expect, because it allows each node to undergo a larger displacement. Because the local perturbation is independent of its lattice location and the translational invariance of the global constraint, the coupling between the two is larger.

3.3.4 A Qualitative Consideration

For a circulant system, we can already work out some of the matrix elements, but we refrain from doing so because it does not add any extra clarity at this point. We do, however, use:

$$\langle 1_N|\hat{K}_0^{-1}|1_N\rangle = N\,\langle n|\hat{K}_0^{-1}|1_N\rangle \tag{3.58}$$

This makes the size dependence of the global determinant terms more explicit. Combining equations (3.53) and (3.57), we recover the full free-energy interaction.

$$\begin{aligned}\Delta\Delta\mathcal{F} =& \frac{1}{2}\log\left(1 - \frac{K'\delta K\,\langle n|\hat{K}_0^{-1}|1_N\rangle^2}{(1+\delta K\,\langle n|\hat{K}_0^{-1}|n\rangle)(1+K'N\,\langle n|\hat{K}_0^{-1}|1_N\rangle)}\right)\\ &+\frac{1}{D}\Bigg[\frac{K'\delta L^2}{2}\frac{K'\delta K\,\langle n|\hat{K}_0^{-1}|1_N\rangle^2}{1+NK'\,\langle n|\hat{K}_0^{-1}|1_N\rangle} + \frac{(K+\delta K)^2\delta a^2}{2}\frac{K'\,\langle n|\hat{K}_0^{-1}|1_N\rangle^2}{1+\delta K\,\langle n|\hat{K}_0^{-1}|n\rangle}\\ &\quad - K'\delta L(K+\delta K)\delta a\,\langle n|\hat{K}_0^{-1}|1_N\rangle\Bigg]\end{aligned} \tag{3.59}$$

In principle, the mismatch parameters δK and δa are fixed by the particular kind of mismatch present in the system. While the length $L = Na$ and inherent structure of the system, i.e. the eigenvalues of the system, are model dependent. This leaves us with two parameters associated with the geometry of the given strain-based sensor: the global stiffness K' and the global deformation δL. Explicitly solving for K' does not reveal much qualitative structure, so instead we focus on δL. Keeping the other parameters fixed, the free-energy interaction term is a parabola as a function of the imposed global deformation.

$$\Delta\Delta\mathcal{F}(\delta L) = A\delta L^2 + B\delta L + C \tag{3.60}$$

Where:

$$A = \frac{1}{D}\frac{K'}{2}\frac{K'\delta K\,\langle n|\hat{K}_0^{-1}|1_N\rangle^2}{1+NK'\,\langle n|\hat{K}_0^{-1}|1_N\rangle} = \frac{K'}{2}\frac{K'\delta K\,\langle n|\hat{K}_0^{-1}|1_N\rangle^2}{DD_g} \tag{3.61}$$

$$B = -\frac{1}{D}K'(K+\delta K)\delta a\,\langle n|\hat{K}_0^{-1}|1_N\rangle = -\frac{K'f_m}{D}\,\langle n|\hat{K}_0^{-1}|1_N\rangle \tag{3.62}$$

$$C = \frac{1}{D}\frac{(K+\delta K)^2\delta a^2}{2}\frac{K'\,\langle n|\hat{K}_0^{-1}|1_N\rangle^2}{1+\delta K\,\langle n|\hat{K}_0^{-1}|n\rangle} - \Delta\Delta\mathcal{S} = \frac{K'f_m^2}{2DD_m}\,\langle n|\hat{K}_0^{-1}|1_N\rangle^2 - \Delta\Delta\mathcal{S} \tag{3.63}$$

The constant term C includes both an energetic term that depends only on the mismatch structure and the entropic contribution. The existence of this term means that, even without additional global deformation, an interaction between the mismatch and the global closing structure is present.

Extremum

First, it is useful to find the parabola's extremum, as it directly influences the optimal sensor performance. The sign of A determines whether the parabola is concave or convex. We know that for stability in the system, all determinants are positive, so that this sign is only dependent on the sign of δK.

- $\delta K > 0 \Rightarrow \Delta\Delta\mathcal{F}(\delta L)$ is a convex parabola. This means that for large δL the interaction term will always be positive and thus destabilising. A stabilising regime may exist in the intermediate deformation range.
- $\delta K = 0 \Rightarrow \Delta\Delta\mathcal{F}(\delta L)$ is a purely geometric linear function of the global deformation interacting with the local structural deformation δa.
- $\delta K < 0 \Rightarrow \Delta\Delta\mathcal{F}(\delta L)$ is a concave parabola. This means that for large δL the interaction term will always be negative and thus stabilising. A destabilising regime for an intermediate deformation may exist, enabling optimal sensor performance.

The extremum is given by:

$$\begin{aligned}\delta L^* &= \frac{(K_0 + \delta K)}{\delta K}\delta a\left(\frac{1}{K' \langle n|\hat{K}_0^{-1}|1_N\rangle} + N\right) \\ &= \frac{(K_0 + \delta K)}{\delta K}\delta a\left(\frac{\tilde{K}_0}{K'} + N\right)\end{aligned} \tag{3.64}$$

The sign of this expression is non-trivial and depends on the signs of δK, δa. Since a physical closing spring requires $K' > 0$, this means that the factor in the parentheses is strictly positive. This leaves the sign of δL^* dependent on the relative signs of δK and δa.

δL^*	$\delta K > 0$	$\delta K < 0$
$\delta a > 0$	+	-
$\delta a < 0$	-	+

Table 3.2: Sign table for δL^* if $K' > 0$

This means that a softening mismatch interacts optimally with the system when the global and local deformation have opposite signs. This is what we would intuitively expect, since the forces arising from these effects counteract each other in that case, increasing the energetic cost. The optimal deformation scales linearly with the system size N, reflecting the greater deformation required to create global frustration in larger systems.
We now consider the extremum value itself, for this we have $\delta L = \delta L^*$ so that:

$$\Delta\Delta\mathcal{F}(\delta L^*) = \Delta\Delta\mathcal{F}^* = A\left(-\frac{B}{2A}\right)^2 + B\left(-\frac{B}{2A}\right) + C = C - \frac{B^2}{4A}$$

Which we now fill in:

$$\begin{aligned}\Delta\Delta\mathcal{F}^* &= -\frac{(K'f_m)^2\left\langle n|\hat{K}_0^{-1}|1_N\right\rangle^2}{D^2}\frac{DD_t}{K'^2\delta K\left\langle n|\hat{K}_0^{-1}|1_N\right\rangle^2} + \frac{K'f_m^2}{2DD_m} - \Delta\Delta\mathcal{S} \\ &= \frac{f_m^2}{2D}\left(\frac{-D_tD_m + K'\delta K\left\langle n|\hat{K}_0^{-1}|1_N\right\rangle^2}{\delta KD_m}\right) - \Delta\Delta\mathcal{S}\end{aligned}$$

But the big factor in the numerator is just the determinant again, we also fill in the entropic-interaction term again:

$$\begin{aligned}\Delta\Delta\mathcal{F}^* =& \frac{1}{2}\log\left(1 - \frac{K'\delta K\left\langle n|\hat{K}_0^{-1}|1_N\right\rangle^2}{(1+\delta K\left\langle n|\hat{K}_0^{-1}|n\right\rangle)(1+NK'\left\langle n|\hat{K}_0^{-1}|1_N\right\rangle)}\right) \\ &- \frac{(K+\delta K)^2\delta a^2}{2\delta K(1+\delta K\left\langle n|\hat{K}_0^{-1}|n\right\rangle)}\end{aligned} \tag{3.65}$$

The energetic part of this extremum value is particularly interesting as it closely resembles the energy stored by a mismatch and is again normalised by the local compliance. This simplifies the nature of the extremum such that it only depends on the sign of δK.

	$\delta K > 0$	$\delta K < 0$
$\Delta\Delta\mathcal{F}^*$	Minimum (-)	Maximum (+)

Table 3.3: Sign and type of the extremum in the interaction free energy for $\delta L = \delta L^*$

Existence of regimes

Since the extremal deformation δL^* has been identified, it is natural to symmetrise the parabola around this extremum. If the interaction free energy possesses two zero crossings, corresponding to the coexistence of stabilising and destabilising regimes, they are located at

$$\begin{aligned}\delta L^0 &= \delta L^* \pm \sqrt{\delta L^{*^2} - \frac{C}{A}} \\ &= \delta L^* \pm \frac{\tilde{K}_0}{K'}\sqrt{\frac{DD_t}{D_m}\left[\frac{(K+\delta K)^2\delta a^2}{\delta K^2} + \frac{\Delta\Delta\mathcal{S}}{\delta K}\right]}\end{aligned} \tag{3.66}$$

To determine the existence of multiple regimes, we must solve for $\Delta\Delta\mathcal{F}^* = 0$ for a critical value of the global stiffness K'_{crit} for which this occurs. This calculation is performed in appendix B.4, the critical K'_{crit} is given by:

$$K'_{\text{crit}} = \tilde{K}_0\left[\frac{D_m\left(1-\exp\left(\frac{(K+\delta K)^2\delta a^2}{\delta KD_m}\right)\right)}{\frac{\delta K}{\tilde{K}_0} - ND_m\left(1-\exp\left(\frac{(K+\delta K)^2\delta a^2}{\delta KD_m}\right)\right)}\right] \tag{3.67}$$

We consider the sign of this critical value. Stability demands that both the zero mode eigenvalue $\tilde{K}_0$ and the rank-one mismatch update D_m are positive, such that the prefactors

in the numerator are positive. The sign is therefore dependent on the exponential terms whose signs depend only on δK.

$$\delta K > 0 \Rightarrow 1 - \exp\left(\frac{(K+\delta K)^2 \delta a^2}{\delta K D_m}\right) < 0 \tag{3.68}$$

$$\delta K < 0 \Rightarrow 1 - \exp\left(\frac{(K+\delta K)^2 \delta a^2}{\delta K D_m}\right) > 0 \tag{3.69}$$

The denominator, too, depends only on the sign of δK, but in the opposite way. This leads to the conclusion that K'_{crit} must be negative. The significance of this result must not be understated. In any physically feasible system, we will have:

$$K'_{\text{phys}} > 0 > K'_{\text{crit}} \tag{3.70}$$

This means, in principle, that the interaction between the mismatch and the system's global frustration will always have both stabilising and destabilising regions. Combining all this, we can write full qualitative sign tables for all cases.

Case 1: $K' > 0$ **and** $\delta K < 0$
This is the physically expected case: a concave free-energy interaction parabola. The mismatch softens the system locally while the global deformation is approximated harmonically with a positive stiffness K'. In the ideal case, it allows us to tune the global deformation δL to the value of maximal destabilisation. Given its physical relevance, we present a qualitative plot in figure 3.5. We note that the sign table of the non-physical case $\delta K > 0$ and $0 > K' > K'_{\text{crit}}$ will look similar.

	δL^-		δL^*		δL^+	
$\Delta\Delta\mathcal{F}$	-	0	+	+	0	-

Table 3.4: Sign table for $\Delta\Delta\mathcal{F}$ if $\delta K < 0$ and $K' > 0$

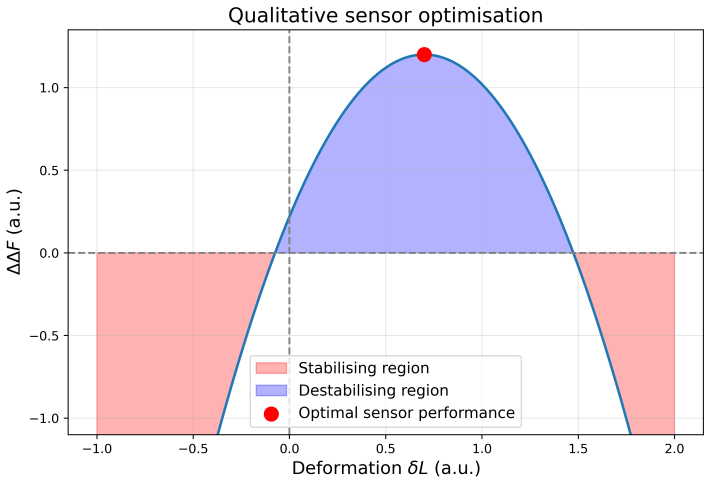

Figure 3.5: Qualitative plot of the interaction term in the physical case $K' > 0, \delta K < 0$, the sensor has a destabilising regime with an optimum at δL^*.

Case 2: $\delta K > 0$ **and** $K' > 0$
The free-energy interaction term is a convex parabola; the interaction is destabilising for large global deformation, but there is a region around the minimum where it is stabilising.

		δL^-		δL^*		δL^+	
$\Delta\Delta\mathcal{F}$	+	0	-	-	0	+

Table 3.5: Sign table for $\Delta\Delta\mathcal{F}$ if $\delta K > 0$ and $K' > 0$

For completeness, we also add two other non-physical cases.

Case 3a: $K' = K'_{\text{crit}}$
In the critical case, only one regime can persist, while the extremum of the interaction term cancels the interaction entirely.

$\Delta\Delta\mathcal{F}$		δL^*	
$\delta K > 0$	-	0	-
$\delta K < 0$	+	0	+

Table 3.6: Sign table for $\Delta\Delta\mathcal{F}$ in the critical case $K' = K'_{\text{crit}}$

Case 3b: $K' < K'_{\text{crit}}$
Beyond the critical case there would only exist one regime.

$\Delta\Delta\mathcal{F}$	
$\delta K > 0$	-
$\delta K < 0$	+

Table 3.7: Sign table for $\Delta\Delta\mathcal{F}$ for $K' < K'_{\text{crit}}$

4 The Kac-Baker Model

Up until this point, we have worked within the general framework of the matched-mode perturbation formalism. Other than including periodic boundary conditions and consequently generating a circulant base system, all qualitative results thus far are general to any positive definite chain-like system. We now choose a specific base model to work with. This will be based on a quadratic coarse-grained description of DNA, namely the cgDNA model. By further coarse-graining, this yields a spatially decaying model reminiscent of the one introduced by Baker in 1961 [23] for Ising-like systems.

4.1 CgDNA

The formalism we introduced is intended to describe real DNA sensors. It is therefore important that the underlying base system is correctly coarse-grained. This means choosing the base stiffness matrix $\hat{K}_0$, which captures effects arising from the combination of the many degrees of freedom present in real DNA.
We therefore base our model on a sequence-dependent coarse-grained DNA model, cgDNA [24, 25, 26]. This model is based upon two base assumptions:

1. Each nucleotide can be represented by a rigid body, neglecting any interactions within. All degrees of freedom consist of interactions between these rigid bodies. This generates 6 intra-base-pair degrees of freedom and 6 other inter-base-pair degrees of freedom. The cgDNA+ model also incorporates phosphate group positions, yielding a total of 24 degrees of freedom.

2. The local energy associated with each interaction is assumed to be quadratic in the relevant degrees of freedom.

4.1.1 Degrees of Freedom

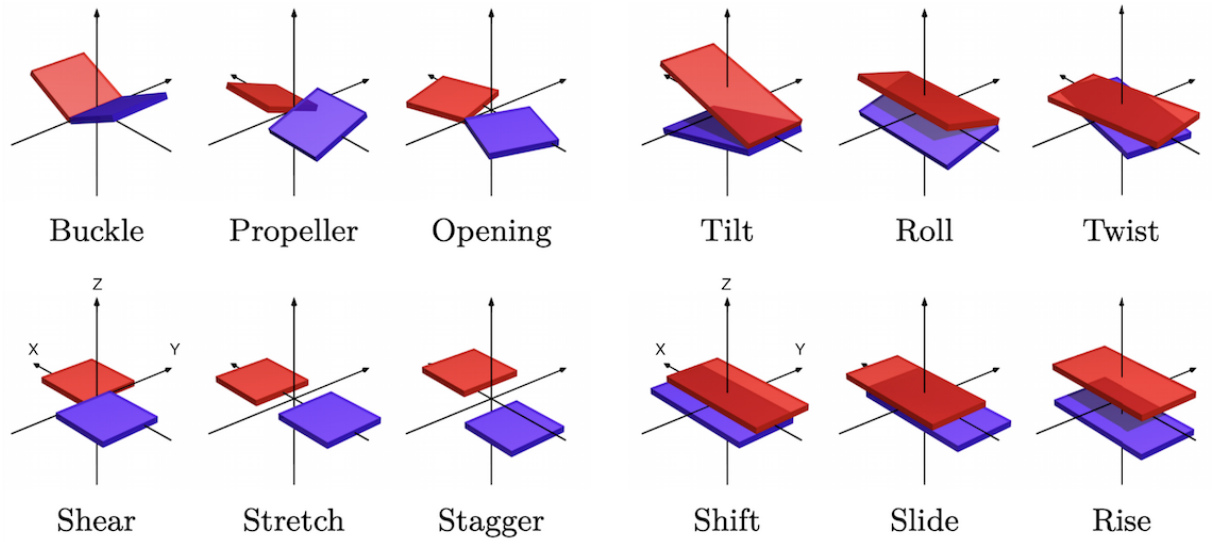

Figure 4.1: The degrees of freedom in the cgDNA model, for the cgDNA+ model, 12 additional degrees of freedom exist by the explicit addition of phosphate groups to the model. (Figure taken from cgNA+ website [24])

CgDNA describes the configuration of the DNA helix in terms of the relative positions of the rigid nucleotides. This introduces 12 degrees of freedom per base pair.

Intra-bp degrees of freedom : (Buckle, Propeller, Opening, Shear, Stretch, Stagger)
Inter-bp degrees of freedom : (Tilt, Roll, Twist, Shift, Slide, Rise)

These degrees of freedom are then combined into a vector for each base pair. Since we use the cgDNA+ model, 12 additional degrees of freedom must be accounted for due to its explicit inclusion of phosphate groups, which improves the model's performance when assessing the q-stiffness of the system [27], a property of particular importance to us for the coupling to the global constraint.

$$|X_n\rangle = \begin{pmatrix} x_{n,\text{buckle}} \\ x_{n,\text{buckle,phosphate}} \\ \vdots \\ x_{n,\text{twist}} \\ x_{n,\text{twist,phosphate}} \\ \vdots \\ x_{n,\text{rise}} \\ x_{n,\text{rise,phosphate}} \end{pmatrix} \leftarrow \text{Twist is the eleventh coefficient for each bp-step} \tag{4.1}$$

4.1.2 Quadratic Model

The key assumption that makes the cgDNA model interesting to us is that it is also quadratic in the local energy conformation for each of the 24 degrees of freedom.

This allows us to write the Hamiltonian in the same way as we treat it in our formalism.

$$\mathcal{H}_{\text{cgDNA+}} = \frac{1}{2} \langle X | \hat{K}_{\text{cgDNA+}} | X \rangle \tag{4.2}$$

Where the state vector $|X\rangle$ takes into account all degrees of freedom of all base pairs. The mathematical treatment is identical to what we introduced in chapter 2, the main difference being the number of coordinates. In an N-base-pair system, the cgDNA+ stiffness matrix is a positive-definite matrix satisfying:

$$\hat{K}_{\text{cgDNA+}} \in \mathbb{R}^{(24N-12)\times(24N-12)} \tag{4.3}$$

This stiffness matrix is constructed using only interactions that reach no further than each rigid nucleotide's five nearest-neighbours, limiting the number of local building blocks. This makes it a banded matrix with overlapping block structures as shown in figure 4.2.

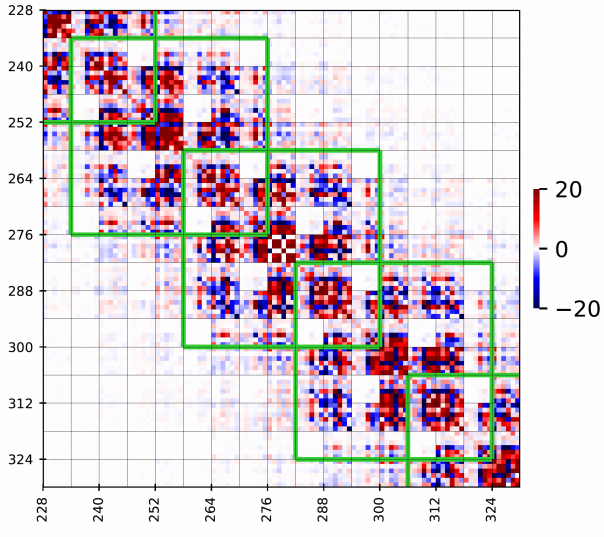

Figure 4.2: Zoom-in image on a cgDNA+ stiffness matrix corresponding to a central base-pair in a strand. The green squares correspond to interactions between rigid bodies, including intra-base-pair and neighbouring base-pair coordinates. (Figure taken from cgNA+ website [24])

It is nearly block-diagonal, meaning that even though the underlying interactions are local, non-local sequence-dependent terms still appear. These arise because each rigid base belongs to multiple neighbouring junctions whose equilibrium geometries are generally incompatible. This results in frustration, forcing the local base-pairs to adopt a compromised configuration that leads to non-local interactions.

4.1.3 Schur Complement

The chain model we use has only one degree of freedom, so we must further coarse-grain the cgDNA+ model. It is known that local microscopic interactions will be retained through the introduction of nonlocal interactions by applying a coarse-graining procedure [28].
For OWL-like sensors, it is observed that the helical periodicity is particularly important for their performance [10]. We therefore postulate that this degree of freedom will be the inter-base-pair twist as shown in figure 4.1. The coarse-graining procedure we use consists of splitting all degrees of freedom and then integrating the additional ones.

We rewrite $|X_n\rangle$ by singling out the twist coordinate:

$$|X_n\rangle = \begin{pmatrix} x_{n,\text{twist}} \\ |x_{n,\text{dropped}}\rangle \end{pmatrix} \tag{4.4}$$

The Hamiltonian for the whole system initially includes all 24 entries for all base-pairs.

$$\mathcal{H}_{\text{cgDNA+}} = \frac{1}{2} \langle X|\hat{K}_{\text{cgDNA+}}|X\rangle \tag{4.5}$$

Splitting this up into the twist coordinate of interest and the 23 other dropped coordinates.

$$\begin{aligned} \mathcal{H}_{\text{cgDNA+}} &= \frac{1}{2} \begin{pmatrix} \langle x_t| & \langle x_d| \end{pmatrix} \begin{pmatrix} \hat{K}_{tt} & \hat{K}_{td} \\ \hat{K}_{dt} & \hat{K}_{dd} \end{pmatrix} \begin{pmatrix} |x_t\rangle \\ |x_d\rangle \end{pmatrix} \\ &= \frac{1}{2} \langle x_t|\hat{K}_{tt}|x_t\rangle + \frac{1}{2} \langle x_d|\hat{K}_{dd}|x_d\rangle + \frac{1}{2} \langle x_d|\hat{K}_{dt}|x_t\rangle + \frac{1}{2} \langle x_t|\hat{K}|x_d\rangle \end{aligned} \tag{4.6}$$

But we know, of course, that the stiffness matrix is symmetric, so that $\hat{K}_{dt} = \hat{K}_{td}^T$.

$$\mathcal{H}_{\text{cgDNA+}} = \frac{1}{2} x_t \hat{K}_{tt} x_t + \frac{1}{2} \langle x_d|\hat{K}_{dd}|x_d\rangle + \langle x_t|\, \hat{K}_{td}\, |x_d\rangle \tag{4.7}$$

To isolate the system's pure twist coordinates, we must project the full cgDNA+ model onto the chain model used here. It is not possible to neglect these dropped coordinates, as they do interact with the twist in the 24×24 blocks of $\hat{K}_{\text{cgDNA+}}$. We can do this by literally integrating them away and working with the marginal distribution. This is possible since the marginal distributions of Gaussian distributions are also Gaussian.

$$P(|x_t\rangle) \propto \int \mathrm{d}\mathbf{x_d} e^{-\mathcal{H}(\mathbf{x}_t, \mathbf{x}_d)} \tag{4.8}$$

Physically, this integral computes the effective energy of a specific twist configuration by allowing the remaining 23 degrees of freedom to thermally equilibrate.
Performing the integration is easily done using the machinery of section 2.3, in terms of the language used there, this gives:

- The quadratic term in the dropped coordinates Hamiltonian $\mathcal{H}_d$ is $\frac{1}{2} \langle x_d|\hat{K}_{dd}|x_d\rangle \Rightarrow \hat{K}_0 = \hat{K}_{dd}$.
- The linear term in $\mathcal{H}_d$ is $\langle x_t|\hat{K}_{td}|x_d\rangle \Rightarrow \langle b| = \langle x_t|\, \hat{K}_{td}$
- The twist contribution to the Hamiltonian is only an additive constant for $\mathcal{H}_d \Rightarrow c = \frac{1}{2} \langle x_t|\hat{K}_{tt}|x_t\rangle$

And now we use the complete-the-square trick to integrate away all these degrees of freedom. For the twist Hamiltonian, all of these add an additive constant, which we can neglect. We get an effective twist Hamiltonian.

$$\begin{aligned} \mathcal{H}_t &= c - \frac{1}{2} \langle b|\hat{K}_0^{-1}|b\rangle \\ &= \frac{1}{2} \langle x_t|\hat{K}_{tt}|x_t\rangle - \frac{1}{2} \langle x_t|\hat{K}_{td}\hat{K}_{dd}^{-1}\hat{K}_{dt}|x_t\rangle \\ &= \frac{1}{2} \langle x_t| \left(\hat{K}_{tt} - \hat{K}_{td}\hat{K}_{dd}^{-1}\hat{K}_{dt}\right) |x_t\rangle \end{aligned} \tag{4.9}$$

Using symmetry again:

$$\mathcal{H}_{\text{twist}} = \frac{1}{2} \langle x_t | \left(\hat{K}_{tt} - \hat{K}_{td} \hat{K}_{dd}^{-1} \hat{K}_{td}^{T} \right) | x_t \rangle \tag{4.10}$$

Which means we get an effective twist stiffness matrix with scalar elements generated from the twist self-interactions and the interactions between the twist and the 23 other degrees of freedom:

$$\hat{K}_{\text{twist}} = \hat{K}_{tt} - \hat{K}_{td} \hat{K}_{dd}^{-1} \hat{K}_{td}^{T} \tag{4.11}$$

This resulting matrix, $\hat{K}_{\text{twist}}$, is known as the Schur complement of the dropped coordinates block. Crucially, because the original full cgDNA+ stiffness matrix is positive definite, its Schur complement is mathematically guaranteed also to be positive definite [29, 30], preserving the physical stability of the system.

While the original pure-twist sub-block $\hat{K}_{tt}$ contains only highly localised interactions, it still relies on the nearly block-diagonal structure shown in figure 4.2. The subtraction of the $\hat{K}_{td} \hat{K}_{dd}^{-1} \hat{K}_{td}^{T}$ term introduces non-local couplings. These appear as off-diagonal couplings representing the effective interactions mediated by the 23 degrees of freedom we integrated out.

We now employ this method on a randomly generated DNA strand, where each letter represents a base pair:

$$\begin{gathered} \text{AGTCCGATTTGACCGTACGATGCTTAGCGGATCCATGGTAC} \\ \text{CTTACGGTAGCTAACGTTCGATGGCATTAACCGTGGATCTAG} \\ \text{CTTACCGGATGATCGTACCGTTAGGCTAACGTTAGCTACGAT} \end{gathered} \tag{4.12}$$

This consists of 120 base pairs to neglect any boundary effects. We plot both the original stiffness matrix for this system as well as the new twist stiffness matrix in figure 4.3

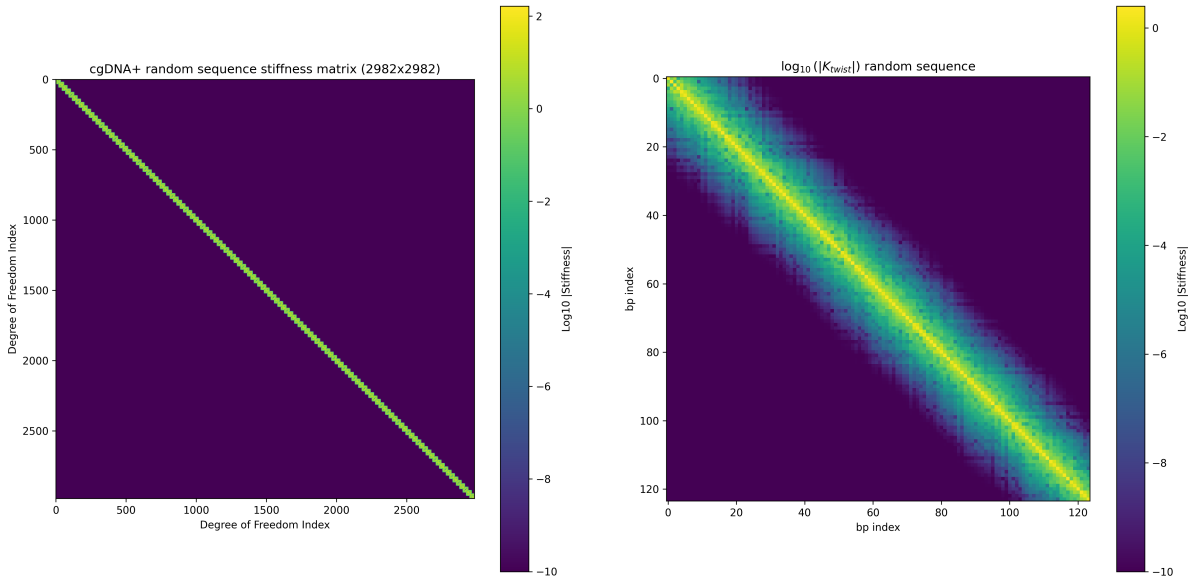

(a) (b)

Figure 4.3: (a) cgDNA+ stiffness matrix for the randomly generated DNA strand 4.12. (b) Reduced twist stiffness matrix obtained through the Schur complement of the same cgDNA+ stiffness matrix.

Although the cgDNA+ model is sequence-dependent, the effective stiffness of the reduced system in figure 4.3b is not very sensitive to this, with only minor fluctuations, which lie mostly in the off-diagonal regions, i.e. longer-range couplings, of the matrix.
The reduced stiffness couplings clearly decay from the diagonal, as we would intuitively expect. Longer-range couplings should be inherently weaker, as they are generated only through couplings to other degrees of freedom, and these couplings are, of course, less strong over this longer range. To capture this, we propose a base stiffness matrix $\hat{K}_0$ in which the non-local couplings decay exponentially with distance away from the diagonal l as:

$$\langle n|\hat{K}_0|n+l\rangle = K_0 e^{-|l|/\lambda} \tag{4.13}$$

We can interpret λ as the length scale of the characteristic interaction in the system, while K_0 is the coupling strength of the self-coupling, i.e. nearest neighbour, in the chain.
We can extract this coupling length by taking the logarithm of the off-diagonal magnitudes and fitting the linear decay:

$$\log|\langle n|\hat{K}_{\text{twist}}|n+l\rangle| = -\frac{|l|}{\lambda} + \text{ct.} \tag{4.14}$$

To discard boundary effects and smooth out local sequence-dependent variations, we average the coupling strengths across the bulk of a sufficiently large and variable twist stiffness matrix. This is why we chose the randomly generated strand 4.12. For this strand, we show the linear fit in figure 4.4. For this particular strand, the decay length is $\lambda = 1.052\ \text{bp}$. Applying this method to several strands, we always find a coupling length of $\lambda \sim 1\ \text{bp}$, with the biggest outlier being a G_{100} strand giving $\lambda = 1.6271\ \text{bp}$. Evidence for increased stiffness in G-rich strands [31, 32] could explain this minor discrepancy. Even though the exact decay length depends weakly on the underlying DNA sequence, the overall exponential form is a general feature. Across all sequences we surveyed, the fitted interaction length remains on the order of one base pair. We thus choose that value for simplicity.

$$\lambda = 1\text{bp} \tag{4.15}$$

This means that the coupling strength decays by one e-fold for each additional bp step, reducing it to about $1/e \approx 0.37$ of its previous value. Indicating a relatively fast decay in coupling strength.
The diagonal element of the reduced stiffness matrix defines the fundamental self-coupling K_0 of the system. To align with contemporary convention, we express it in nanometres. Extracting it from the random sequence of equation (4.12) yields:

$$K_0 \approx 38\text{nm} \tag{4.16}$$

The most relevant model describing DNA twist is the twistable worm-like-chain (TWLC), a purely quadratic chain model that incorporates both the bending (tilt and roll) and twist modes present in the helix [33]. This is based on the twist persistence length of the system, the typical correlation length. Due to the addition of long-range couplings to the system, the response is determined not only by the local self-coupling but also by the effective long-range interactions. For the periodic system, we can capture the long-wavelength response by incorporating these effects through the global stiffness eigenvalue $\tilde{K}_0$ of the stiffness matrix. In the following section, we will derive its dependence on the fundamental coupling K_0 and coupling length λ explicitly.

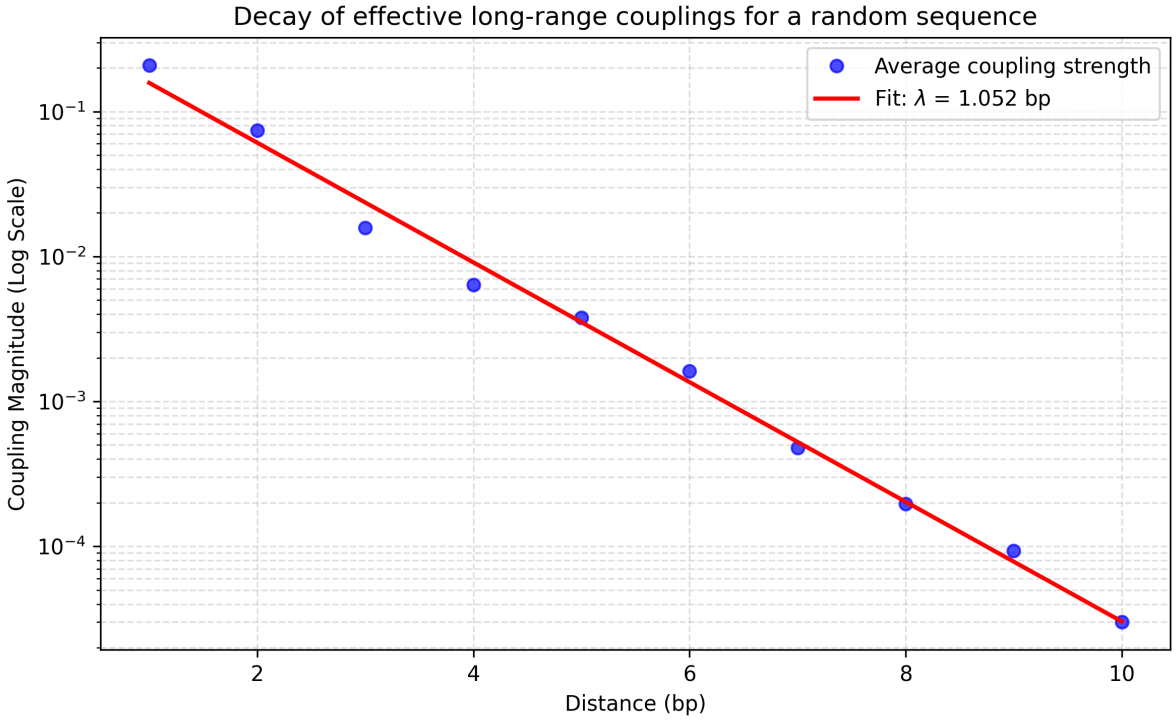

Figure 4.4: Decay fit of the random sequence equation (4.12) versus the distance away from the diagonal coupling.

The intrinsic torsional stiffness of DNA in the TWLC model is commonly taken to be:

$$C \approx 110\text{nm} \tag{4.17}$$

When the twist-bend coupling is included, though, this value is renormalised to a value of [34]:

$$\kappa_t = 75\text{nm} \tag{4.18}$$

Because the Schur complement of the cgDNA+ matrix preserves the effective couplings between twist and the eliminated bending degrees of freedom, the renormalised value κ_t provides the most appropriate reference for comparison.

4.2 Kac-Baker Couplings

The exponentially decaying coupling we imposed in the previous section has been studied before in lattices. Kac showed that a potential of this kind has a solvable partition sum [35], while Baker applied it two years later to a generalised Ising system with a similar setup to the one we have here [23]. Because of their foundational work, these models are sometimes referred to as Kac-Baker couplings in quadratic models [36, 37].

4.2.1 A Banded Circulant Matrix

We initially consider a general Hamiltonian that includes interactions between displacements at the n-th and l-th sites, mediated by $\hat{K}_{|n-l|}$, with the possibility of couplings to

m neighbours. In this model, these couplings no longer directly correspond to physical springs, as that would create a more complex circulant model. Instead, the couplings can be interpreted as harmonic interactions spanning long distances.

$$\mathcal{H}_0 = \frac{1}{2}\sum_{n=0}^{N-1}\sum_{l=1}^{m} K_{|n-l|}x_n x_l \tag{4.19}$$

We reorder the sum by defining $j \equiv n - l$ it now runs from $-m$ to m:

$$\begin{aligned}\mathcal{H}_0 &= \frac{1}{2}\sum_{n=0}^{N-1}\sum_{j=-m}^{m} K_{|j|}x_n x_{n+j} \\ &= \frac{1}{2}\langle x|\left[\sum_{n=0}^{N-1}\sum_{j=-m}^{m} K_{|j|}|n\rangle\langle n+j|\right]|x\rangle\end{aligned}$$

We recognise that the coupling can be written using the discrete translational shift operators (2.59):

$$\langle n+j| = (|n+j\rangle)^t = \left(\hat{S}^{tj}|n\rangle\right)^t = \langle n|\hat{S}^j \tag{4.20}$$

Such that the base Hamiltonian becomes:

$$\mathcal{H}_0 = \frac{1}{2}\langle x|\left[\sum_{l=-m}^{m} K_{|l|}\hat{S}^l\right]|x\rangle \tag{4.21}$$

And our base $\hat{K}_0$ matrix is thus given by:

$$\hat{K}_0 = \sum_{l=-m}^{m} K_{|l|}\hat{S}^l \tag{4.22}$$

This is a canonical form of a circulant matrix as written in equation (2.63), only limited by the range of the couplings m. A particularly nice form, as we have already developed a theoretical description for it in section 2.6. The result is a banded matrix:

$$\hat{K}_0 = \begin{pmatrix} K_0 & K_1 & \cdots & K_m & 0 & \cdots & 0 & K_m & \cdots & K_1 \\ K_1 & K_0 & K_1 & \cdots & K_m & 0 & \cdots & 0 & \ddots & \vdots \\ \vdots & K_1 & K_0 & \ddots & \ddots & \ddots & & & & K_m \\ K_m & \vdots & \ddots & \ddots & \ddots & \ddots & \ddots & 0 & \cdots & 0 \\ 0 & K_m & \ddots & \ddots & K_0 & K_1 & \cdots & K_m & & \vdots \\ \vdots & 0 & \ddots & \ddots & K_1 & K_0 & K_1 & \ddots & \ddots & 0 \\ 0 & \vdots & & \ddots & \vdots & \ddots & \ddots & \ddots & \ddots & K_m \\ K_m & 0 & & & K_m & \cdots & K_1 & K_0 & K_1 & \vdots \\ \vdots & \ddots & & & 0 & K_m & \cdots & K_1 & K_0 & K_1 \\ K_1 & \cdots & K_m & 0 & \cdots & 0 & K_m & \cdots & K_1 & K_0 \end{pmatrix} \tag{4.23}$$

Notice the effect of the periodic boundary conditions, as the corners fill up from $K_1 \to K_m$ as the off-diagonal terms do. These arise from the sequential application of the shift matrices, which have corner terms (2.60).

From equations (2.63) and (2.68) we know immediately what the coefficients for the discrete Fourier transformed eigenvalues will be. These are the coefficients next to the shift matrices themselves.

$$\tilde{K}_q = \sum_{l=-m}^{m} K_{|l|} e^{\frac{2\pi i}{N} ql} \tag{4.24}$$

To identify the fundamental self-coupling K_0 explicitly, we split up the sum into the negative and positive l parts.

$$\tilde{K}_q = \sum_{l=-m}^{-1} K_{-l} e^{\frac{2\pi i}{N} ql} + K_0 + \sum_{l=1}^{m} K_l e^{\frac{2\pi i}{N} ql}$$

These negative and positive parts are nearly identical under $l \to -l$ conversion, such that:

$$\begin{aligned} \tilde{K}_q &= K_0 + \sum_{l=1}^{m} K_l \left(e^{\frac{2\pi i}{N} ql} + e^{-\frac{2\pi i}{N} ql} \right) \\ &= K_0 + 2 \sum_{l=1}^{m} K_l \cos\left(\frac{2\pi}{N} ql \right) \end{aligned} \tag{4.25}$$

The $q = 0$ global eigenmode of the system is now also revealed. As discussed in detail in section 2.6, it is equal to the row sum of the matrix, as confirmed by inspection of the matrix (4.23).

$$\text{Row sum}(\hat{K}_0) = \langle n | \hat{K}_0 | 1_N \rangle = \tilde{K}_0 = K_0 + 2 \sum_{l=1}^{m} K_l \tag{4.26}$$

4.2.2 Circulant Kac-Baker

At this point, we move our attention to the Kac-Baker couplings we defined earlier:

$$\hat{K}_{|i-j|} = K_0 \exp\left(-\frac{|i-j|}{\lambda} \right) = K_0 r^{-|i-j|} \tag{4.27}$$

Where r is a number greater than 1 defined by the coupling length λ:

$$r = e^{1/\lambda} \tag{4.28}$$

The Hamiltonian in displacement coordinates is then given by:

$$\mathcal{H}_0 = \frac{K_0}{2} \sum_{n=0}^{N-1} \sum_{l=-m}^{m} x_n x_{n+l} \exp\left(-\frac{|l|}{\lambda} \right) \tag{4.29}$$

This is the simplest way to interpret the spatial decay in the chain model, as it physically links displacements in the system via a decaying harmonic coupling. The stiffness matrix of the system is now given by:

$$\hat{K}_0 = K_0 \sum_{l=-m}^{m} \hat{S}^l \exp\left(-\frac{|l|}{\lambda} \right) \tag{4.30}$$

To determine the eigenvalues of the stiffness matrix, we must now fill in the sum in equation (4.25)

$$\begin{aligned}\tilde{K}_q &= K_0 + 2\sum_{l=1}^{m} K_l \cos\left(\frac{2\pi}{N} ql\right) \\ &= K_0\left[1 + 2\sum_{l=1}^{m} r^{-l}\cos\left(\frac{2\pi}{N} ql\right)\right] \\ &= K_0\left[1 + \frac{r\cos\left(\frac{2\pi}{N}q\right) - 1 + r^{-m}\left(\cos\left(\frac{2\pi}{N}mq\right) - \cos\left(\frac{2\pi}{N}(m+1)q\right)\right)}{r^2 - 2r\cos\left(\frac{2\pi}{N}q\right) + 1}\right]\end{aligned} \tag{4.31}$$

For the zero mode eigenvalue, this simplifies to:

$$\tilde{K}_0 = K_0\left[1 + 2\frac{1 - r^{-m}}{r - 1}\right] \tag{4.32}$$

For the matrix elements $\langle n|\hat{K}_0^{-1}|n\rangle$, we need to sum over all eigenvalues, though, which is not analytically viable for the m-coupling chain.

Short range limit

Given that the characteristic coupling length λ we found from the reduced cgDNA+ matrix is only 1 base pair, it is reasonable to consider the short-range limit of the Kac-Baker coupling. As shown in figure 4.4, couplings beyond the first few base pairs do not contribute appreciably to the geometric sums in equation (4.25) and (4.26). Since the coupling length is an order of magnitude smaller than the system size (an additional requirement for periodic systems), it is therefore justified and analytically favourable to take the limit $m \to \infty$ in our system, as the geometric sums, due to their exponentially decaying nature, converge and simplify significantly.

$$\begin{aligned}\tilde{K}_q &= K_0\left[1 + 2\frac{r\cos\left(\frac{2\pi}{N}q\right) - 1}{r^2 - 2r\cos\left(\frac{2\pi}{N}q\right) + 1}\right] \\ &= K_0\left(\frac{r^2 - 1}{r^2 - 2r\cos\left(\frac{2\pi}{N}q\right) + 1}\right)\end{aligned} \tag{4.33}$$

and

$$\tilde{K}_0 = K_0\left(1 + 2\frac{1}{r - 1}\right) = K_0\left(\frac{r + 1}{r - 1}\right) \tag{4.34}$$

Which reveals an elegant result if we use $r = e^{1/\lambda}$:

$$\begin{aligned}\tilde{K}_0 &= K_0\frac{e^{1/\lambda} + 1}{e^{1/\lambda} - 1} \\ &= K_0\frac{e^{1/2\lambda} + e^{-1/2\lambda}}{e^{1/2\lambda} - e^{-1/2\lambda}} \\ &= K_0\coth\left(\frac{1}{2\lambda}\right)\end{aligned} \tag{4.35}$$

This establishes the link between the long-wavelength behaviour of our system, the fundamental coupling K_0 and the characteristic decay length of the couplings. As we required to compare the result of the coarse-graining procedure we applied with the renormalised stiffness of the twistable worm-like-chain (4.18). For the given decay length of 1 base pair and fundamental coupling of 38nm, the resulting value is given by:

$$\tilde{K}_0 \approx 38\text{nm}\coth\left(\frac{1}{2}\right) \approx 83\text{nm} \tag{4.36}$$

Which is remarkably close, given that we coarse-grained 23 relevant degrees of freedom of the cgDNA+ model into a single twist degree of freedom. While at the same time choosing to work with a translationally invariant system, a feature not present in these TWLC models.

Matrix elements

As discussed in chapter 3, we require three matrix elements of the system's structure matrix $\hat{K}_0^{-1}$ to quantify the relevant free energy landscapes. We already have the row sum:

$$\langle n|\hat{K}_0^{-1}|1_N\rangle = \frac{1}{\tilde{K}_0} = \frac{1}{K_0}\tanh\left(\frac{1}{2\lambda}\right) \tag{4.37}$$

This immediately yields the global constraint matrix element as well.

$$\langle 1_N|\hat{K}_0^{-1}|1_N\rangle = \frac{N}{K_0}\tanh\left(\frac{1}{2\lambda}\right) \tag{4.38}$$

For the final matrix element, we need to consider the sum of all eigenvalues (3.15), using the short-range limit eigenvalues equation (4.33), this sum yields:

$$\langle n|\hat{K}_0^{-1}|n\rangle = \frac{1}{NK_0(r^2-1)}\sum_{q=0}^{N-1}\left((r^2+1) - 2r\cos\left(\frac{2\pi}{N}q\right)\right) = \frac{1}{K_0}\frac{r^2+1}{r^2-1} \tag{4.39}$$

We can neglect the cosine-dependent term, as it will cancel after the summation over all q modes. Reverting back to λ, we recover another elegant form:

$$\langle n|\hat{K}_0^{-1}|n\rangle = \frac{1}{K_0}\coth\left(\frac{1}{\lambda}\right) \tag{4.40}$$

Due to their particular importance, it is useful to list these matrix elements:

$$\langle n|\hat{K}_0^{-1}|n\rangle = \frac{1}{K_0}\coth(1/\lambda) \tag{4.41}$$

$$\langle n|\hat{K}_0^{-1}|1_N\rangle = \frac{1}{K_0}\tanh(1/2\lambda) \tag{4.42}$$

$$\langle 1_N|\hat{K}_0^{-1}|1_N\rangle = \frac{N}{K_0}\tanh(1/2\lambda) \tag{4.43}$$

To get a feeling for the magnitude of the terms, we plot them for a range of characteristic lengths in figure 4.5.

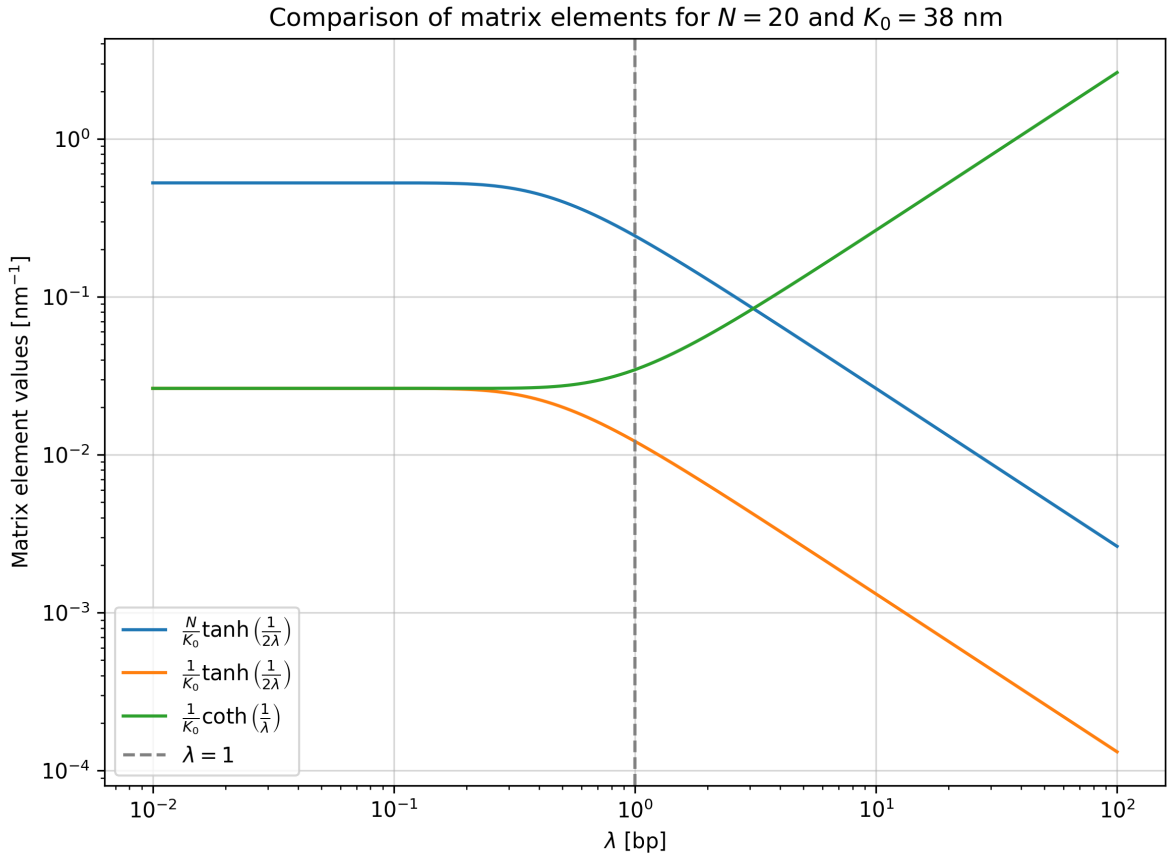

Figure 4.5: A plot of the relevant matrix elements in the Kac-Baker model.

We see, of course, that the global interaction $\langle 1_N|\hat{K}_0^{-1}|1_N\rangle$ is always an order of magnitude greater than the mixing term $\langle n|\hat{K}_0^{-1}|1_N\rangle$ due to the factor $N = 20\text{bp}$. The interesting part of this graph lies in the comparison between the global term and the local mismatch term. For $\lambda \gtrsim 1$ bp, their respective magnitudes switch in relative importance. Since we have already determined $\lambda = 1\text{bp}$, we are in a regime in which these contributions are consequently of a similar order.
For sufficiently short decay lengths $(\lambda \lesssim 0.1\text{bp})$ the matrix elements are nearly independent of it as:

$$\lim_{\lambda\to 0}\coth(1/\lambda) = \lim_{\lambda\to 0}\tanh(1/2\lambda) = 1 \tag{4.44}$$

This is the regime in which the Kac-Baker model reduces to the decoupled chain model.

4.2.3 Correlations

To cross-check the value of λ, it is physically interesting to examine correlations between distant displacements. To find these correlations, we can use equation (2.23) by filling in $f(\mathbf{x}) = x_n x_m$.

$$\begin{aligned}\langle x_n x_m \rangle &= \frac{\partial}{\partial b_n}\left[\frac{\partial}{\partial b_m} e^{\frac{1}{2}\langle b|\hat{K}_0^{-1}|b\rangle}\right]_{|b\rangle=0} \\ &= \frac{1}{2}\frac{\partial}{\partial b_m}\left[\langle n|\hat{K}_0^{-1}|b\rangle\, e^{\frac{1}{2}\langle b|\hat{K}_0^{-1}|b\rangle}\right]_{|b\rangle=0} \\ &= \langle n|\hat{K}_0^{-1}|m\rangle \end{aligned} \tag{4.45}$$

These correlations are thus directly related to the off-diagonal elements of the structure matrix $\hat{K}_0^{-1}$. It is therefore often referred to as the covariance/correlation matrix in the literature [27]. This is a general feature of any Gaussian theory, where these correlations yield the propagator of the theory [13].

Structure matrix

To find these off-diagonal elements, it is once again useful to switch to Fourier space.

$$\langle n|\hat{K}_0^{-1}|m\rangle = \sum_{q=0}^{N-1} \frac{\langle n|q\rangle\,\langle q|m\rangle}{\tilde{K}_q} \tag{4.46}$$

Using the discrete Fourier expansion of the eigenvectors in real space (2.66) and the eigenvalues we found for the Kac-Baker couplings(4.33), this yields.

$$\begin{aligned}\langle n|\hat{K}_0^{-1}|m\rangle &= \frac{1}{N}\sum_{q=0}^{N-1} \exp\left(\frac{2\pi i}{N}q(n-m)\right)\frac{r^2 - 2r\cos\left(\frac{2\pi}{N}q\right) - 1}{r^2+1} \\ &= \frac{1}{NK_0}\left[\frac{r^2-1}{r^2+1}\sum_{q=0}^{N-1}\exp\left(\frac{2\pi i}{N}q(n-m)\right) - \frac{2r}{r^2+1}\sum_{q=0}^{N-1}\exp\left(\frac{2\pi i}{N}q(n-m)\right)\cos\left(\frac{2\pi}{N}q\right)\right]\end{aligned}$$

Using Euler's formula, we can write the cosine as the sum of two exponentials.

$$\cos\left(\frac{2\pi}{N}q\right) = \frac{e^{\frac{2\pi i}{N}q} + e^{-\frac{2\pi i}{N}q}}{2} \tag{4.47}$$

And now use the orthonormality of the Fourier modes:

$$\sum_{q=0}^{N-1}\exp\left(\frac{2\pi i}{N}q(k-l)\right) = \delta_{kl} \tag{4.48}$$

This has profound consequences. The Kac-Baker couplings in the circulant model do not allow correlations beyond the next-nearest-neighbours. This is no coincidence, as this model is the dual of the next-nearest-neighbour coupling chain (see Skoruppa *et al.* [22]), where we see the more conventional picture of exponentially decaying correlations. This exponential decay of spatial correlations is also observed for all three degrees of freedom in the

twistable worm-like-chain and has been reported extensively [38, 39, 40, 41]. The absence of these longer-range, decaying correlations in this theory suggests to us that translational invariance in chain models must be broken to capture this effect and apply the relevant Schur-complement coarse-graining procedure. This interpretation is supported by an apparent connection between Kac-Baker-like couplings and field-theoretic descriptions of the Markovian Ornstein-Uhlenbeck process, where exponentially decaying interactions correspond to screened correlations [42].
We recognise the diagonal element of the structure matrix from before. For the off-diagonal elements, the prefactor is given by:

$$\frac{r}{r^2-1} = \frac{e^{1/\lambda}}{e^{2/\lambda}-1} = \frac{1}{e^{1/\lambda}-e^{-1/\lambda}} = \frac{1}{2}\operatorname{csch}(1/\lambda) \tag{4.49}$$

So finally, the matrix elements are given by:

$$\langle n|\hat{K}_0^{-1}|m\rangle = \frac{1}{K_0}\coth(1/\lambda)\,\langle n|m\rangle - \frac{1}{2K_0}\operatorname{csch}(1/\lambda)(\langle n|m+1\rangle + \langle n|m-1\rangle) \tag{4.50}$$

We can use the shift matrices to simplify this:

$$\hat{K}_0^{-1} = \frac{\operatorname{csch}(1/\lambda)}{K_0}\left[\cosh(1/\lambda) - \frac{1}{2}\left(\hat{S}+\hat{S}^t\right)\right]\mathbb{1} \tag{4.51}$$

4.3 Strain-Mismatch in the Kac-Baker Model

Now that we have established the key features of the Kac-Baker coupling circulant chain model, we move on to its application within our matched-mode perturbations formalism, which describes the interaction between mismatches and the system's global strain. The qualitative description in chapter 3 provided us with a first glimpse of how this interaction works within the general formalism. But to obtain quantitative information, we require the fully developed Kac-Baker model.

4.3.1 Stability

As we discussed in section 3.3.1, for any meaningful comparison among the several perturbed systems, we must first ensure that all are stable, which imposes several demands on the system. We can now impose these constraints quantitatively.

Base eigenvalues

For the base system, the eigenvalues are given by equation (4.33). These must be positive, which imposes:

$$\frac{r^2-1}{r^2-2r\cos\left(\frac{2\pi}{N}q\right)+1} > 0 \qquad \forall q \in \{0,\dots,N-1\} \tag{4.52}$$

Since the denominator has no real roots, we can assume it is positive, which shifts the requirement to the numerator. It is useful to recast this in terms of the decay length λ.

$$\begin{cases} K_0 > 0 \\ \lambda > 0 \end{cases} \tag{4.53}$$

This indicates that the couplings can only decay over distance, as is physically reasonable.

Global constraint term

The determinant condition for the global constraint update is given by:

$$K' \langle 1_N | \hat{K}_0^{-1} | 1_N \rangle > -1 \tag{4.54}$$

Using equation (4.42), we can then write down a condition on the global constraint spring constant K'.

$$K' > -\frac{K_0}{N} \coth\left(\frac{1}{2\lambda}\right) \tag{4.55}$$

A negative closing spring is therefore permitted, and notably, it can become progressively stronger as the coupling length increases, as shown in figure 4.6.
As λ increases, the long-range couplings add collective stiffness to the system, raising the lowest eigenvalue and improving overall stability. This means a more negative quadratic coupling K' is required to destabilise the uniform $\tilde{K}_0$ eigenmode response, so the system can tolerate increasingly negative K' as interactions become more nonlocal.

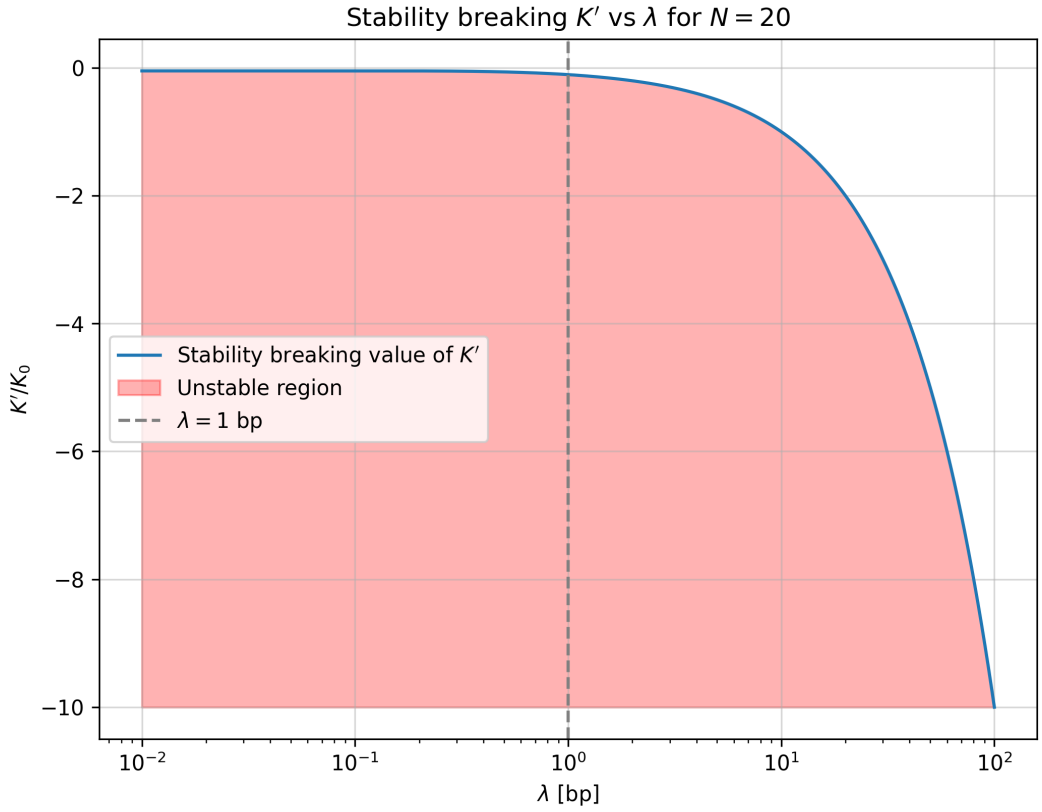

Figure 4.6: Stability curve for K' for global constraint.

Interpreting what a negative spring implies is counterintuitive, as it would exert a force that strengthens as we move away from its equilibrium length (with increasing $|\delta L|$). Alone, such a coupling would be unstable. However, it could be used to approximate a locally repulsive interaction; this idea is not explored further here.

Local perturbation

Now we move on to the condition on the mismatch for which we alter the local coupling at the n-th displacement $K_0 \to K_0 + \delta K$.

$$\delta K \, \langle n|\hat{K}_0^{-1}|n\rangle > -1 \tag{4.56}$$

For the Kac-Baker chain, then:

$$\delta K > -K_0 \tanh\left(\frac{1}{\lambda}\right) \tag{4.57}$$

We expect mismatches to be locally softening so that $\delta K < 0$. This condition thus places a strict limit on how destabilising the mismatch can be in this model. In particular, we see that if the coupling length increases, mismatches quickly become destabilising enough so that the whole system is no longer positive definite and thus no longer stable. For the present model, in which λ is chosen as 1 base pair, the critical value breaking stability is:

$$\frac{\delta K_{\text{crit}}}{K_0} \approx -0.76 \tag{4.58}$$

In the limit of $\lambda \to 0$, the criticality curve converges to -1. Intuitively, we can interpret this as physically removing the spring from the decoupled chain.

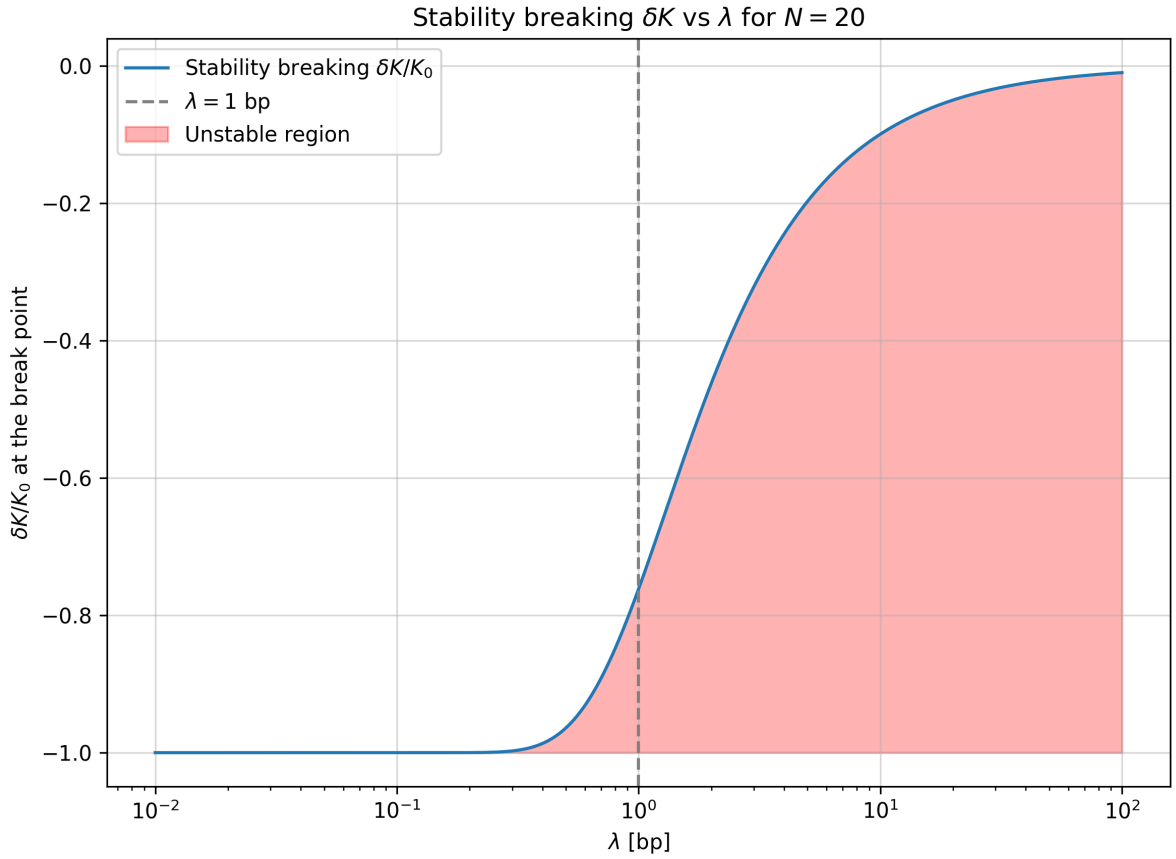

Figure 4.7: Stability curve for δK for both a mismatch term.

Interaction term

Finally, we can also consider the system's stability when both the mismatch and the global strain are present. For a rank-two update, we had: We require D (3.44), the determinant of the 2×2 update matrix, to be positive. We see the determinants of the individual perturbations appearing separately, and we have already required them to be positive so that we can write:

$$K'\delta K \langle n|\hat{K}_0^{-1}|1_N\rangle^2 < \left(1 + K' \langle 1_N|\hat{K}_0^{-1}|1_N\rangle\right)\left(1 + \delta K \langle n|\hat{K}_0^{-1}|n\rangle\right) \tag{4.59}$$

For the Kac-Baker model, this becomes:

$$K'\delta K \tanh(1/2\lambda)^2 < (K_0 + NK' \tanh(1/2\lambda))(K_0 + \delta K \coth(1/\lambda)) \tag{4.60}$$

Since the physically relevant case for a closing spring has K' positive, which preserves stability, we do not consider K' a relevant parameter here. Instead, we solve for δK as the softening mismatch can break stability. This stability curve for this demand is plotted in figure 4.8.

$$\delta K > \frac{K_0(K_0 + NK' \tanh(1/2\lambda))}{K' \tanh(1/2\lambda)^2 - NK' \coth(1/\lambda) \tanh(1/2\lambda) - K_0 \coth(1/\lambda)} \tag{4.61}$$

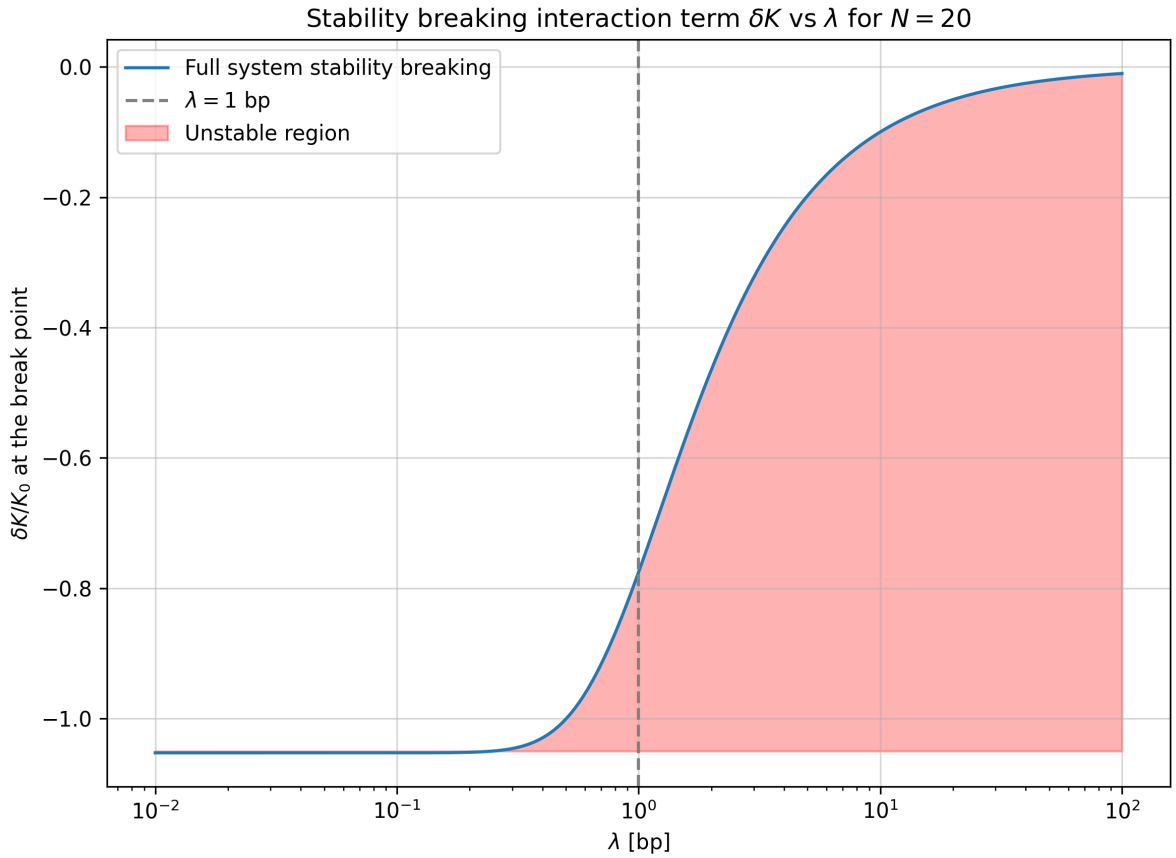

Figure 4.8: Stability curve for δK for the interaction term.

It is a less restrictive condition than the pure mismatch stability condition. This observation is nearly independent of the strength or sign of the closing spring. In theory, this means that there exist systems in which the presence of the closing spring is stabilising enough that what would normally be unstable becomes stable. In particular, in the decoupled chain, a "negative" spring in the mismatched chain can interact with the global strain, ensuring that the overall system remains positive definite. Since we care about the existence of the mismatch-only system, we are not considering that case at this time.

4.3.2 Strain

Because we have already developed the entire formalism to describe global frustration in the system, it is now simply a case of filling in the relevant zero-mode eigenvalue $\tilde{K}_0$ in equation (3.36).

$$\Delta\mathcal{F}_g = \frac{1}{2}\log\left(1 + N\frac{K'}{K_0}\tanh\left(\frac{1}{2\lambda}\right)\right) + \frac{K_0K'}{2(K_0 + NK'\tanh(1/2\lambda))}\delta L^2 \tag{4.62}$$

Or in the rigid limit:

$$\Delta\mathcal{F}_r = -\frac{1}{2}\log\left(K_0\coth\left(\frac{1}{2\lambda}\right)\right) + \frac{K_0\coth(1/2\lambda)}{2N}\delta L^2 \tag{4.63}$$

Torque

There is a fundamental limit to the torsional strain a DNA molecule can withstand [43]. Over long enough distances (i.e. beyond the persistence length), it behaves approximately as an isotropic flexible rod. As twist turns are added through the application of torsion, the extension of the molecule remains nearly constant. That is, until a critical torque $\tau_{\text{crit}+}$ is reached, after which the molecule buckles and forms interwinding structures. Beyond $\tau_{\text{crit}+}$, adding turns decreases the spatial extension of the molecule, since twist is converted into writhe. Undergoing the supercoiling phase transition. Schematically, we can see this as the DNA strand climbing the free energy hill (which we approximated harmonically in equation (4.62)) by applying the torque to the system before it reaches the top of this climb and starts to loop to release the strain, as shown in figure 4.9.

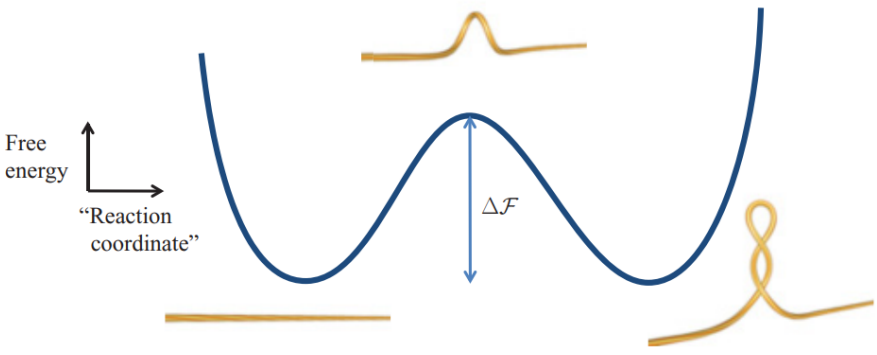

Figure 4.9: The free energy landscape of the straight and supercoiled states (taken from [44]).

There also exists a limit on how much negative torque we can apply $\tau_{\text{crit}-}$. Negative torque underwinds the helix and can promote local strand separation or denaturation at relatively small torques compared to the positive critical value [45]. Bryant et al.(2003) [43] determined the values for $\tau_{\text{crit}\pm}$ using relaxation curves of a bead applying torque on a 14.8 kbp long molecule as shown in figure 4.10.

$$\tau_{\text{crit}+} = 34\text{pNnm} \approx 8.3 k_B T/\text{rad} \tag{4.64}$$
$$\tau_{\text{crit}-} = -9.6\text{pNnm} \approx -2.3 k_B T/\text{rad} \tag{4.65}$$

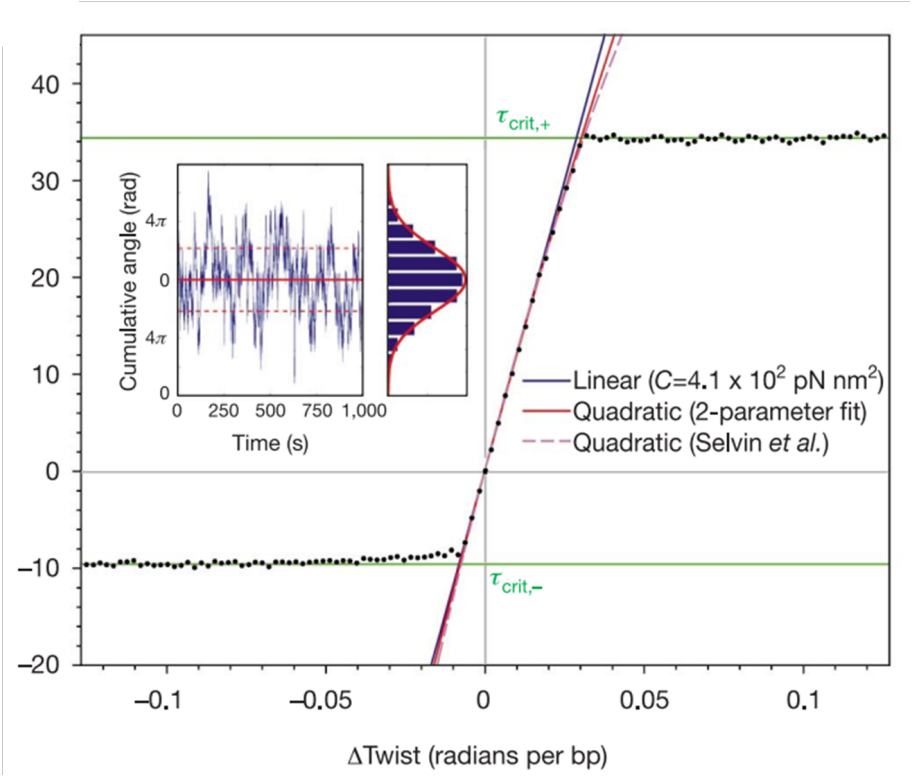

Figure 4.10: Averaged twist elasticity data obtained by Bryant et al. (2003) [43], with clear indications of $\tau_{\text{crit}\pm}$.

The system's closure is regulated by the closing strength K'. Due to the tight nature of this closing, we predict a relatively strong K' compared to the fundamental K_0 coupling. But as we will see, neither the qualitative nor the quantitative prediction of the MMP formalism is very sensitive to the strength of K'; it therefore suffices to take $K' \gtrsim 2K_0$. The global twist is stored between this closing spring and all other nodes in the system.
The global under/overwinding δL is limited by the global torque through an effective closing strength.

$$K'_{\text{eff}} = \frac{K_0 K'}{K_0 + N K' \tanh(1/2\lambda)} \tag{4.66}$$

Ideally, we decouple K' and δL entirely. The most obvious way would be to work in the rigid limit and to take $K' \to \infty$ in every equation we have come across. This is, however, unnecessary as the $NK' \tanh(1/2\lambda)$ term in the denominator will be of a greater order of

magnitude for any sensible choice of K', i.e. not a very soft closing spring. This is shown explicitly in figure 4.11.

$$K'_{\text{eff}} = \frac{K_0}{N \tanh(1/2\lambda)} \approx 4.11\text{nm} \tag{4.67}$$

Which can now be used to impose limits on the global twist.

$$\delta L_{\text{crit}+} = \frac{\tau_{\text{crit}+}}{K'_{eff}} \approx 2.0\text{rad} \approx 0.32 \text{ Helical turns} \tag{4.68}$$

$$\delta L_{\text{crit}-} = \frac{\tau_{\text{crit}-}}{K'_{eff}} \approx -0.57\text{rad} \approx -0.091 \text{ Helical turns} \tag{4.69}$$

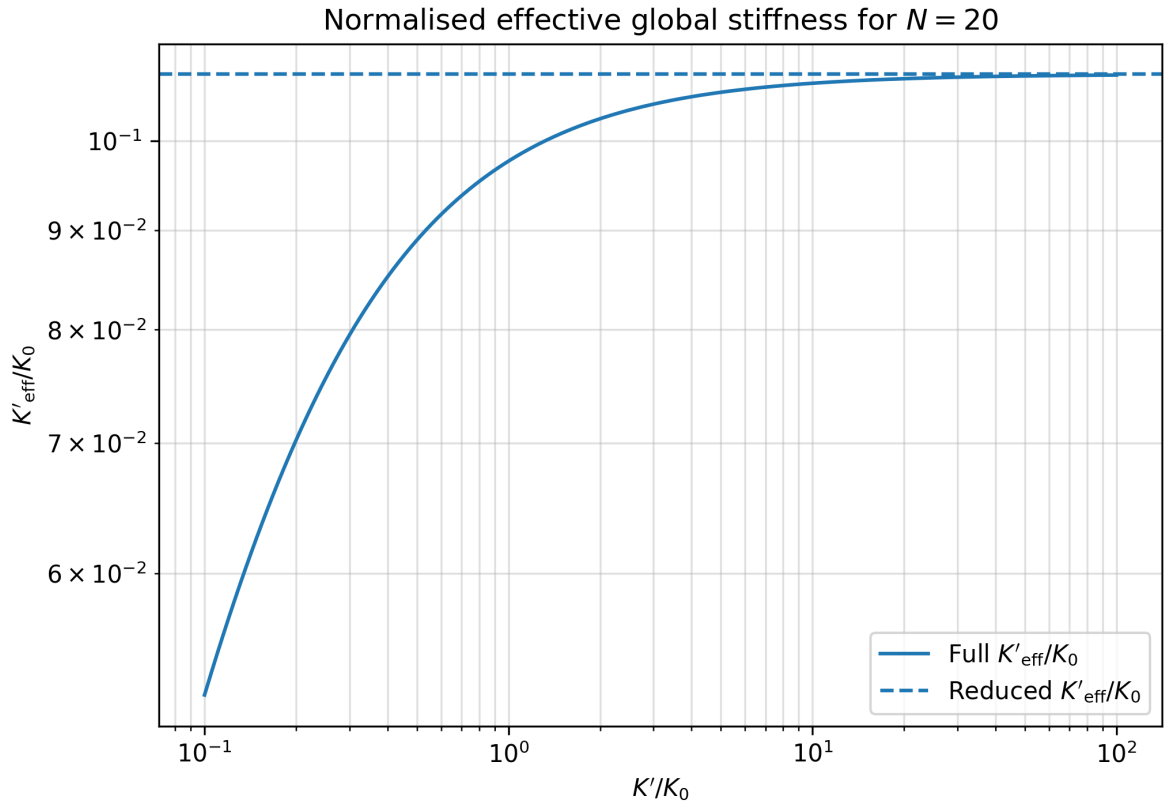

Figure 4.11: Comparison of the effective global closing spring.

4.3.3 Mismatches

We now consider the mismatching case in the Kac-Baker model, we fill in the free-energy penalty (3.12):

$$\Delta\mathcal{F}_m = \frac{1}{2}\log\left(1 + \frac{\delta K}{K_0}\coth\left(\frac{1}{\lambda}\right)\right) + \frac{K_0 + \delta K}{2}\delta a^2\left(\frac{1 - \coth(1/\lambda)}{1 + \frac{\delta K}{K_0}\coth(1/\lambda)}\right) \tag{4.70}$$

The matched-mode perturbation formalism cannot fully capture the free-energy penalty arising from a softening mismatch, as it predicts that the mismatch has a stabilising effect on the helix. Contradicting its definition.

An increase in entropy is natural to the model. The local softening increases the available states in phase space. It is therefore a natural choice to extract the softening parameter δK straight from this contribution. We invert the entropic contribution in equation (4.70).

$$\frac{\delta K}{K_0} = (\exp(-2\Delta\mathcal{S}) - 1)\tanh\left(\frac{1}{\lambda}\right) \tag{4.71}$$

In the original OWL sensor, the inhT mismatch is considered [10], which consists of a G-T mismatch flanked by matching T-A pairs. We fit this using the nearest-neighbour model, considering the mismatching AGC/TTC case from table 5 of Allawi and SantaLucia [46]. To get the full value of our model's ΔS, though, we must compare it with the matching case, which is found in Table 1 of the same paper and in [47].

$$\Delta S_{\mathrm{m}} = \Delta S_{GT} - \left(\Delta S_{AG/TC} + \Delta S_{GC/CG}\right) = 35.2 \pm 5.6\mathrm{eu} \tag{4.72}$$

We convert these entropy units back to the dimensionless value by dividing by $R = 1.987\mathrm{cal\,mol^{-1}\,K^{-1}}$, which gives:

$$\Delta\mathcal{S}_m = 17.7 \pm 2.8 \tag{4.73}$$

For any value within the confidence interval, however, the contribution of the exponential term is tiny compared to the order 1 term. This means that we can neglect this term, which yields:

$$\frac{\delta K}{K_0} \approx -\tanh\left(\frac{1}{\lambda}\right) \tag{4.74}$$

Exactly the stability condition for the local mismatch insertion (4.57). As this would make the model unstable, we deem this method insufficient to fit the parameter. Since we cannot infer them from the nearest-neighbour model, there is no direct determination of the mismatch parameters $\{\delta K, \delta a\}$, as both influence the overall free energy landscape.
Literature [48, 49, 20] suggests that the effect of the G-T mismatch on helical parameters or local twist is relatively minor compared with its destabilising effect on local pairing within the stacking environment. This is further supported by the sequence dependence of the thermodynamic effect of the mismatch [48].
In the matched-mode-perturbation formalism, this suggests treating the elastic response to the mismatch as a local softening effect in the system. We therefore expect the stiffness perturbation δK to be the leading coarse-grained parameter. To ensure we are working in the regime where the harmonic approximation holds and remains relevant, we choose its value to be in the range:

$$-0.6 \leq \frac{\delta K}{K_0} \leq -0.4 \tag{4.75}$$

The geometry-altering perturbation δa is interpreted as a smaller correction term that is important for coupling to the global deformation δL in the interaction term. Due to its local nature, we expect it to be significantly smaller. The interaction between the global strain and the mismatch is optimised if the effects present competing contributions, as we can infer from the extremum δL^* in equation (3.64). This suggests that for a twist-based sensor, the δa parameter is a small local underwinding of the helix.

$$\delta a \sim -10^{-2}\delta L_{\max} \tag{4.76}$$

There exists some evidence from molecular dynamics simulations supporting this claim in the context of G-T mismatches [50].

Heuristic argument

The formalism clearly omits some of the fundamental interactions of the DNA mismatch. We see this mainly in the stabilising energetic response independent of the sign of the local stiffness perturbation δK. To address this shortcoming, we must therefore include another additive effect in the local interaction potential, effectively modelling many factors not captured by this elastic approximation [51, 52].

$$\mathcal{V} = -\mathcal{E}_0 + \frac{K_0}{2}x^2 \tag{4.77}$$

To this end, we present a heuristic argument based on the rigid-body description of DNA shown in figure 4.12.

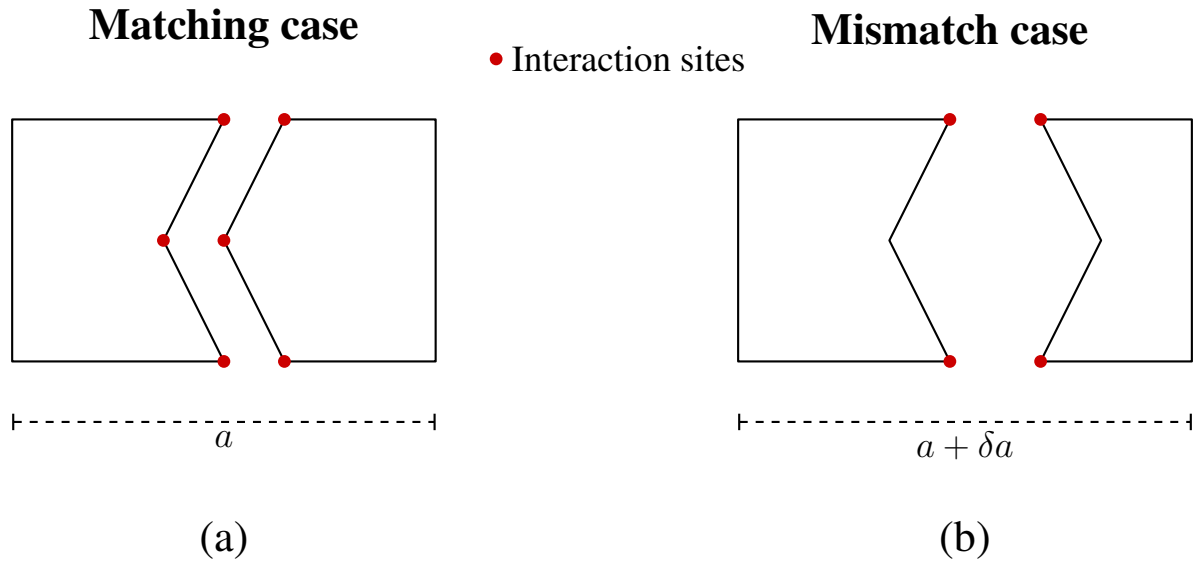

Figure 4.12: A heuristic argument for why a mismatch has a stabilising effect in the MMP formalism.

We presume each interaction site between the bases carries some effective energy background $\mathcal{E}_0$ plus the quadratic energy that our model captures. For the matching case, then:

$$\mathcal{V}_{\text{Match}} = -3\mathcal{E}_0 + \frac{3}{2}K_0(u-a)^2 \tag{4.78}$$

While the mismatch has only two interaction sites.

$$\mathcal{V}_{\text{Mismatch}} = -2\mathcal{E}_0 + \frac{2}{2}(K_0+\delta K)(u-a-\delta a)^2 \tag{4.79}$$

This interaction-site-based model thus indeed features a lower elastic energy component for the mismatch case than for the matching case. But due to the presence of the extra effective interaction, the matching case will have a lower overall potential-energy equilibrium, as shown explicitly in figure 4.13.

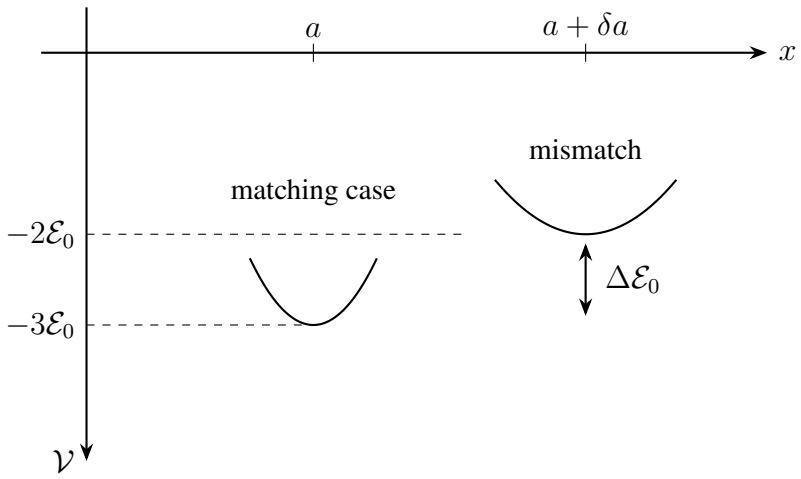

Figure 4.13: The potential energy of the matching case is lower in the equilibrium state due to the presence of an additional stabilising interaction site.

The free-energy-interaction term is the fundamental quantity of this thesis and is only connected to the global strain through the MMP formalism. The additive energetic contributions, which capture the other effective parameters, will consequently not influence this. We can therefore safely ignore these effects.

4.3.4 The Interaction Term

The lack of certainty about the mismatch-dependent parameters introduces some ambiguity into the model, but this does not prevent us from establishing a quantitative free-energy interaction term. It is given by:

$$\begin{aligned}\Delta\Delta\mathcal{F} =& \frac{1}{2}\log\left(1 - \frac{K'\delta K\tanh(1/2\lambda)^2}{(K_0 + NK'\tanh(1/2\lambda))(K_0 + \delta K\coth(1/\lambda))}\right)\\ &+ \frac{K'}{K_0}\frac{\tanh(1/2\lambda)}{D}\left[\frac{K'\delta L^2}{2}\frac{\delta K\tanh(1/2\lambda)}{K_0 + NK'\tanh(1/2\lambda)}\right.\\ &+ \frac{(K_0+\delta K)^2\delta a^2}{2}\frac{\tanh(1/2\lambda)}{K_0 + \delta K\coth(1/\lambda)}\\ &\left.- (K_0+\delta K)\delta a\delta L\right]\end{aligned} \tag{4.80}$$

Rigid limit

Another source of ambiguity is the strength of the global strain K'. However, as shown in figure 4.14, the interaction term quickly converges to its rigid limit value. A derivation of the general rigid-free-energy-interaction term is found in appendix B.5. For the Kac-Baker

couplings, it is given by:

$$\begin{aligned}\Delta\Delta\mathcal{F}_r = \frac{1}{2}\log\left(1 - \frac{\delta K \tanh(1/2\lambda)}{N(K_0 + \delta K \coth(1/\lambda))}\right) \\ + \frac{K_0}{N(K_0 + \delta K \coth(1/\lambda)) - \delta K \tanh(1/2\lambda)}\left[\frac{\delta K}{2N}\delta L^2\right. \\ \left. - (K_0 + \delta K)\delta a \delta L + \frac{(K_0 + \delta K)^2 \delta a^2}{2}\frac{\tanh(1/2\lambda)}{K_0 + \delta K \coth(1/\lambda)}\right]\end{aligned} \tag{4.81}$$

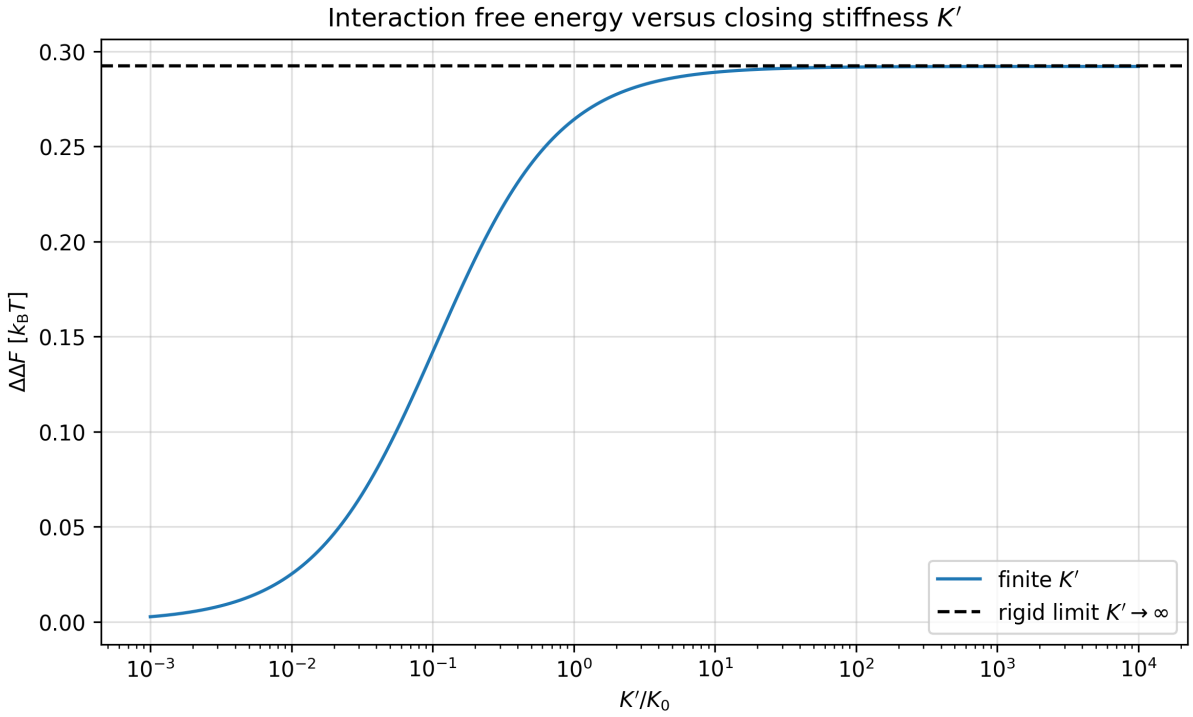

Figure 4.14: Convergence of the free-energy-interaction term to the rigid limit.

The motivation of this rigid limit lies in the architecture of the OWL sensor itself [10]. As explained in detail in the introduction, a large part of the improved mismatch selectivity is attributed to the nearly circular geometry of the SNV-matching probe (P) strand. Its 3' and 5' ends are stabilised by stacking interactions, creating what is described as a structural lock [11]. The resulting global constraint in our model must therefore act as a mechanically significant closing spring with an effective stiffness expected to exceed the intrinsic stiffness of the linear branch. For the relevant parameter set, choosing $K' \gtrsim 2K_0$ is sufficient to remain within 5% of the exact result as shown in figure 4.15. Due to the model's coarse-grained nature, this approximation error is minor compared to the inherent uncertainty linked to the effective parameters. This makes the rigid limit a natural approximation of the system's global constraint.

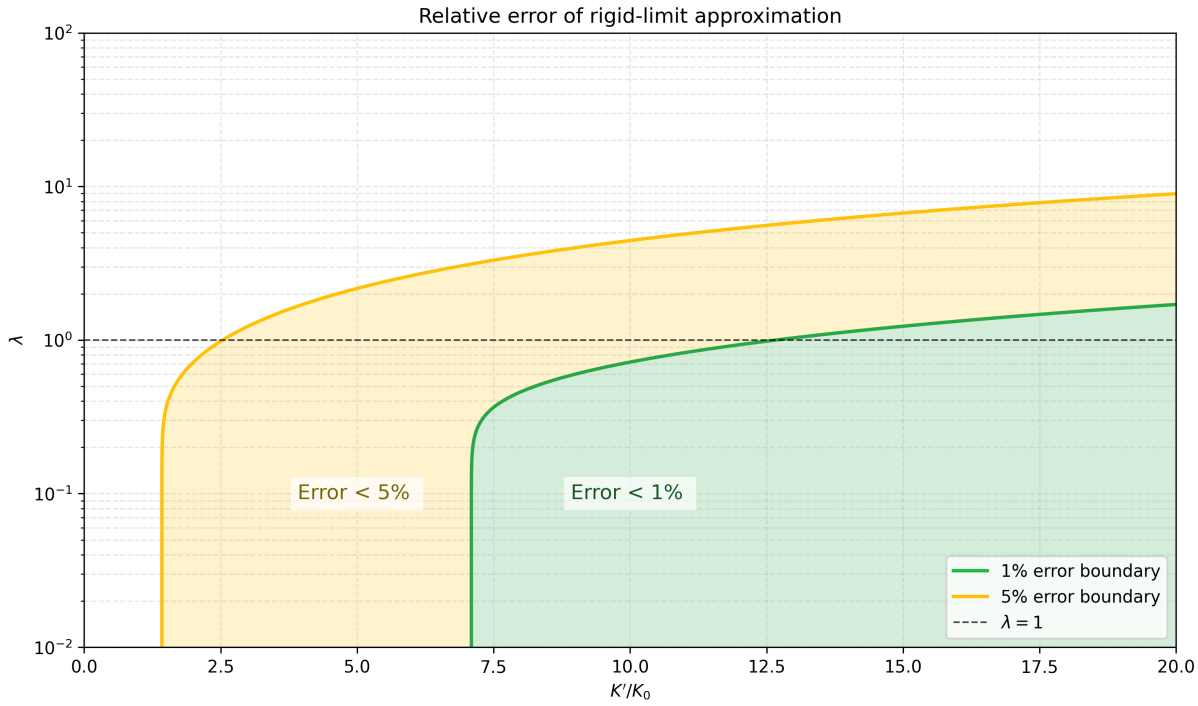

Figure 4.15: Relative error of the rigid limit interaction free energy.

Quantitative analysis

We can now consider a quantitative analysis of the interaction term. The amount of deformation theoretically maximising the free-energy interaction term in the rigid limit is independent of the model as the $1/K'$ term in equation (3.64) drops.

$$\delta L^* = N\delta a\left(1 + \frac{K_0}{\delta K}\right) \tag{4.82}$$

Dependent on the mismatch parameters, this yields two cases which we plot for $\delta a = -0.12\text{rad}$ in figure 4.16:

$$\delta L^* > \delta L_{\max} \quad \text{(Limited case)} \tag{4.83}$$
$$\delta L^* \leq \delta L_{\max} \quad \text{(Optimal case)} \tag{4.84}$$

We first consider a limiting case in which the optimal interaction term is constrained by the allowed range of δL, as shown in figure 4.16. This yields a monotonic increase in destabilisation from the interaction term. The sensor thus operates in a regime where achievable selectivity is limited by the maximum torque that can be imposed globally before supercoiling, rather than by the intrinsic optimum of the interaction term. Optimising sensor performance is therefore impossible, as it would require driving the system close to the supercoiling phase transition, which proceeds via an unstable equilibrium state [44], as shown in figure 4.9.

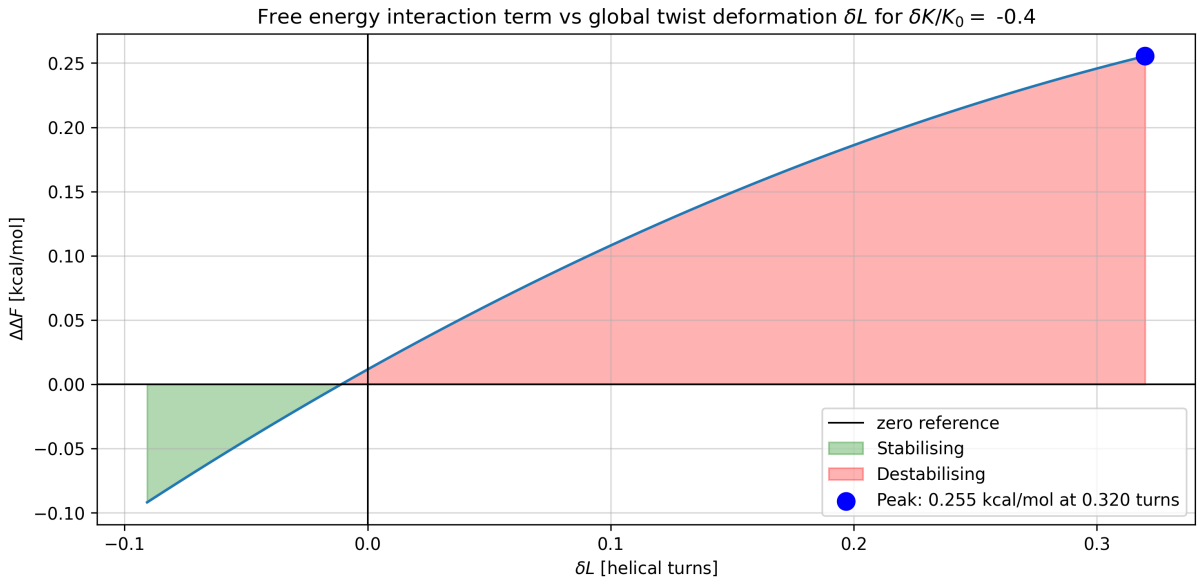

Figure 4.16: Limited case of interaction: The mismatch is not softening enough for the manifestation of a maximum in the free-energy interaction term

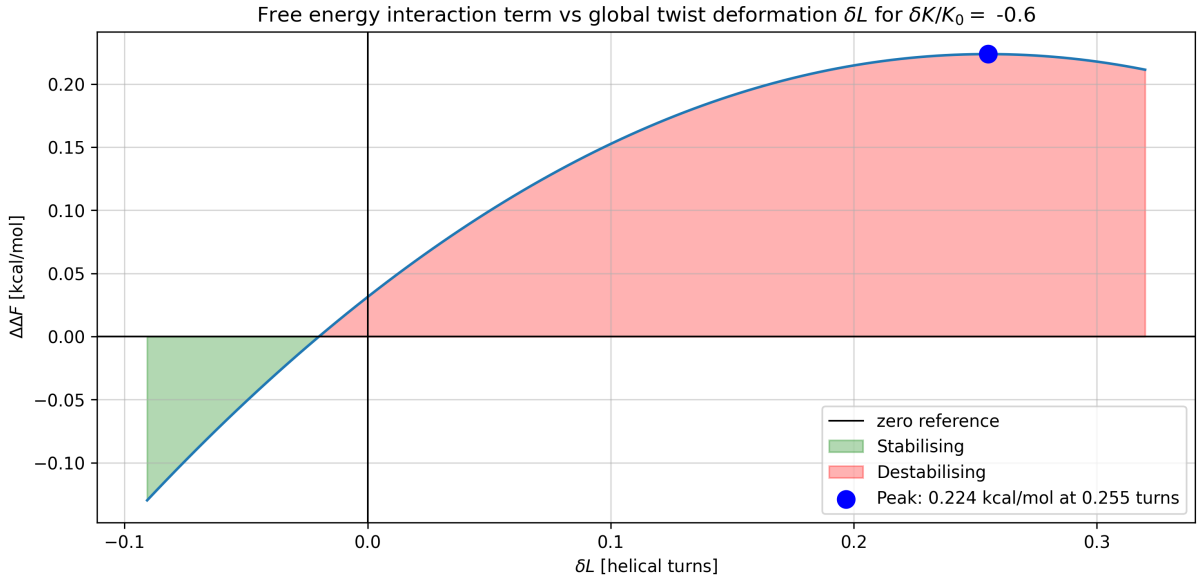

Figure 4.17: Optimal case of interaction: The mismatch is softening enough for the manifestation of a maximum in the free-energy interaction term

More interesting is the optimal case, which, in principle, allows us to optimise sensor performance within the allowed deformation range. Physically, the maximum arises due to the switch from a competing to a cooperative effect. While initially, the increase in global deformation increases the coupling between the mismatch and the imposed strain, this is no longer the case beyond δL^*. The over-application of the global strain starts to compensate for any mismatch-related effects at the local site, leading to a decrease in the interaction term. In the rigid limit approximation, the optimal interaction term depends only on the

mismatch-related parameters.

$$\Delta\Delta\mathcal{F}_r^* = \frac{1}{2}\log\left(1 - \frac{\delta K \tanh(1/2\lambda)}{N(K_0 + \delta K \coth(1/\lambda))}\right) - \frac{(K_0+\delta K)^2 \delta a^2}{2\delta K(1 + \frac{\delta K}{K_0}\coth(1/\lambda))} \tag{4.85}$$

Dependent on the exact combination of the mismatch parameters, this optimum lies within the ballpark of the interaction term reported by Stulens *et al.* of around 0.26 kcal/mol. The accessible region allows for higher values than this, though, as shown in figure 4.18. As we currently do not fully capture the effect of a mismatch in the model, this result can help us further narrow the parameter space. It suggests that we should explore the regime of significant softening, where a mismatch yields a local coupling strength around 40% of that in the matching case. Whilst also limiting the local structural perturbation δa to values slightly stricter than the originally proposed $-10^{-2}\delta L_{\max}$.

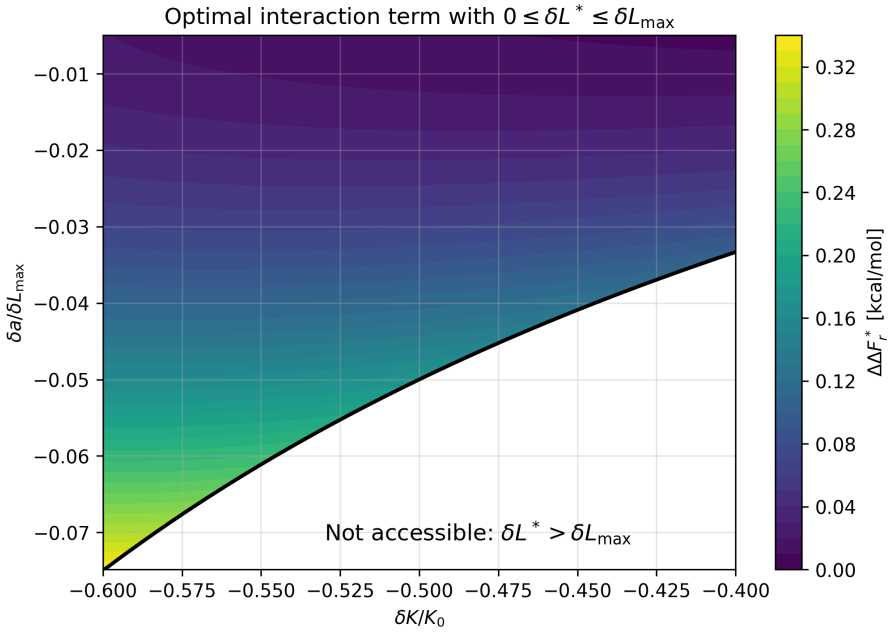

Figure 4.18: Optimal interaction term in the approximate accessible parameter space of the mismatch.

Figure 4.18 shows that the parameter space slightly shifts the optimal working regime. The value of the optimal interaction term varies less with the softening effect than with the local geometric perturbation. This is also evident in equation (4.85). The entropic term is strongly suppressed by the system size $N = 20$ compared with the $\mathcal{O}(1)$ terms that remain after cancellation of the K_0-dependent terms by the choice $\delta K \propto -K_0$. We therefore expect the optimal working regime to be dominated by the energetic interaction term. This scales quadratically with the δa parameter, making it relatively more important than the local softening. We must note, though, that the accessibility of the optimum, i.e. its position (4.82), is determined equally by both.

Finally, we note the dependence of the interaction term on the system size N. For twist-based sensors, this is not a suitable reference, as it immediately alters the system's helical periodicity. For OWL sensors, the interaction term disappears unless the probe size is finely tuned to 9 base pairs [10]. However, single-molecule force spectroscopy has revealed that

mismatches alter the force-extension response, which leads to changes in the free-energy landscape of hairpin formation [53], for example, suggesting that, after the appropriate coarse-graining, other inter-base-pair step coordinates can be modelled by the present formalism. This could present opportunities to develop even smaller sensors.

5 Source of Strain

The previous chapters provide an overview of the analytical model we developed for the strain-mismatch interaction in DNA. As we have established, though, the formalism needn't be limited to torque-based sensors. For OWL sensors, there are strong indications that this is indeed the case, but no guarantee. In this chapter, we identify the source of strain in an OWL-like sensor using a combination of molecular dynamics simulations with the LAMMPS oxDNA2 module and base-pair step analysis in 3DNA.

5.1 OxDNA

Contemporary simulations of DNA consist of two main classes. Monte Carlo-based simulations (e.g., the cgDNA model we described earlier [25]) sample states according to the Boltzmann distribution and subsequently yield parameters after analysis. And molecular dynamics (MD) simulations. This method involves numerically integrating the classical equations of motion. This can be combined with stochastic dynamics via a Langevin integrator [54]. For complex systems involving multiple bound DNA strands, this is often preferred because these systems must access states that are difficult to reach with equilibrium sampling. The computational power required to integrate all translational and rotational degrees of freedom of all atoms grows quickly with system size, however. To this end, the coarse-grained molecular dynamics oxDNA model was developed [55], capturing all essential physics while remaining computationally efficient. It achieves this by approximating DNA as rigid nucleotide structures, coarse-graining the underlying atomic structure.

5.1.1 OxView

One of the major challenges of simulating DNA nanostructures is their construction. For setting up oxDNA simulations, the web-based structure builder and editor oxView was developed by the Šulc group [56, 57]. This allows the construction of sequence-dependent many-strand systems and the modification of their backbone structure. This structure can subsequently be exported as native oxDNA topology and configuration files. The topology file contains all sequence-dependent information and backbone connections, while the configuration file records the initial positions and orientations of all rigid nucleotides. Initial pre-equilibration, the relaxation of highly constrained systems, is also possible on oxView via base-cluster formation and rigid-body dynamics of the backbone. Our interpretation of an OWL sensor before equilibration in oxView is shown in figure 5.1, where the bottom-left bound strand represents the SNV-matching probe region.

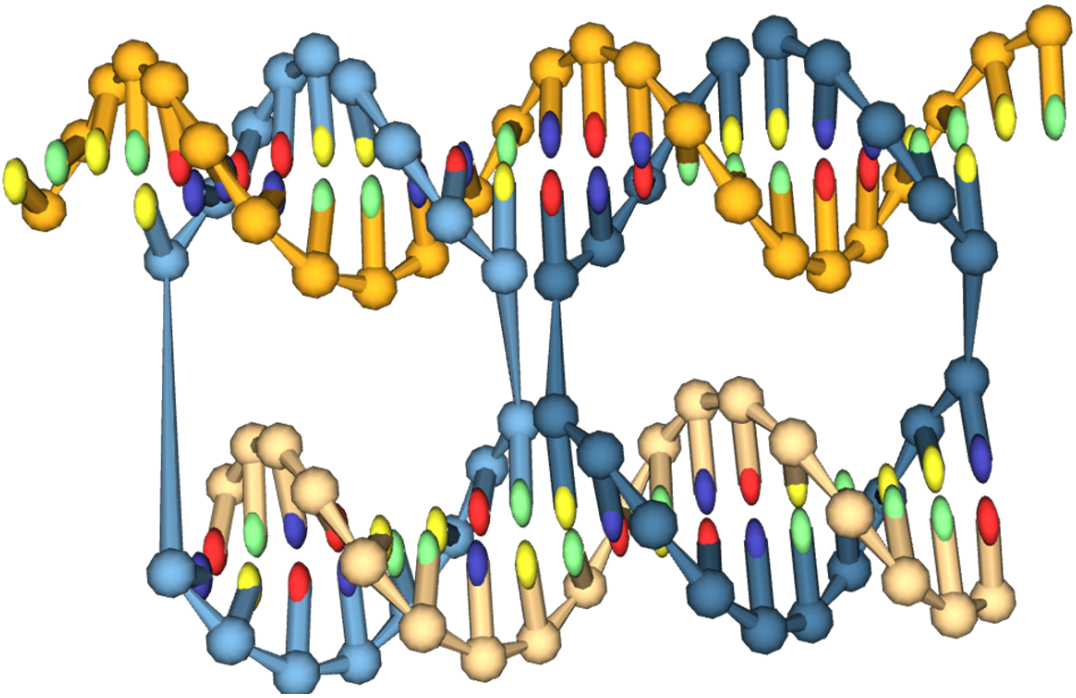

Figure 5.1: Initial oxView representation of the unequilibrated OWL-like sensor. The SNV-containing target is bound in the bottom-left region. (Figure created with OxView [56, 57])

OxView also provides a visual interpretation of the system's dynamics: all simulated timesteps in the trajectory can be played sequentially as a video, which is useful for debugging unphysical phenomena and for generating visuals.

5.1.2 Underlying Physics

We base our discussion on an introductory paper by Sengar *et al.* [58].
The version we use, oxDNA2, is a sequence-dependent model that treats nucleotides as rigid building blocks and accounts for groove asymmetry in DNA [59]. The differences between the several versions of oxDNA are relatively minor for the purposes of this thesis, so we refer to it as oxDNA from here. The oxDNA model consists of bonded interactions between nearest-neighbour backbone nucleotides and non-bonded interactions between nucleotides on the same or different backbones, as shown in figure 5.2. These depend only on the relative orientation between the relevant rigid bases. Each nucleotide is modelled using an internal reference frame defined by two orthogonal vectors that modulate these interactions: the $\mathbf{n}$ vector, along the helical direction, captures backbone and stacking interactions, while the $\mathbf{b}$ vector represents the hydrogen-bonding plane. These combine to give the following potential energy, a sum of pairwise contributions:

$$V_0 = \sum_{\langle ij \rangle} (V_{\text{backbone}} + V_{\text{stack}} + V'_{\text{exc}}) + \sum_{i,j \notin \langle ij \rangle} (V_{\text{H-Bond}} + V_{\text{cross stack}} + V_{\text{exc}} + V_{\text{coax}}) + V_{\text{DH}} \quad (5.1)$$

Where the first sum runs over neighbours $\langle ij \rangle$ along the same single strand, while the second sum goes beyond single-stranded interactions. The potentials have the following interpretations:

- V_{backbone}: Connectivity between neighbouring bases via the backbone. This potential is modelled by Finite-Extensible-Nonlinear-Elastic (FENE) springs that mimic the covalent bonds along the strand. It is the only potential that is independent of the orientation of the nucleotides.
- V_{stack}: Stacking interactions between adjacent bases on the same strand. The equilibrium length of this stacking interaction is deliberately chosen to be shorter than the backbone equilibrium length, such that helical stacked structures form naturally.
- V'_{exc} and V_{exc}: Excluded volume interactions between adjacent bases and non-adjacent bases, respectively.
- $V_{\text{H-Bond}}$: Hydrogen bonding between opposing bases. Non-complementary base pairing results in weaker hydrogen bonding, allowing mismatches to be modelled [60].
- $V_{\text{cross stack}}$: Stacking interactions between bases on other strands.
- V_{coax}: Coaxial stacking interactions between bases across strand ends. This interaction is important in our context as it generates the locked ends in the OWL structure.
- V_{DH}: Debye-Hückel electrostatic interaction, representing screened electrostatic repulsion between DNA backbones in solution. Only present in the OxDNA2 model.

For exact forms of these potentials, we refer the reader to Ouldridge *et al.* [61].

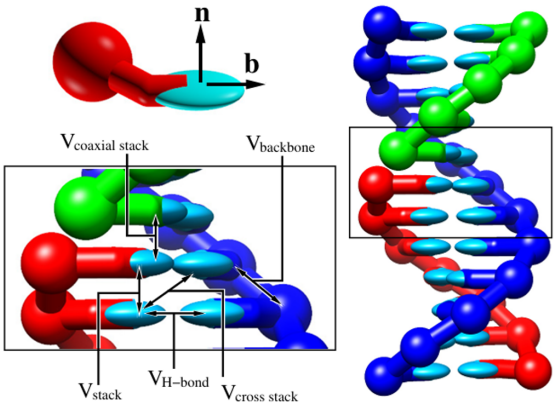

Figure 5.2: OxDNA interactions are orientation-based between nearest neighbours (figure adapted from [62])

5.1.3 Pipeline

LAMMPS

OxDNA also has the advantage of being available as a Large-scale Atomic/Molecular Massively Parallel Simulator (LAMMPS) package [63, 64]. Albeit with some minor modifications to the parametrisation of the quaternion coordinates used by oxDNA to the three-dimensional coordinates used by the LAMMPS rigid body integrator. To convert any oxDNA/OxView-related files to LAMMPS-related files and back, we used the helpful tacoxDNA software [65]. Most significantly, it allows us to convert the complex geometry we build in OxView (see figure 5.1) to a LAMMPS configuration file describing initial conditions of all particles/bonds

in the system. For the input file required by LAMMPS, we based ourselves on a file by Matthies *et al.* [55]. This utilises an oxDNA2 NVE-type rigid-body integrator with Langevin thermostat to include stochastic dynamics.

3DNA

Since oxDNA is a coarse-grained model, the full atomistic structure of the helix is not considered by either oxDNA or LAMMPS. For further analysis, we use the TacoxDNA converter to generate a Protein Data Bank (PDB) file. This conversion retains the position and orientation of each coarse-grained nucleotide and constructs an approximate atomistic representation of the corresponding base and backbone geometry. This also allows us to construct the rigid-block structure we saw in cgDNA (see e.g. figure 4.1). We visualise, using ChimeraX [66], both the full-atomistic model and the rigid-block-nucleotide structure in figure 5.3. We note the atomistic representation of the ends of the strands in figure 5.3a. This particularly highlights the coaxial stacking interactions that give rise to the locked-ends OWL structure.

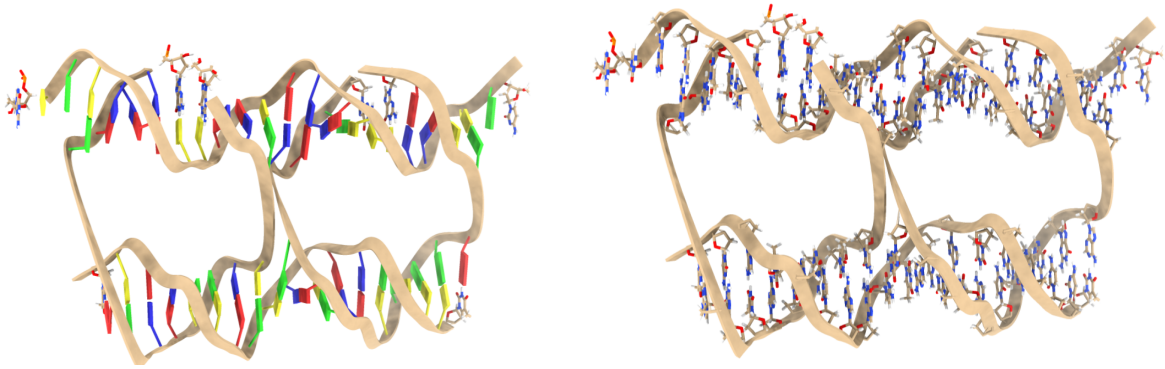

(a) (b)

Figure 5.3: A comparison of the rigid-block-nucleotide structure and full atomistic resolution of the same OWL structure created in oxView in figure 5.1. (Figures made with ChimeraX [66]) (a): Rigid-block nucleotide structure of the OWL sensor, the colour coding is as follows: A = red, T = blue, G = green, C = yellow. (b): Full atomistic model of the OWL sensor. Note that this is an approximation made by the converter, and the atomistic model is not used in simulations.

We analysed the rigid-body structure in the PDB file using 3DNA [67]. Software specifically designed to identify and analyse base interactions in PDB files of nucleic acids by constructing an internal reference frame for each base. For residues in close contact, i.e., base pairs, it builds a similar quadratic matrix-based approach to cgDNA to determine a set of rigid-body parameters, which are shown in figure 5.4.

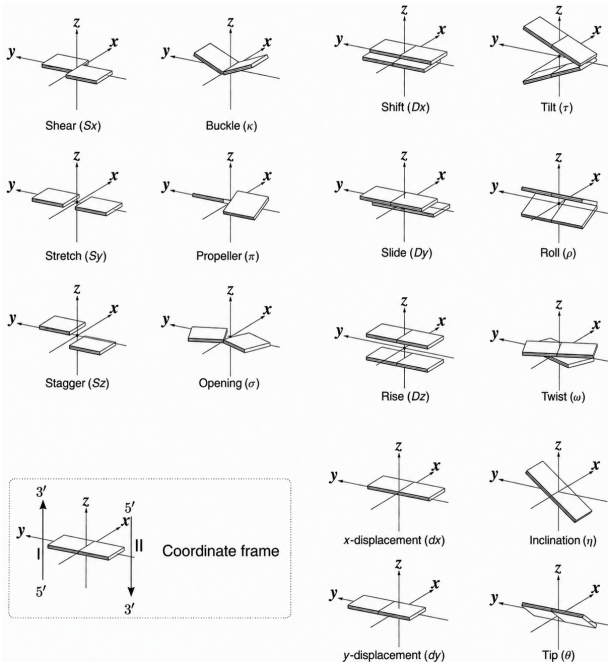

Figure 5.4: 3DNA rigid-body base parameters, 6 intra base-pair (Shear, Buckle, Stretch, Propeller, Stagger, Opening), 6 inter base-pair (Shift, Tilt, Slide, Roll, Rise, Twist) and 4 helical parameters (x-, y-displacement, Inclination, Tip). (Figure from [67])

To determine the source of strain in OWL sensors, we construct several OWL-like geometries and compare the relative values of the inter-base-pair 3DNA parameters for the SNV-matching probe strand. To do this, we developed the pipeline shown in figure 5.5. The structures are first designed in oxView and then exported as oxDNA topology and configuration files. These are subsequently converted using tacoxDNA into a LAMMPS configuration file, combined with a universal input file. In LAMMPS, the system is first equilibrated, after which trajectory steps are sampled. Since the saved LAMMPS coordinates may wrap around the periodic simulation box, the selected frames are unwrapped before being converted back to oxDNA files, which are then immediately converted to PDB files. 3DNA then identifies all base pairs, constructs the base-pair reference frame, and finally analyses the inter-base-pair-step coordinates.

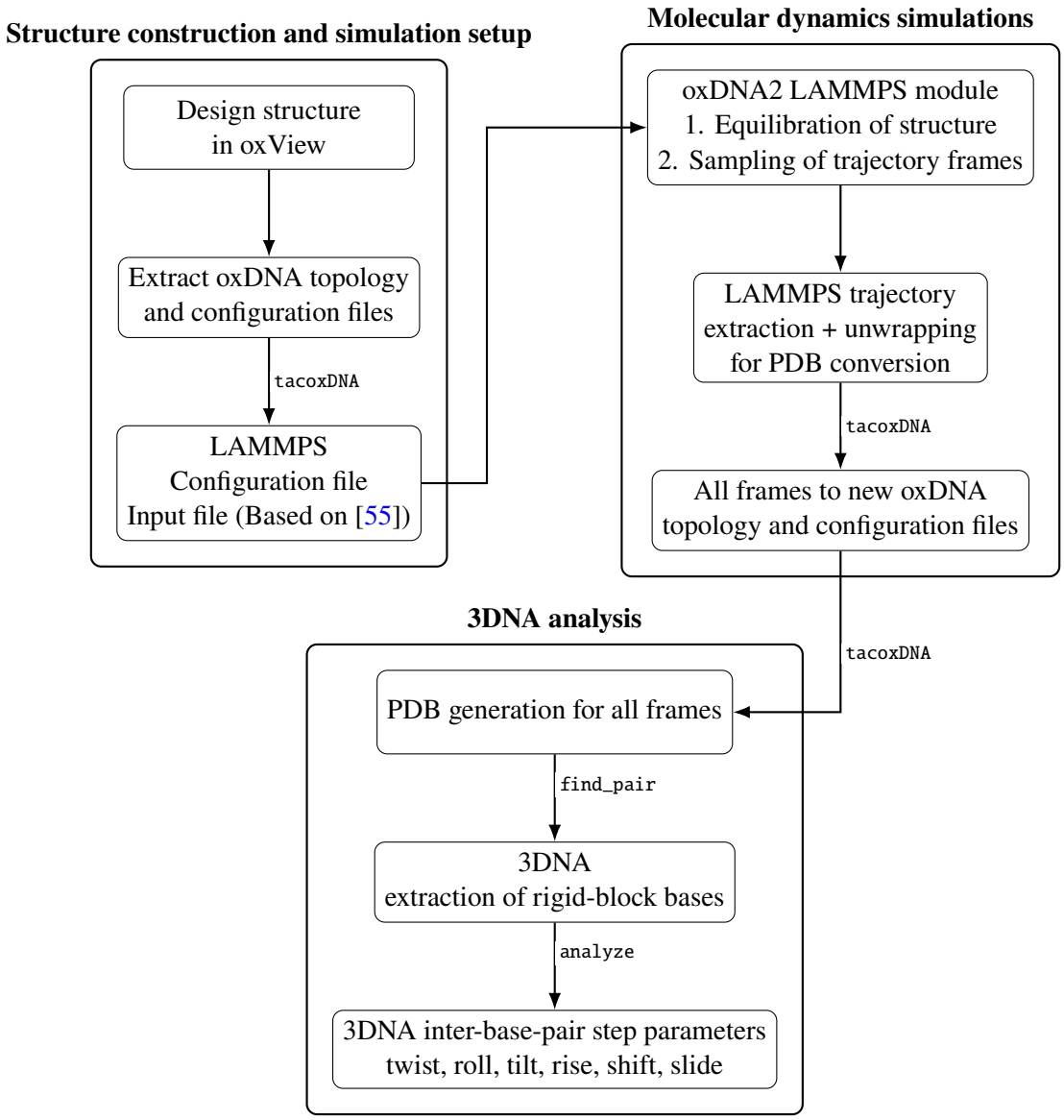

Figure 5.5: The pipeline to investigate inter-bp-step 3DNA parameters from a structure initially built in oxView.

5.2 Structural Comparison of OWL Geometries

5.2.1 Investigated geometries

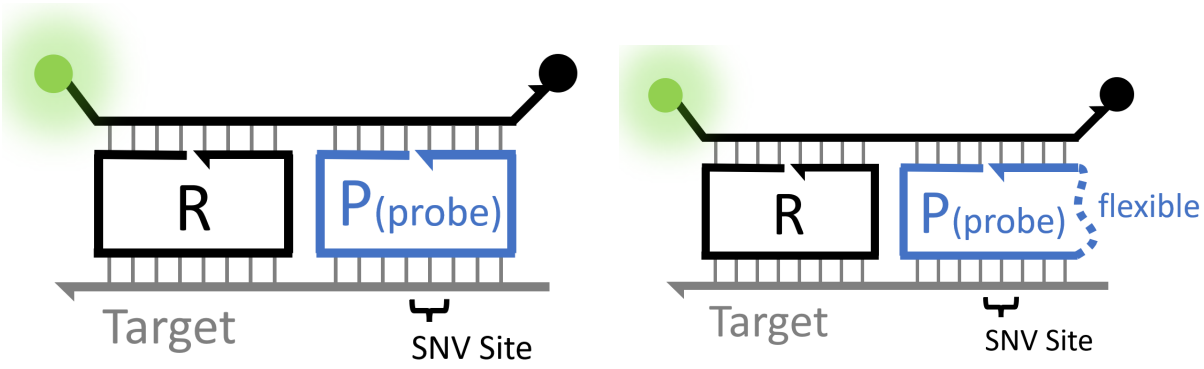

(a) (b)

Figure 5.6: Schematic of strained OWL sensors (a) and OWL sensors closed by a flexible linker relieving strain. (Figures from [1])

Multiple designs were considered when OWL was first conceived by Karadeema *et al.* [10]. The main difference between the designs is the number of nucleotides hybridising to the target strand in both the P and R strands, as shown in figure 5.6a. The most stable design was the R_{10}/P_{10} design, in which both strands hybridise with 10 nucleotides to the target strand. However, this structure is stable enough to accommodate a mismatch and thus is not selective towards the SNV-binding analyte. The best design appears to be the R_{10}/P_9 design, which consistently distinguishes SNVs from the wild-type DNA background. This is why the twist parameter was considered responsible for the strain in the complex, as 9 nucleotides create an imperfect helical structure compared with the 10-nucleotide counterpart. This provides the first useful comparison between the 9-bp-binding OWL9 and the 10-bp-binding OWL10.
Another way to relieve the strain in the sensor is the introduction of a flexible linker, as shown in figure 5.6b [1]. We cannot model this exactly in oxView, so we simulate it by cutting the backbone connecting the lower and upper parts of the P strand of the OWL9. We refer to this as OWL9-cut. All three designs are shown after equilibration in figure 5.7. Once again, we place the SNV on the lower left double strand.

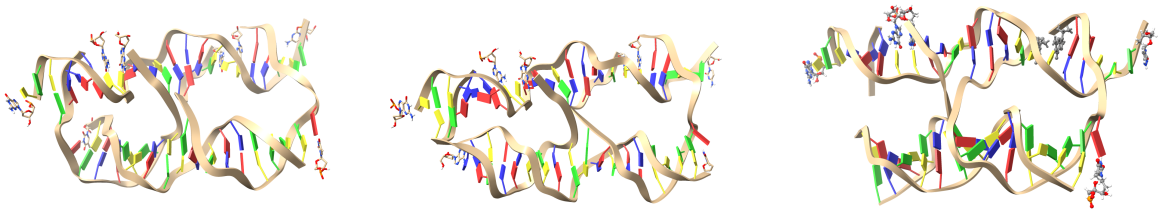

(a) OWL9 (b) OWL10 (c) OWL9-cut

Figure 5.7: Comparison of the three OWL designs, strain should be relieved in (b) and (c). (Figures made with ChimeraX [66])

For each geometry we compare, we sampled 10^7 timesteps to obtain precise results, reducing uncertainty in almost all cases to a level small enough for qualitative statements. An easy way to see this is that the Standard Error of the Mean (SEM) error bars are not distinguishable in most plots, even though they are present. We then compare the three structures to each other and to expected values in B-DNA as listed in Olson *et al.* [68].

5.2.2 Twist

As we expect the helical imperfection in OWL9 to be the primary source of strain in the system, we first consider the twist parameter of the SNV-matching strand. Plots of the relative twist between the rigid-base-pair steps are given in figure 5.8 in units of degrees.

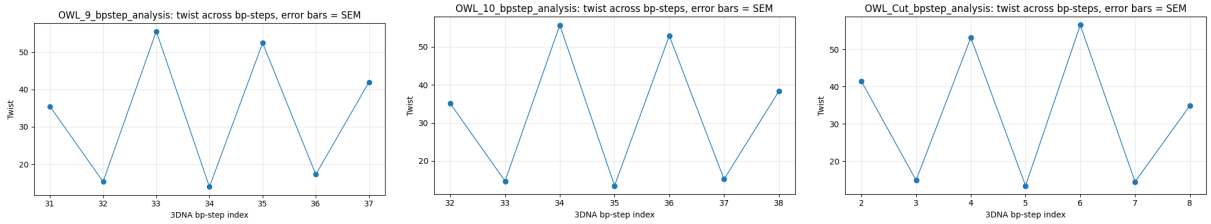

(a) OWL9 (b) OWL10 (c) OWL9-cut

Figure 5.8: Comparison of twist between the three designs from figure 5.7.

All three structures exhibit nearly identical twist distributions along the probe strand as the twist fluctuates around the B-DNA equilibrium value of approximately 36°. No significant difference is observed between the strained OWL9 and its less strained counterparts. This suggests that twist is not the primary source of strain in the OWL9 sensor, as we expect it to yield a global deformation, yet none is observed.
We observe strong oscillations in the twist parameter between base-pair steps in all cases. This is unlikely to be due to global strain, as such strain should be relieved in OWL9-cut and, to a lesser extent, in OWL10. This is supported by the fact that the oscillations average around the canonical B-DNA value. Given the small error bars, the pattern is reproduced across many timesteps, ruling out thermal fluctuations. A possible explanation is sequence-dependent local geometry: the same sequence is analysed in all three designs, and neighbouring base-pair steps can have distinct preferred twist values due to their local stacking interactions. Similar sequence-dependent variations have been observed in other sequence-dependent simulations before [69, 70].

5.2.3 Bending

The largest differences between OWL9, OWL10, and OWL9-cut are observed for the two bending parameters, tilt and roll.

Tilt

For the tilt parameter, shown in figure 5.9, we observe a significantly different distribution for OWL9-cut compared with the closed-loop OWL9 and OWL10. As tilt represents bending transverse to the helical axis, this can be interpreted as the upper part of the sensor's P

strand pulling the lower strand towards it. This is even visible in figure 5.7 for both the equilibrated OWL9 and OWL10 designs. The equilibrium tilt of B-DNA is around 0°, so any significant deviation from zero indicates bending strain on the local geometry. This suggests that the imposed strain is expressed as a deformation of the local tilt parameter. The deformation is somewhat larger in OWL9 than in OWL10, while it is nearly absent in OWL9-cut.

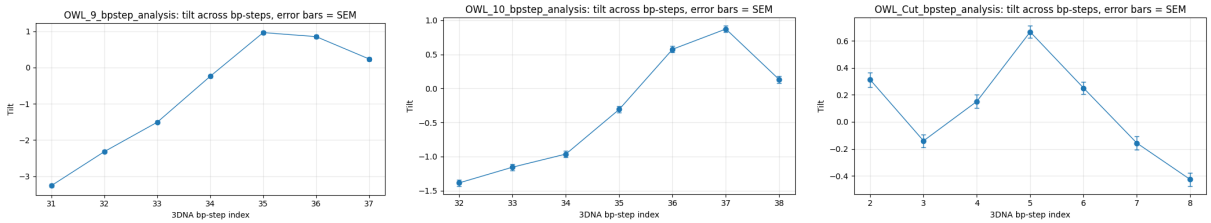

(a) OWL9 (b) OWL10 (c) OWL9-cut

Figure 5.9: Comparison of tilts between the three designs from figure 5.7.

Roll

Roll represents bending of the local helical axis in the groove direction and is expected to be close to 0° as well. As shown in figure 5.10, the roll profiles display a similar qualitative behaviour to the Tilt profiles. OWL9 and OWL10 both show a broad positive Roll deformation along the probe strand, with the deformation appearing stronger in OWL9 and again, providing evidence that the closed-loop structure provides a contribution. The OWL9-cut structure also exhibits a nonzero bending profile, suggesting that loop-closing cannot be the sole contribution.

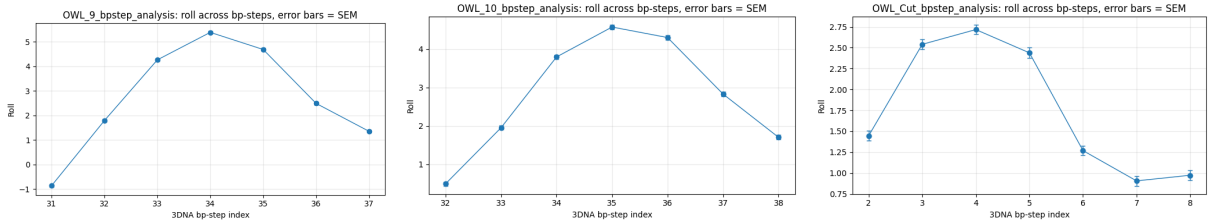

(a) OWL9 (b) OWL10 (c) OWL9-cut

Figure 5.10: Comparison of rolls between the three designs from figure 5.7.

The larger deviation from the equilibrium values in OWL9 compared with OWL10 suggests that the same amount of bending is imposed on the shorter hybridised strand. The missing base pair in OWL9 does not appear to introduce a qualitatively different deformation, as suggested by the proposed helical imperfection, but rather concentrates the imposed deformation over a shorter bound strand. This could explain why the OWL9 design is more sensitive to mismatches than the OWL10 design.
The other parameters do not exhibit any significant deviation between the geometries. Plots for these are therefore redacted to the appendix C.1.

6 Conclusions

6.1 Analytical Model

The matched-mode perturbation formalism from which we built our analytical model provides promising insights into DNA mechanics. Since it is entirely general to systems with quadratic degrees of freedom, it can be used to describe a multitude of perturbations to DNA or other elastic systems. It gives an intuitive explanation of how an interaction term arises between the MMP and how a non-zero mixing term $\langle \hat{s} | \hat{K}_0^{-1} | \hat{t} \rangle$ is a signature of interaction. The quadratic form of the free-energy interaction term with respect to the force terms also makes it relatively easy to analyse and interpret results.
The correct coarse-graining procedure is important for this, as it determines the matrix elements that govern the exact effect of the perturbations on the system. The fact that coarse-graining generates long-range couplings, together with its mathematical elegance, makes the Kac-Baker model a natural candidate for a one-dimensional base model of DNA. Its current circulant form somewhat limits its use for purely local effects, as it lacks correlations beyond next-nearest neighbours. This limitation can be addressed by abandoning the idea of translational invariance, albeit at the cost of losing some general results for the circulant MMP formalism and making it harder to find a closed-form expression for the eigenvalues.

6.2 The Strain-Mismatch Interaction

The MMP formalism offers a consistent explanation of the strain-mismatch interaction in strain-based biosensors and produces significant results. The interaction is guaranteed to have a destabilising regime under a positive harmonic strain, independent of the underlying base couplings. These sensors precisely require this to enhance their ability to distinguish mutations from wild-type DNA. Additionally, it allows us to identify a maximum in the free-energy interaction term, corresponding to the optimal working regime of the sensors, limited only by the mismatch-dependent parameters. For twist-based strain, quantitative analysis shows that this optimal working regime is accessible under certain assumptions about the elastic effect of the mismatch. This optimal working regime lies within a range that significantly stretches the limits of mutation detection.

6.3 Outlook

Molecular dynamics simulations of OWL-type sensors reveal a rather surprising result: strain is mainly manifested in local bending parameters. Fortunately, the model's generality also allows us to describe this after refitting the strain- and mismatch-dependent parameters. It also shows that there are several ways to induce strain due to DNA's unique geometric features. The main result of the thesis is thus best shown by figure 6.1, which is an arbitrary representation of an optimisable interaction term for an arbitrary quadratic degree of freedom in DNA. Optimisable designs for strain-based biosensors are not limited to twist alone, which opens the door to more efficient mutation detection.

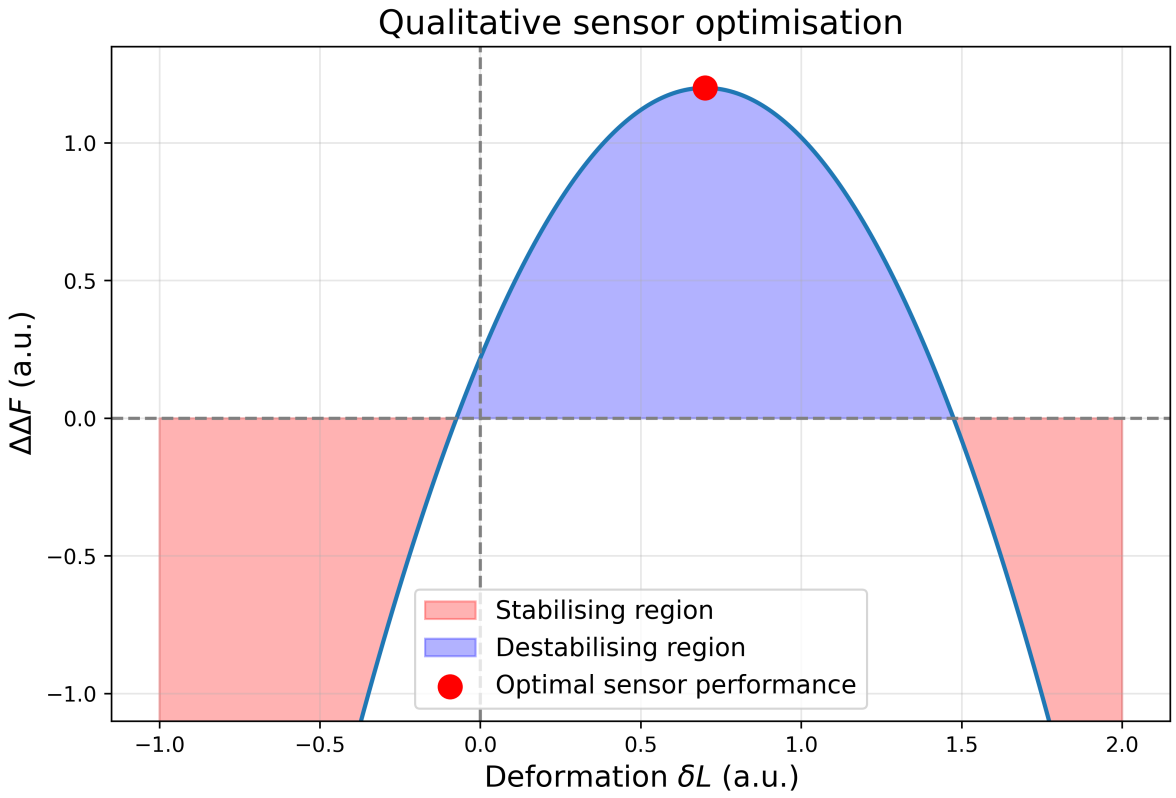

Figure 6.1: Qualitative plot of the interaction term. The analytical model shows that any suitable quadratic degree of freedom yields a significant destabilising region that allows for optimisation.

Bibliography

[1] Yannick Stulens et al. “Breaking the Limit of Hybridization Selectivity by Strain-forming Probes and Wild-type Blocker”. Unpublished manuscript.

[2] Liwei Ma et al. “Liquid biopsy in cancer: current status, challenges and future prospects”. In: *Signal Transduction and Targeted Therapy* 9.1 (Dec. 2024), p. 336. DOI: 10.1038/s41392-024-02021-w. URL: https://doi.org/10.1038/s41392-024-02021-w.

[3] Stefania Napolitano et al. “Liquid Biopsy at Home: Delivering Precision Medicine for Patients with Cancer During the COVID-19 Pandemic”. In: *The Oncologist* 27.8 (Mar. 2022), e633–e641. DOI: 10.1093/oncolo/oyac071. URL: https://doi.org/10.1093/oncolo/oyac071.

[4] Alex Nesta, Denisse Tafur, and Christine Beck. “Hotspots of Human Mutation”. In: *Trends in Genetics* 37 (Nov. 2020). DOI: 10.1016/j.tig.2020.10.003.

[5] Khin Zay Yar Myint et al. “Identification of circulating tumour DNA (ctDNA) from the liquid biopsy results: Findings from an observational cohort study”. In: *Cancer Treatment and Research Communications* 35 (Jan. 2023), p. 100701. DOI: 10.1016/j.ctarc.2023.100701. URL: https://doi.org/10.1016/j.ctarc.2023.100701.

[6] OpenAI. *Schematic Illustration of Circulating Tumour DNA (ctDNA) and Wild-Type DNA (wtDNA) Released by Tumour Cells into the Bloodstream*. Image generated using ChatGPT (GPT-5.5) by OpenAI. Generated on 20 May 2026. Available at: https://chat.openai.com/. San Francisco, CA, 2026.

[7] International Society of Genetic Genealogy. *Single-nucleotide polymorphism*. ISOGG Wiki. 2024. URL: https://isogg.org/wiki/Single-nucleotide_polymorphism (visited on 04/27/2026).

[8] Rebekka Van Hoof et al. “Depletion of wild-type target enhances the hybridization-based sensitivity of low-abundant mutation detection by reference capture probes”. In: *Sensors and Actuators B Chemical* 368 (June 2022), p. 132175. DOI: 10.1016/j.snb.2022.132175. URL: https://doi.org/10.1016/j.snb.2022.132175.

[9] Yannick Stulens et al. “Hybridization-based sensor with large dynamic range for detection of circulating tumor DNA in clinical samples”. In: *Biosensors and Bioelectronics* 281 (Apr. 2025), p. 117342. DOI: 10.1016/j.bios.2025.117342. URL: https://doi.org/10.1016/j.bios.2025.117342.

[10] Rebekah J. Karadeema et al. “The owl sensor: a ‘fragile’ DNA nanostructure for the analysis of single nucleotide variations”. In: *Nanoscale* 10.21 (Jan. 2018), pp. 10116–10122. DOI: 10.1039/c8nr01107a. URL: https://doi.org/10.1039/c8nr01107a.

[11] Brittany L. Mueller, Mark J. Liberman, and Dmitry M. Kolpashchikov. "OWL2: a molecular beacon-based nanostructure for highly selective detection of single-nucleotide variations in folded nucleic acids". In: *Nanoscale* 15.12 (Jan. 2023), pp. 5735–5742. DOI: 10.1039/d2nr05590b.

[12] Cai-Hong Yun et al. "The T790M mutation in EGFR kinase causes drug resistance by increasing the affinity for ATP". In: *Proceedings of the National Academy of Sciences* 105.6 (Jan. 2008), pp. 2070–2075. DOI: 10.1073/pnas.0709662105. URL: https://doi.org/10.1073/pnas.0709662105.

[13] Hugh Osborn. *Advanced Quantum Field Theory*. https://www.damtp.cam.ac.uk/user/ho/AQFTNotes.pdf. Lecture notes, Department of Applied Mathematics and Theoretical Physics, University of Cambridge; Lent Term 2013. Originally typeset by Steffen Gielen (2007), revised by Carl Turner (2013), latest update October 30, 2019. 2019.

[14] Wikipedia contributors. *Matrix determinant lemma — Wikipedia, The Free Encyclopedia*. https://en.wikipedia.org/w/index.php?title=Matrix_determinant_lemma&oldid=1301760752. [Online; accessed 27-September-2025]. 2025.

[15] Yue Hao and Valeria Simoncini. "The Sherman–Morrison–Woodbury formula for generalized linear matrix equations and applications". In: *Numerical Linear Algebra with Applications* 28 (May 2021). DOI: 10.1002/nla.2384.

[16] Stephen Pollock. "Circulant matrices and time-series analysis". In: *International Journal of Mathematical Education in Science and Technology* 33 (Jan. 2002), pp. 213–230. DOI: 10.1080/00207390110118953.

[17] P.J. Davis. *Circulant Matrices*. AMS Chelsea Publishing Series. American Mathematical Society, 2013. ISBN: 9780821891650. URL: https://books.google.be/books?id=OpHbzQEACAAJ.

[18] Robert M. Gray. "Toeplitz and Circulant Matrices: A Review". In: *Foundations and Trends in Communications and Information Theory* 2.3 (2006), pp. 155–239. DOI: 10.1561/0100000006. URL: https://ee.stanford.edu/~gray/toeplitz.pdf.

[19] Giulia Rossetti et al. "The structural impact of DNA mismatches". In: *Nucleic Acids Research* 43.8 (Apr. 2015), pp. 4309–4321. ISSN: 0305-1048. DOI: 10.1093/nar/gkv254. eprint: https://academic.oup.com/nar/article-pdf/43/8/4309/17436586/gkv254.pdf. URL: https://doi.org/10.1093/nar/gkv254.

[20] William N. Hunter et al. "Refined crystal structure of an octanucleotide duplex with G · T mismatched base-pairs". In: *Journal of Molecular Biology* 190.4 (1986), pp. 605–618. ISSN: 0022-2836. DOI: https://doi.org/10.1016/0022-2836(86)90246-9. URL: https://www.sciencedirect.com/science/article/pii/0022283686902469.

[21] Herbert Goldstein. *Classical Mechanics*. Addison-Wesley, 1980.

[22] Enrico Skoruppa et al. "Length-scale-dependent elasticity in DNA from coarse-grained and all-atom models". In: *Phys. Rev. E* 103 (4 Apr. 2021), p. 042408. DOI: 10.1103/PhysRevE.103.042408. URL: https://link.aps.org/doi/10.1103/PhysRevE.103.042408.

[23] George A. Baker Jr. "One-Dimensional Order-Disorder Model Which Approaches a Phase Transition". In: *Phys. Rev.* 122 (5 June 1961), pp. 1477–1484. DOI: 10.1103/PhysRev.122.1477. URL: https://link.aps.org/doi/10.1103/PhysRev.122.1477.

[24] Rahul Sharma et al. "cgNA+web : A Visual Interface to the cgNA+ Sequence-dependent Statistical Mechanics Model of Double-stranded Nucleic Acids". In: *Journal of Molecular Biology* 435.14 (2023). Computation Resources for Molecular Biology, p. 167978. ISSN: 0022-2836. DOI: https://doi.org/10.1016/j.jmb.2023.167978. URL: https://www.sciencedirect.com/science/article/pii/S0022283623000347.

[25] D. Petkevičiūtė et al. "cgDNA: a software package for the prediction of sequence-dependent coarse-grain free energies of B-form DNA". In: *Nucleic Acids Research* 42.20 (Sept. 2014), e153. DOI: 10.1093/nar/gku825. URL: https://doi.org/10.1093/nar/gku825.

[26] Alessandro Samuele Patelli. "A sequence-dependent coarse-grain model of B-DNA with explicit description of bases and phosphate groups parametrised from large scale Molecular Dynamics simulations". In: *Infoscience (Ecole Polytechnique Fédérale de Lausanne)* (Jan. 2019). DOI: 10.5075/epfl-thesis-9552. URL: https://infoscience.epfl.ch/handle/20.500.14299/159987.

[27] Wout Laeremans et al. "Insights into elastic properties of coarse-grained DNA models: q-stiffness of cgDNA vs cgDNA+". In: *The Journal of Chemical Physics* 160.14 (Apr. 2024). ISSN: 1089-7690. DOI: 10.1063/5.0197053. URL: http://dx.doi.org/10.1063/5.0197053.

[28] Qiang Du, Xiantao Li, and Liming Yuan. "Analysis of Coarse-Grained lattice models and connections to nonlocal interactions". In: *CSIAM Transactions on Applied Mathematics* 1.1 (Apr. 2020), pp. 155–185. DOI: 10.4208/csiam-am.2020-0009. URL: https://doi.org/10.4208/csiam-am.2020-0009.

[29] Jean Gallier. *Geometric Methods and Applications*. Springer, Jan. 2011. DOI: 10.1007/978-1-4419-9961-0. URL: https://doi.org/10.1007/978-1-4419-9961-0.

[30] Chris Yeh. *Schur complements and the Matrix inversion Lemma*. May 2021. URL: https://chrisyeh96.github.io/2021/05/19/schur-complement.html.

[31] Xavier Viader-Godoy, Maria Manosas, and Felix Ritort. "Stacking correlation length in single-stranded DNA". In: *Nucleic Acids Research* 52.21 (Oct. 2024), pp. 13243–13254. DOI: 10.1093/nar/gkae934. URL: https://doi.org/10.1093/nar/gkae934.

[32] Mario González-Jiménez et al. "Low-frequency vibrational modes in G-quadruplexes reveal the mechanical properties of nucleic acids". In: *Physical Chemistry Chemical Physics* 23.23 (Jan. 2021), pp. 13250–13260. DOI: 10.1039/d0cp05404f. URL: https://doi.org/10.1039/d0cp05404f.

[33] Midas Segers et al. "Mechanical properties of nucleic acids and the non-local twistable wormlike chain model". In: *The Journal of Chemical Physics* 156.23 (June 2022). ISSN: 1089-7690. DOI: 10.1063/5.0089166. URL: http://dx.doi.org/10.1063/5.0089166.

[34] Stefanos K. Nomidis et al. "Twist-bend coupling and the statistical mechanics of the twistable wormlike-chain model of DNA: Perturbation theory and beyond". In: *Physical review. E* 99.3 (Mar. 2019), p. 032414. DOI: 10.1103/physreve.99.032414. URL: https://doi.org/10.1103/physreve.99.032414.

[35] Mark Kac. “On the Partition Function of a One-Dimensional Gas”. In: *Phys. Fluids* 2 (1 Jan. 1959), pp. 8–12. DOI: 10.1063/1.1724399. URL: https://doi.org/10.1063/1.1724399.

[36] Serge F. Mingaleev et al. “Kinks in the discrete sine-Gordon model with Kac-Baker long-range interactions”. In: *Physical Review E* 61.4 (Apr. 2000), pp. 4454–4461. ISSN: 1095-3787. DOI: 10.1103/physreve.61.4454. URL: http://dx.doi.org/10.1103/PhysRevE.61.4454.

[37] Klaus B Møller and Niels E Henriksen. “On wave-packet dynamics in a decaying quadratic potential”. In: *Physica Scripta* 55.5 (May 1997), p. 542. DOI: 10.1088/0031-8949/55/5/005. URL: https://doi.org/10.1088/0031-8949/55/5/005.

[38] Midas Segers et al. “Mechanisms of DNA-Mediated Allostery”. In: *Physical Review Letters* 131.23 (Dec. 2023). ISSN: 1079-7114. DOI: 10.1103/physrevlett.131.238402. URL: http://dx.doi.org/10.1103/PhysRevLett.131.238402.

[39] Andrey A. Gorin, Victor B. Zhurkin, and Wilma K. “B-DNA Twisting Correlates with Base-pair Morphology”. In: *Journal of Molecular Biology* 247.1 (1995), pp. 34–48. ISSN: 0022-2836. DOI: https://doi.org/10.1006/jmbi.1994.0120. URL: https://www.sciencedirect.com/science/article/pii/S0022283684701203.

[40] H Herzel et al. “Interpreting correlations in biosequences”. In: *Physica A: Statistical Mechanics and its Applications* 249.1 (1998), pp. 449–459. ISSN: 0378-4371. DOI: https://doi.org/10.1016/S0378-4371(97)00505-0. URL: https://www.sciencedirect.com/science/article/pii/S0378437197005050.

[41] Chung-Kang Peng et al. “Long Range Correlations in Nucleotide Sequences”. In: *Nature* 356 (Apr. 1992), pp. 168–70. DOI: 10.1038/356168a0.

[42] Riccardo Fantoni. “Exact Results for One Dimensional Fluids Through Functional Integration”. In: *Journal of Statistical Physics* 163.6 (2016), pp. 1247–1267. DOI: 10.1007/s10955-016-1510-3. URL: https://doi.org/10.1007/s10955-016-1510-3.

[43] Zev Bryant et al. “Structural transitions and elasticity from torque measurements on DNA”. In: *Nature* 424.6946 (2003), pp. 338–341. DOI: 10.1038/nature01810. URL: https://doi.org/10.1038/nature01810.

[44] Bryan C. Daniels and James P. Sethna. “Nucleation at the DNA supercoiling transition”. In: *Physical Review E* 83.4 (Apr. 2011), p. 041924. DOI: 10.1103/physreve.83.041924. URL: https://doi.org/10.1103/physreve.83.041924.

[45] Terence Hwa et al. “Localization of denaturation bubbles in random DNA sequences”. In: *Proceedings of the National Academy of Sciences* 100.8 (Apr. 2003), pp. 4411–4416. DOI: 10.1073/pnas.0736291100. URL: https://doi.org/10.1073/pnas.0736291100.

[46] Hatim Allawi and John Santalucia. “Thermodynamics and NMR of internal GT mismatches in DNA”. In: *Biochemistry* 36 (Sept. 1997), pp. 10581–94. DOI: 10.1021/bi962590c.

[47] Hatim T. Allawi and John SantaLucia. “Nearest Neighbor Thermodynamic Parameters for Internal G·A Mismatches in DNA”. In: *Biochemistry* 37.8 (1998). PMID: 9485363, pp. 2170–2179. DOI: 10.1021/bi9724873. eprint: https://doi.org/10.1021/bi9724873. URL: https://doi.org/10.1021/bi9724873.

[48] H. Allawi and John SantaLucia. “NMR solution structure of a DNA dodecamer containing single G*T mismatches”. In: *Nucleic Acids Research* 26.21 (Nov. 1998), pp. 4925–4934. DOI: 10.1093/nar/26.21.4925. URL: https://doi.org/10.1093/nar/26.21.4925.

[49] Masayuki Shibata, Theresa Julia Zielinski, and Robert Rein. “A molecular dynamics study of the effect of G · T mispairs on the conformation of DNA in solution”. In: *Biopolymers* 31.2 (Feb. 1991), pp. 211–232. DOI: 10.1002/bip.360310209. URL: https://doi.org/10.1002/bip.360310209.

[50] Petra Imhof and Mai Zahran. “The effect of a G:T mispair on the dynamics of DNA”. In: *PLoS ONE* 8.1 (Jan. 2013), e53305. DOI: 10.1371/journal.pone.0053305. URL: https://doi.org/10.1371/journal.pone.0053305.

[51] Pablo D. Dans et al. “Exploring polymorphisms in B-DNA helical conformations”. In: *Nucleic Acids Research* 40.21 (Nov. 2012), pp. 10668–10678. ISSN: 0305-1048. DOI: 10.1093/nar/gks884. eprint: https://academic.oup.com/nar/article-pdf/40/21/10668/16962473/gks884.pdf. URL: https://doi.org/10.1093/nar/gks884.

[52] Ivonne Otero-Navas and Jorge M. Seminario. “Molecular electrostatic potentials of DNA base–base pairing and mispairing”. In: *Journal of Molecular Modeling* 18.1 (Apr. 2011), pp. 91–101. DOI: 10.1007/s00894-011-1028-1. URL: https://doi.org/10.1007/s00894-011-1028-1.

[53] F. Landuzzi et al. “Detection of single DNA mismatches by force spectroscopy in short DNA hairpins”. In: *The Journal of Chemical Physics* 152.7 (Feb. 2020), p. 074204. DOI: 10.1063/1.5139284. URL: https://doi.org/10.1063/1.5139284.

[54] E. Carlon, M. Laleman, and S. Nomidis. “Computational Physics: Molecular Dynamics Simulations”. Unpublished lecture notes, KU Leuven, Academic Year 2025–2026. 2025.

[55] Michael Matthies, Matthew Sample, and Petr Šulc. *Coarse-grained simulations of DNA and RNA systems with oxDNA and oxRNA models: Introductory tutorial*. 2023. arXiv: 2308.01455 [physics.bio-ph]. URL: https://arxiv.org/abs/2308.01455.

[56] Joakim Bohlin et al. “Design and simulation of DNA, RNA and hybrid protein–nucleic acid nanostructures with oxView”. In: *Nature Protocols* 17.8 (June 2022), pp. 1762–1788. DOI: 10.1038/s41596-022-00688-5. URL: https://doi.org/10.1038/s41596-022-00688-5.

[57] Erik Poppleton et al. “Design, optimization and analysis of large DNA and RNA nanostructures through interactive visualization, editing and molecular simulation”. In: *Nucleic Acids Research* 48.12 (May 2020), e72. DOI: 10.1093/nar/gkaa417. URL: https://doi.org/10.1093/nar/gkaa417.

[58] A. Sengar et al. “A Primer on the oxDNA Model of DNA: When to Use it, How to Simulate it and How to Interpret the Results”. In: *Frontiers in Molecular Biosciences* 8 (June 2021), p. 693710. DOI: 10.3389/fmolb.2021.693710. URL: https://doi.org/10.3389/fmolb.2021.693710.

[59] Benedict E. K. Snodin et al. “Introducing improved structural properties and salt dependence into a coarse-grained model of DNA”. In: *The Journal of Chemical Physics* 142.23 (June 2015). DOI: 10.1063/1.4921957. URL: https://doi.org/10.1063/1.4921957.

[60] Natalie Haley et al. “Design of hidden thermodynamic driving for non-equilibrium systems via mismatch elimination during DNA strand displacement”. In: *Nature Communications* 11 (May 2020), p. 2562. DOI: 10.1038/s41467-020-16353-y.

[61] Thomas E. Ouldridge, Ard A. Louis, and Jonathan P. K. Doye. “Structural, mechanical, and thermodynamic properties of a coarse-grained DNA model”. In: *The Journal of Chemical Physics* 134.8 (Feb. 2011), p. 085101. DOI: 10.1063/1.3552946. URL: https://doi.org/10.1063/1.3552946.

[62] A. Sengar et al. “A Primer on the oxDNA Model of DNA: When to Use it, How to Simulate it and How to Interpret the Results”. In: *Frontiers in Molecular Biosciences* 8 (June 2021). ISSN: 2296-889X. DOI: 10.3389/fmolb.2021.693710. URL: http://dx.doi.org/10.3389/fmolb.2021.693710.

[63] Oliver Henrich et al. “Coarse-grained simulation of DNA using LAMMPS: An implementation of the oxDNA model and its applications”. In: *The European Physical Journal E* 41.5 (May 2018). ISSN: 1292-895X. DOI: 10.1140/epje/i2018-11669-8. URL: http://dx.doi.org/10.1140/epje/i2018-11669-8.

[64] A. P. Thompson et al. “LAMMPS - a flexible simulation tool for particle-based materials modeling at the atomic, meso, and continuum scales”. In: *Comp. Phys. Comm.* 271 (2022), p. 108171. DOI: 10.1016/j.cpc.2021.108171.

[65] Antonio Suma et al. “TacoxDNA: A user-friendly web server for simulations of complex DNA structures, from single strands to origami”. In: *Journal of Computational Chemistry* 40.29 (2019), pp. 2586–2595. DOI: https://doi.org/10.1002/jcc.26029. eprint: https://onlinelibrary.wiley.com/doi/pdf/10.1002/jcc.26029. URL: https://onlinelibrary.wiley.com/doi/abs/10.1002/jcc.26029.

[66] Eric F. Pettersen et al. “UCSF ChimeraX: Structure visualization for researchers, educators, and developers”. In: *Protein Science* 30.1 (Sept. 2020), pp. 70–82. DOI: 10.1002/pro.3943. URL: https://doi.org/10.1002/pro.3943.

[67] X.-j. Lu and Wilma K. Olson. “3DNA: a software package for the analysis, rebuilding and visualization of three-dimensional nucleic acid structures”. In: *Nucleic Acids Research* 31.17 (Aug. 2003), pp. 5108–5121. DOI: 10.1093/nar/gkg680. URL: https://doi.org/10.1093/nar/gkg680.

[68] Wilma K Olson et al. “A standard reference frame for the description of nucleic acid base-pair geometry”. In: *Journal of Molecular Biology* 313.1 (Oct. 2001), pp. 229–237. DOI: 10.1006/jmbi.2001.4987. URL: https://doi.org/10.1006/jmbi.2001.4987.

[69] David R. Bevan et al. “Molecular Dynamics Simulations of the d(CCAACGTTGG)2 Decamer: Influence of the Crystal Environment”. In: *Biophysical Journal* 78.2 (Feb. 2000), pp. 668–682. DOI: 10.1016/s0006-3495(00)76625-2. URL: https://doi.org/10.1016/s0006-3495(00)76625-2.

[70] Minjung Kim et al. “Sequence-dependent twist-bend coupling in DNA minicircles”. In: *Nanoscale* 13.47 (Jan. 2021), pp. 20186–20196. DOI: 10.1039/d1nr04672a. URL: https://doi.org/10.1039/d1nr04672a.

[71] D.C. Lay. *Linear Algebra and Its Applications*. Addison-Wesley, 2012. ISBN: 9780321385178. URL: https://books.google.be/books?id=_4bjtgAACAAJ.

A Statement on the use of GenAI

The following table shows where GenAI was used during this thesis. It was converted from the KU Leuven Word template to LaTeX. Coincidentally, this conversion of a Word table was performed with ChatGPT.
For more information, see: https://www.kuleuven.be/english/education/student/educational-tools/responsible-use-of-generative-artificial-intelligence#Transparency.

Table A.1: Use of generative AI tools during the thesis.

GenAI assistance for	**Used**	**Tool(s)**	**Purpose**
Language assistance for reviewing or improving self-written text	Yes	Grammarly	Spelling, grammar, and text improvement suggestions.
Paraphrasing tool	Yes	Grammarly	Rewording and improving phrasing.
Search engine for information or existing research	Yes	Gemini Pro, Elicit, ChatGPT Premium	Finding relevant information and understanding papers.
Literature search	Yes	Gemini Pro, Elicit, ChatGPT Premium	Gathering papers to read.
Generating programming code	Yes	Gemini Pro, ChatGPT Premium	Generating plots, handling simulation input/output files, and analysing output files.
Generating new research ideas	Yes	Gemini Pro	Exploring how to coarse-grain the cgDNA+ matrix.
Generating synthetic data	Yes	Gemini Pro	Generating a random DNA strand for Chapter 4.
Generating visuals, video, or audio	Yes	Gemini Pro, ChatGPT Premium	Creating the liquid biopsy figure in the introduction, figures 1.2, 2.2 to 2.5, 3.1 to 3.4, 4.12, 4.13 and 5.5 were drawn by hand and then converted to TikZ using GenAI.

B Mathematical Derivations

B.1 Theorems

Theorem B.1 (Spectral Theorem for Stability)**.** *Let $\hat{A} \in \mathbb{R}^{n\times n}$ be a symmetric matrix. $\hat{A}$ is positive definite ($\hat{A} \succ 0$) if and only if there exists an orthogonal matrix Q such that:*

$$\hat{A} = Q\Lambda Q^T, \quad \textit{with } \lambda_i > 0 \ \forall i$$

This ensures $\det\left(\hat{A}\right) = \prod \lambda_i > 0$, guaranteeing the existence of $\hat{A}^{-1}$ and a stable quadratic form [71].

Theorem B.2 (Gaussian integrals)**.** *Suppose $\hat{A}$ is a symmetric positive definite $N \times N$ matrix, then:*

$$\int d\mathbf{x} e^{-\frac{1}{2}\langle x|\hat{A}|x\rangle} = \sqrt{\frac{(2\pi)^N}{\det \hat{A}}} = \sqrt{\frac{(2\pi)^N}{\prod_{n=1}^N \lambda_n}} \tag{B.1}$$

where $\{\lambda_n\}$ are the eigenvalues of $\hat{A}$.

Theorem B.3 (Sherman-Morrison)**.** *For any square invertible matrix A and column vectors $|u\rangle, |v\rangle$ the inverse of $A + |u\rangle\langle v|$ is given by [15]:*

$$(A + |u\rangle\langle v|)^{-1} = A^{-1} - \frac{A^{-1}|u\rangle\langle v|A^{-1}}{1 + \langle v|A^{-1}|u\rangle} \tag{B.2}$$

and a consequence of said theorem, the matrix-determinant lemma.

Lemma B.4 (Matrix-determinant)**.** *For any square invertible matrix A and column vector $|u\rangle, |v\rangle$ [14]:*

$$\det(A + |u\rangle\langle v|) = \det A\big[1 + \langle v|A^{-1}|u\rangle\big] \tag{B.3}$$

Theorem B.5 (Woodbury matrix identity)**.** *Let A_0, U, C, V have the right dimensions and $A = A_0 + U^t C V$ then [15]:*

$$A^{-1} = A_0^{-1} - A_0^{-1}U^t(C^{-1} + VA_0^{-1}U^t)^{-1}VA_0^{-1} \tag{B.4}$$

and for the determinant:

$$\det A = \det(A_0)\det(C)\det\left(C^{-1} + U^t A_0^{-1} V\right) \tag{B.5}$$

Theorem B.6. *If $\hat{C}$ is symmetric, positive definite and circulant, then $\hat{C}^{-1}$ is also symmetric (a), positive definite (b) and circulant. Moreover (c),*

$$\hat{C}^{-1} = \hat{U}\hat{\Psi}^{-1}\hat{U}^\dagger. \tag{B.6}$$

Proof a.

$$\begin{aligned} CC^{-1} &= \mathbb{1} \\ \left(CC^{-1}\right)^t &= \mathbb{1} \\ \left(C^{-1}\right)^t C^t &= \mathbb{1} \\ \left(C^{-1}\right)^t C &= \mathbb{1} \\ \left(C^{-1}\right)^t &= C^{-1} \end{aligned}$$

□

Proof b. Let $|u\rangle = C\,|v\rangle$ then:

$$\langle u|C^{-1}|u\rangle = \langle v|CC^{-1}C|v\rangle = \langle v|C|v\rangle > 0$$

since $C \succ 0$ □

Proof c.

$$\begin{aligned} CU\Psi^{-1}U^\dagger &= U\Psi U^\dagger U\Psi^{-1}U^\dagger \\ &= U\Psi\Psi^{-1}U^\dagger \\ &= UU^\dagger \\ &= \mathbb{1} \end{aligned}$$

□

Corollary B.6.1. *Let $\hat{C}$ be an invertible circulant matrix. Then the row sum of $\hat{C}^{-1}$ is the inverse of the row sum of $\hat{C}$. Equivalently, using the all-ones vector notation.*

$$\frac{\langle 1_N|\hat{C}^{-1}|1_N\rangle}{N} = \frac{N}{\langle 1_N|\hat{C}|1_N\rangle}. \tag{B.7}$$

Proof.

$$\begin{aligned} CC^{-1} &= \mathbb{1} \\ \sum_{k=0}^{N-1} C_{ik}C^{-1}_{kj} &= \delta_{ij} \\ \sum_{j=0}^{N-1}\sum_{k=0}^{N-1} C_{ik}C^{-1}_{kj} &= \sum_{j=0}^{N-1}\delta_{ij} \\ \sum_{k=0}^{N-1} C_{ik}\sum_{j=0}^{N-1} C^{-1}_{kj} &= 1 \end{aligned}$$

Now we use the fact that C^{-1} is also a circulant matrix, so that the sum over any row will be the same:

$$\sum_{j=0}^{N-1} C^{-1}_{kj} = \sum_{j=0}^{N-1} C^{-1}_{ij}$$

We get:

$$\sum_{k=0}^{N-1} C_{ik} \sum_{j=0}^{N-1} C_{ij}^{-1} = 1$$

$$\sum_{j=0}^{N-1} C_{ij}^{-1} = \frac{1}{\sum_{k=0}^{N-1} C_{ik}}$$

$$\text{Row sum}\big(C^{-1}\big) = \frac{1}{\text{Row sum}(C)}$$

□

B.2 Perturbing Twice

B.2.1 Woodbury for Rank-2 Update

For the presence of two matched-mode perturbations, we use the Woodbury matrix identity B.5 for a rank-2 update.

$$\begin{aligned} A &= A_0 + |u\rangle\langle u| + |v\rangle\langle v| \\ &= \begin{pmatrix} |u\rangle & |v\rangle \end{pmatrix} \mathbb{1}_2 \begin{pmatrix} \langle u| \\ \langle v| \end{pmatrix} \\ &\equiv A_0 + VV^t \end{aligned} \tag{B.8}$$

The new inverse is then given by:

$$A^{-1} = A_0^{-1} - A_0^{-1} V \big(\mathbb{1}_2^{-1} + V^t A_0^{-1} V\big)^{-1} V^t A_0^{-1} \tag{B.9}$$

It might not be immediately obvious, but we can treat this as a 2×2 block matrix problem. We first compute the term within the brackets:

$$\begin{aligned} \mathbb{1}_2 + V^t A_0^{-1} V &= \begin{pmatrix} 1 & 0 \\ 0 & 1 \end{pmatrix} + \begin{pmatrix} \langle u| \\ \langle v| \end{pmatrix} A_0^{-1} \begin{pmatrix} |u\rangle & |v\rangle \end{pmatrix} \\ &= \begin{pmatrix} 1 + \langle u|A_0^{-1}|u\rangle & \langle u|A_0^{-1}|v\rangle \\ \langle v|A_0^{-1}|u\rangle & 1 + \langle v|A_0^{-1}|v\rangle \end{pmatrix} \end{aligned}$$

So that its inverse is given by:

$$\big(\mathbb{1}_2 + V^t A_0^{-1} V\big)^{-1} = \frac{1}{D} \begin{pmatrix} 1 + \langle v|A_0^{-1}|v\rangle & -\langle u|A_0^{-1}|v\rangle \\ -\langle v|A_0^{-1}|u\rangle & 1 + \langle u|A_0^{-1}|u\rangle \end{pmatrix} \tag{B.10}$$

Where D is the determinant of this 2×2 matrix:

$$D = (1 + \langle v|A_0^{-1}|v\rangle)(1 + \langle u|A_0^{-1}|u\rangle) - \langle u|A_0^{-1}|v\rangle^2 \tag{B.11}$$

So that:

$$\begin{aligned}
A^{-1} =& A_0^{-1} - \frac{1}{D} A_0^{-1} \begin{pmatrix} |u\rangle & |v\rangle \end{pmatrix} \begin{pmatrix} 1 + \langle v|A_0^{-1}|v\rangle & -\langle u|A_0^{-1}|v\rangle \\ -\langle v|A_0^{-1}|u\rangle & 1 + \langle u|A_0^{-1}|u\rangle \end{pmatrix} \begin{pmatrix} \langle u| \\ \langle v| \end{pmatrix} A_0^{-1} \\
&= A_0^{-1} - \frac{A_0^{-1}}{D} \big[(1 + \langle v|A_0^{-1}|v\rangle) |u\rangle\langle u| + (1 + \langle u|A_0^{-1}|u\rangle) |v\rangle\langle v| - \langle u|A_0^{-1}|v\rangle \left(|u\rangle\langle v| + |v\rangle\langle u| \right) \big] A_0^{-1} \\
&= A_0^{-1} - \frac{1}{D} \big[(1 + \langle v|A_0^{-1}|v\rangle) A_0^{-1} |u\rangle\langle u| A_0^{-1} + (1 + \langle u|A_0^{-1}|u\rangle) A_0^{-1} |v\rangle\langle v| A_0^{-1} \\
&- \langle u|A_0^{-1}|v\rangle \left(A_0^{-1} |v\rangle\langle u| A_0^{-1} + A_0^{-1} |u\rangle\langle v| A_0^{-1} \right) \big] \qquad \text{(B.12)}
\end{aligned}$$

For the determinant of the updated matrix, we follow a similar procedure to find:

$$\det A = \det(A_0) \det\left(\mathbb{1}_2^{-1} + V^t A_0^{-1} V \right) = \det(A_0) D \qquad \text{(B.13)}$$

B.2.2 Energetic Interaction Term

To find the energetic contribution resulting from the joint application of the MMPs, we evaluate the shift in the quadratic form using the perturbed inverse:

$$\begin{aligned}
\Delta\mathcal{E}_{s,t} =& \frac{1}{2D} \Big[\xi \Big(1 + \kappa \langle \hat{s}|\hat{K}_0^{-1}|\hat{s}\rangle \Big) \Big(f_s \langle \hat{s}\big|\hat{K}_0^{-1}\big|\hat{t}\rangle + f_t \langle \hat{t}\big|\hat{K}_0^{-1}\big|\hat{t}\rangle \Big)^2 \\
&+ \kappa \Big(1 + \xi \langle \hat{t}\big|\hat{K}_0^{-1}\big|\hat{t}\rangle \Big) \Big(f_s \langle \hat{s}|\hat{K}_0^{-1}|\hat{s}\rangle + f_t \langle \hat{s}\big|\hat{K}_0^{-1}\big|\hat{t}\rangle \Big)^2 \\
&- 2\kappa\xi \langle \hat{s}\big|\hat{K}_0^{-1}\big|\hat{t}\rangle \Big(f_s \langle \hat{s}|\hat{K}_0^{-1}|\hat{s}\rangle + f_t \langle \hat{s}\big|\hat{K}_0^{-1}\big|\hat{t}\rangle \Big) \Big(f_s \langle \hat{s}\big|\hat{K}_0^{-1}\big|\hat{t}\rangle + f_t \langle \hat{t}\big|\hat{K}_0^{-1}\big|\hat{t}\rangle \Big) \Big] \\
&- \frac{1}{2} \Big(f_s^2 \langle \hat{s}|\hat{K}_0^{-1}|\hat{s}\rangle + f_t^2 \langle \hat{t}\big|\hat{K}_0^{-1}\big|\hat{t}\rangle + 2 f_s f_t \langle \hat{s}\big|\hat{K}_0^{-1}\big|\hat{t}\rangle \Big) + c \qquad \text{(B.14)}
\end{aligned}$$

Note that the second and third lines still lie within the big square brackets, and we used the fact that $\hat{K}_0^{-1}$ is symmetric. We can simplify this by expanding each term:

$$\begin{aligned}
(i) &= \xi \Big(1 + \kappa \langle \hat{s}|\hat{K}_0^{-1}|\hat{s}\rangle \Big) \Big(f_s^2 \langle \hat{s}\big|\hat{K}_0^{-1}\big|\hat{t}\rangle^2 + 2 f_s f_t \langle \hat{s}\big|\hat{K}_0^{-1}\big|\hat{t}\rangle \langle \hat{t}\big|\hat{K}_0^{-1}\big|\hat{t}\rangle + f_t^2 \langle \hat{t}\big|\hat{K}_0^{-1}\big|\hat{t}\rangle^2 \Big) \\
(ii) &= \kappa \Big(1 + \xi \langle \hat{t}\big|\hat{K}_0^{-1}\big|\hat{t}\rangle \Big) \Big(f_s^2 \langle \hat{s}|\hat{K}_0^{-1}|\hat{s}\rangle^2 + 2 f_s f_t \langle \hat{s}\big|\hat{K}_0^{-1}\big|\hat{t}\rangle \langle \hat{s}|\hat{K}_0^{-1}|\hat{s}\rangle + f_t^2 \langle \hat{s}\big|\hat{K}_0^{-1}\big|\hat{t}\rangle^2 \Big) \\
(iii) &= 2\kappa\xi \langle \hat{s}\big|\hat{K}_0^{-1}\big|\hat{t}\rangle \Big[f_s^2 \langle \hat{s}|\hat{K}_0^{-1}|\hat{s}\rangle \langle \hat{s}\big|\hat{K}_0^{-1}\big|\hat{t}\rangle + f_s f_t \Big(\langle \hat{s}|\hat{K}_0^{-1}|\hat{s}\rangle \langle \hat{t}\big|\hat{K}_0^{-1}\big|\hat{t}\rangle + \langle \hat{s}\big|\hat{K}_0^{-1}\big|\hat{t}\rangle^2 \Big) \\
&\quad + f_t^2 \langle \hat{s}\big|\hat{K}_0^{-1}\big|\hat{t}\rangle \langle \hat{t}\big|\hat{K}_0^{-1}\big|\hat{t}\rangle \Big]
\end{aligned}$$

We first simplify the $\mathcal{O}(f_s^2)$ terms:

$$\begin{aligned}
&\mathcal{O}(f_s^2): \\
&\xi \Big(1 + \kappa \langle \hat{s}|\hat{K}_0^{-1}|\hat{s}\rangle \Big) \langle \hat{s}\big|\hat{K}_0^{-1}\big|\hat{t}\rangle^2 + \kappa \Big(1 + \xi \langle \hat{t}\big|\hat{K}_0^{-1}\big|\hat{t}\rangle \Big) \langle \hat{s}|\hat{K}_0^{-1}|\hat{s}\rangle^2 - 2\kappa\xi \langle \hat{s}\big|\hat{K}_0^{-1}\big|\hat{t}\rangle^2 \langle \hat{s}|\hat{K}_0^{-1}|\hat{s}\rangle \\
&= \xi \Big(1 - \kappa \langle \hat{s}|\hat{K}_0^{-1}|\hat{s}\rangle \Big) \langle \hat{s}\big|\hat{K}_0^{-1}\big|\hat{t}\rangle^2 + \kappa \Big(1 + \xi \langle \hat{t}\big|\hat{K}_0^{-1}\big|\hat{t}\rangle \Big) \langle \hat{s}|\hat{K}_0^{-1}|\hat{s}\rangle^2 \qquad \text{(B.15)}
\end{aligned}$$

The $\mathcal{O}(f_t^2)$ terms follow by symmetry ($s \leftrightarrow t$ and $\kappa \leftrightarrow \xi$):

$$\mathcal{O}(f_t^2): \kappa \Big(1 - \xi \langle \hat{t}\big|\hat{K}_0^{-1}\big|\hat{t}\rangle \Big) \langle \hat{s}\big|\hat{K}_0^{-1}\big|\hat{t}\rangle^2 + \xi \Big(1 + \kappa \langle \hat{s}|\hat{K}_0^{-1}|\hat{s}\rangle \Big) \langle \hat{t}\big|\hat{K}_0^{-1}\big|\hat{t}\rangle^2 \qquad \text{(B.16)}$$

While the $\mathcal{O}(f_s f_t)$ terms are given by:

$$\begin{aligned}
&\mathcal{O}(f_s f_t):\\
&2\xi\Big(1+\kappa\,\langle\hat{s}|\hat{K}_0^{-1}|\hat{s}\rangle\Big)\,\langle\hat{s}\big|\hat{K}_0^{-1}\big|\hat{t}\rangle\,\langle\hat{t}\big|\hat{K}_0^{-1}\big|\hat{t}\rangle + 2\kappa\Big(1+\xi\,\langle\hat{t}\big|\hat{K}_0^{-1}\big|\hat{t}\rangle\Big)\,\langle\hat{s}\big|\hat{K}_0^{-1}\big|\hat{t}\rangle\,\langle\hat{s}|\hat{K}_0^{-1}|\hat{s}\rangle\\
&-2\kappa\xi\,\langle\hat{s}\big|\hat{K}_0^{-1}\big|\hat{t}\rangle\Big(\,\langle\hat{s}|\hat{K}_0^{-1}|\hat{s}\rangle\,\langle\hat{t}\big|\hat{K}_0^{-1}\big|\hat{t}\rangle + \langle\hat{s}\big|\hat{K}_0^{-1}\big|\hat{t}\rangle^2\Big)\\
&=2\,\langle\hat{s}\big|\hat{K}_0^{-1}\big|\hat{t}\rangle\Big(\xi\,\langle\hat{t}\big|\hat{K}_0^{-1}\big|\hat{t}\rangle + \kappa\,\langle\hat{s}|\hat{K}_0^{-1}|\hat{s}\rangle + \kappa\xi\,\langle\hat{s}|\hat{K}_0^{-1}|\hat{s}\rangle\,\langle\hat{t}\big|\hat{K}_0^{-1}\big|\hat{t}\rangle - \kappa\xi\,\langle\hat{s}\big|\hat{K}_0^{-1}\big|\hat{t}\rangle^2\Big)
\end{aligned} \tag{B.17}$$

While the single MMP terms outside the bracket will cancel in the interaction term, the same does not hold for the $\langle\hat{s}\big|\hat{K}_0^{-1}\big|\hat{t}\rangle$ term, we thus bring it inside the bracket as well by multiplying by the 2×2 update determinant.

$$\begin{aligned}
2D\,\langle\hat{s}\big|\hat{K}_0^{-1}\big|\hat{t}\rangle &= 2\,\langle\hat{s}\big|\hat{K}_0^{-1}\big|\hat{t}\rangle\Big[\Big(1+\kappa\,\langle\hat{s}|\hat{K}_0^{-1}|\hat{s}\rangle\Big)\Big(1+\xi\,\langle\hat{t}\big|\hat{K}_0^{-1}\big|\hat{t}\rangle\Big) - \kappa\xi\,\langle\hat{s}\big|\hat{K}_0^{-1}\big|\hat{t}\rangle^2\Big]\\
&= 2\,\langle\hat{s}\big|\hat{K}_0^{-1}\big|\hat{t}\rangle\Big(1+\kappa\,\langle\hat{s}|\hat{K}_0^{-1}|\hat{s}\rangle + \xi\,\langle\hat{t}\big|\hat{K}_0^{-1}\big|\hat{t}\rangle + \kappa\xi\,\langle\hat{s}|\hat{K}_0^{-1}|\hat{s}\rangle\,\langle\hat{t}\big|\hat{K}_0^{-1}\big|\hat{t}\rangle\\
&\quad - \kappa\xi\,\langle\hat{s}\big|\hat{K}_0^{-1}\big|\hat{t}\rangle^2\Big)
\end{aligned} \tag{B.18}$$

We see that almost all terms at $\mathcal{O}(f_s f_t)$ thus cancel out and we are left with:

$$\mathcal{O}(f_s f_t) = -2\,\langle\hat{s}\big|\hat{K}_0^{-1}\big|\hat{t}\rangle \tag{B.19}$$

Order by order, then the rank-2 energy penalty is given by:

$$\begin{aligned}
\Delta\mathcal{E}_{s,t} = \frac{1}{2D}\big[&f_s^2\Big(\xi\Big(1-\kappa\,\langle\hat{s}|\hat{K}_0^{-1}|\hat{s}\rangle\Big)\,\langle\hat{s}\big|\hat{K}_0^{-1}\big|\hat{t}\rangle^2 + \kappa\Big(1+\xi\,\langle\hat{t}\big|\hat{K}_0^{-1}\big|\hat{t}\rangle\Big)\,\langle\hat{s}|\hat{K}_0^{-1}|\hat{s}\rangle^2\Big)\\
&+ f_t^2\Big(\kappa\Big(1-\xi\,\langle\hat{t}\big|\hat{K}_0^{-1}\big|\hat{t}\rangle\Big)\,\langle\hat{s}\big|\hat{K}_0^{-1}\big|\hat{t}\rangle^2 + \xi\Big(1+\kappa\,\langle\hat{s}|\hat{K}_0^{-1}|\hat{s}\rangle\Big)\,\langle\hat{t}\big|\hat{K}_0^{-1}\big|\hat{t}\rangle^2\Big) - 2f_s f_t\,\langle\hat{s}\big|\hat{K}_0^{-1}\big|\hat{t}\rangle\big]\\
&- \frac{f_s^2}{2}\,\langle\hat{s}|\hat{K}_0^{-1}|\hat{s}\rangle - \frac{f_t^2}{2}\,\langle\hat{t}\big|\hat{K}_0^{-1}\big|\hat{t}\rangle
\end{aligned} \tag{B.20}$$

For the interaction term, we still need to subtract the two separate rank-1 energies given by equation (2.36) from this:

$$\begin{aligned}
\Delta\Delta\mathcal{E}_{st} &= \Delta\mathcal{E}_{st} - (\Delta\mathcal{E}_s + \Delta\mathcal{E}_t)\\
&= \frac{1}{2D}[\dots] - \frac{f_s^2}{2}\frac{\kappa\,\langle\hat{s}|\hat{K}_0^{-1}|\hat{s}\rangle^2}{1+\kappa\,\langle\hat{s}|\hat{K}_0^{-1}|\hat{s}\rangle} - \frac{f_t^2}{2}\frac{\xi\,\langle\hat{t}\big|\hat{K}_0^{-1}\big|\hat{t}\rangle^2}{1+\xi\,\langle\hat{t}\big|\hat{K}_0^{-1}\big|\hat{t}\rangle}
\end{aligned} \tag{B.21}$$

This means we get two more $\mathcal{O}(f_s^2)$ and $\mathcal{O}(f_t^2)$ terms. We bring these into the big bracket term by multiplying with the determinant D, for the $\mathcal{O}(f_s^2)$ term, this yields:

$$\begin{aligned}
&D\frac{\kappa\,\langle\hat{s}|\hat{K}_0^{-1}|\hat{s}\rangle^2}{1+\kappa\,\langle\hat{s}|\hat{K}_0^{-1}|\hat{s}\rangle}\\
&=\Big(\Big(1+\xi\,\langle\hat{t}\big|\hat{K}_0^{-1}\big|\hat{t}\rangle\Big)\Big(1+\kappa\,\langle\hat{s}|\hat{K}_0^{-1}|\hat{s}\rangle\Big) - \kappa\xi\,\langle\hat{s}\big|\hat{K}_0^{-1}\big|\hat{t}\rangle^2\Big)\frac{\kappa\,\langle\hat{s}|\hat{K}_0^{-1}|\hat{s}\rangle^2}{1+\kappa\,\langle\hat{s}|\hat{K}_0^{-1}|\hat{s}\rangle}\\
&=\kappa\Big(1+\xi\,\langle\hat{t}\big|\hat{K}_0^{-1}\big|\hat{t}\rangle\Big)\,\langle\hat{s}|\hat{K}_0^{-1}|\hat{s}\rangle^2 - \frac{\kappa^2\xi\,\langle\hat{s}\big|\hat{K}_0^{-1}\big|\hat{t}\rangle^2\,\langle\hat{s}|\hat{K}_0^{-1}|\hat{s}\rangle^2}{1+\kappa\,\langle\hat{s}|\hat{K}_0^{-1}|\hat{s}\rangle}
\end{aligned} \tag{B.22}$$

So that the $\mathcal{O}(f_s^2)$ within the bracket becomes:

$$\begin{aligned}
&\mathcal{O}\left(f_s^2\right): \\
&\xi\Big(1-\kappa\left\langle\hat{s}\right|\hat{K}_0^{-1}\left|\hat{s}\right\rangle\Big)\left\langle\hat{s}\right|\hat{K}_0^{-1}\left|\hat{t}\right\rangle^2+\kappa\Big(1+\xi\left\langle\hat{t}\right|\hat{K}_0^{-1}\left|\hat{t}\right\rangle\Big)\left\langle\hat{s}\right|\hat{K}_0^{-1}\left|\hat{s}\right\rangle^2 \\
&-\kappa\Big(1+\xi\left\langle\hat{t}\right|\hat{K}_0^{-1}\left|\hat{t}\right\rangle\Big)\left\langle\hat{s}\right|\hat{K}_0^{-1}\left|\hat{s}\right\rangle^2+\frac{\kappa^2\xi\left\langle\hat{s}\right|\hat{K}_0^{-1}\left|\hat{t}\right\rangle^2\left\langle\hat{s}\right|\hat{K}_0^{-1}\left|\hat{s}\right\rangle^2}{1+\kappa\left\langle\hat{s}\right|\hat{K}_0^{-1}\left|\hat{s}\right\rangle} \\
&=\xi\left\langle\hat{s}\right|\hat{K}_0^{-1}\left|\hat{t}\right\rangle^2\left(1-\kappa\left\langle\hat{s}\right|\hat{K}_0^{-1}\left|\hat{s}\right\rangle+\frac{\kappa^2\left\langle\hat{s}\right|\hat{K}_0^{-1}\left|\hat{s}\right\rangle^2}{1+\kappa\left\langle\hat{s}\right|\hat{K}_0^{-1}\left|\hat{s}\right\rangle}\right) \\
&=\frac{\xi\left\langle\hat{s}\right|\hat{K}_0^{-1}\left|\hat{t}\right\rangle^2}{1+\kappa\left\langle\hat{s}\right|\hat{K}_0^{-1}\left|\hat{s}\right\rangle}
\end{aligned} \tag{B.23}$$

The calculation for the $\mathcal{O}(f_t^2)$ terms is identical. The final expression for the interaction energy of a rank-2 update is then:

$$\Delta\Delta\mathcal{E}_{st}=\frac{1}{D}\left[\frac{f_s^2}{2}\frac{\xi\left\langle\hat{s}\right|\hat{K}_0^{-1}\left|\hat{t}\right\rangle^2}{1+\kappa\left\langle\hat{s}\right|\hat{K}_0^{-1}\left|\hat{s}\right\rangle}+\frac{f_t^2}{2}\frac{\kappa\left\langle\hat{s}\right|\hat{K}_0^{-1}\left|\hat{t}\right\rangle^2}{1+\xi\left\langle\hat{t}\right|\hat{K}_0^{-1}\left|\hat{t}\right\rangle}-f_sf_t\left\langle\hat{s}\right|\hat{K}_0^{-1}\left|\hat{t}\right\rangle\right] \tag{B.24}$$

B.3 Constrained Coordinates

Consider a general translationally invariant system described by a symmetric positive definite circulant stiffness matrix $\hat{K}$. In the presence of the closing spring, the Hamiltonian takes the form

$$\mathcal{H}=\frac{1}{2}\left\langle x\right|\hat{K}\left|x\right\rangle+\frac{K'}{2}(\left\langle 1_N\right|x\rangle-\delta L)^2 \tag{B.25}$$

In the rigid limit $K'\to\infty$, the additional term in the Hamiltonian yields a Dirac δ-function in the partition sum.

$$\exp\left[-\frac{K'}{2}(\left\langle 1_N\right|x\rangle-\delta L)^2\right]\propto\delta(\left\langle 1_N\right|x\rangle+\delta L) \tag{B.26}$$

This constrains the system to an $(N-1)$-dimensional subspace of the non-rigid system. The partition sum retains only the constrained Hamiltonian:

$$\begin{aligned}
Z&=\int d^N\mathbf{x}\exp(-\mathcal{H}(x_0,\ldots,x_{N-1}))\delta(\left\langle 1_N\right|x\rangle-\delta L) \\
&=\int d^{N-1}\mathbf{y}\exp(-\mathcal{H}_{\text{constrained}})
\end{aligned} \tag{B.27}$$

To isolate the constrained mode, we use the orthonormal Fourier basis $\{\left|q\right\rangle\}$ starting from the zero mode.

$$\left|1_N\right\rangle=\sqrt{N}\left|q=0\right\rangle \tag{B.28}$$

Expanding the displacement vector in this basis:

$$\left|x\right\rangle=\sum_{q=0}^{N-1}y_q\left|q\right\rangle \tag{B.29}$$

The constraint becomes:

$$\langle 1_N|x\rangle = \sqrt{N}y_0 = \delta L$$

such that

$$y_0 = \frac{\delta L}{\sqrt{N}} \tag{B.30}$$

The zeroth Fourier mode thus completely absorbs the rigid constraint, while the remaining $N-1$ Fourier modes remain unconstrained. Since the $\hat{K}$ is circulant, the Fourier modes diagonalise the system and:

$$\hat{K}\,|1_N\rangle = \tilde{K}_0\,|1_N\rangle \tag{B.31}$$

This decomposes the Hamiltonian into a constraint term and a sum over the remaining eigenmodes.

$$\begin{aligned}\mathcal{H} &= \frac{1}{2}\tilde{K}_0 y_0^2 + \frac{1}{2}\sum_{q=1}^{N-1}\tilde{K}_q y_q^2 \\ &= \frac{\tilde{K}_0}{2N}\delta L^2 + \frac{1}{2}\sum_{n=1}^{N-1}\tilde{K}_q y_q^2\end{aligned} \tag{B.32}$$

The constrained partition sum is then given by integrating over the $N-1$-dimensional subspace, with the addition of the extra term.

$$Z = \exp\left(-\frac{\tilde{K}_0}{2N}\delta L^2\right)\int d^{N-1}\mathbf{y}\,\exp\left[-\frac{1}{2}\sum_{q=1}^{N-1}\tilde{K}_q y_q^2\right] \tag{B.33}$$

Since the Hamiltonian is diagonal in this subspace, the eigenvalues fully determine the Gaussian integral.

$$Z = (2\pi)^{\frac{N-1}{2}}\left(\prod_{q=1}^{N-1}\tilde{K}_q\right)^{-1/2}\exp\left(-\frac{\tilde{K}_0}{2N}\delta L^2\right) \tag{B.34}$$

Such that the free energy of the constrained chain is given by:

$$\mathcal{F}_r = \frac{1}{2}\left[\sum_{q=1}^{N-1}\log\left(\tilde{K}_q\right) - (N-1)\log(2\pi)\right] + \frac{\tilde{K}_0}{2N}\delta L^2 \tag{B.35}$$

Which yields a free energy penalty compared to the free circulant model of:

$$\Delta\mathcal{F}_r = -\frac{1}{2}\log\left(\tilde{K}_0\right) + \frac{\tilde{K}_0}{2N}\delta L^2 + \text{ additive term} \tag{B.36}$$

B.4 Critical Global Constraint Stiffness

For the existence of zero points for the free energy interaction parabola, we must solve:

$$\frac{(K_0+\delta K)^2\delta a^2}{2\delta K(1+\delta K\,\langle n|\hat{K}_0^{-1}|n\rangle)} - \frac{1}{2}\log\left(1 - \frac{K'\delta K\,\langle n|\hat{K}_0^{-1}|1_N\rangle^2}{(1+\delta K\,\langle n|\hat{K}_0^{-1}|n\rangle)(1+NK'\,\langle n|\hat{K}_0^{-1}|1_N\rangle)}\right) = 0 \tag{B.37}$$

for the global closing stiffness K'_{crit}. We first define the reduced mismatch energy:

$$\Delta\varepsilon_m \equiv \frac{(K_0+\delta K)^2\delta a^2}{2\delta K(1+\delta K\,\langle n|\hat{K}_0^{-1}|n\rangle)} \tag{B.38}$$

$$\begin{aligned}
&\log\left(1-\frac{K'_{\text{crit}}\delta K\,\langle n|\hat{K}_0^{-1}|1_N\rangle^2}{(1+\delta K\,\langle n|\hat{K}_0^{-1}|n\rangle)(1+NK'_{\text{crit}}\,\langle n|\hat{K}_0^{-1}|1_N\rangle)}\right)=2\Delta\varepsilon_m\\
&1-\frac{K'_{\text{crit}}\delta K\,\langle n|\hat{K}_0^{-1}|1_N\rangle^2}{(1+\delta K\,\langle n|\hat{K}_0^{-1}|n\rangle)(1+NK'_{\text{crit}}\,\langle n|\hat{K}_0^{-1}|1_N\rangle)}=\exp(2\Delta\varepsilon_m)\\
&K'_{\text{crit}}\delta K\,\langle n|\hat{K}_0^{-1}|1_N\rangle^2=D_m(1+NK'\,\langle n|\hat{K}_0^{-1}|1_N\rangle)(1-\exp(2\Delta\varepsilon_m))\\
&K'_{\text{crit}}\Big(\delta K\,\langle n|\hat{K}_0^{-1}|1_N\rangle^2+ND_m\,\langle n|\hat{K}_0^{-1}|1_N\rangle\,(\exp(2\Delta\varepsilon_m)-1)\Big)=D_m(1-\exp(2\Delta\varepsilon_m))\\
&K'_{\text{crit}}=\frac{1}{\langle n|\hat{K}_0^{-1}|1_N\rangle}\frac{D_m(1-\exp(2\Delta\varepsilon_m))}{\delta K\,\langle n|\hat{K}_0^{-1}|n\rangle-ND_m(1-\exp(2\Delta\varepsilon_m))}
\end{aligned}$$

We can simplify this some more by using

$$\langle n|\hat{K}_0^{-1}|1_N\rangle=\frac{1}{\tilde{K}_0} \tag{B.39}$$

So that we can link back to the zero-mode eigenvalue:

$$K'_{\text{crit}}=\tilde{K}_0\left[\frac{D_m\Big(1-\exp\Big(\frac{(K_0+\delta K)^2\delta a^2}{\delta KD_m}\Big)\Big)}{\frac{\delta K}{\tilde{K}_0}-ND_m\Big(1-\exp\Big(\frac{(K_0+\delta K)^2\delta a^2}{\delta KD_m}\Big)\Big)}\right] \tag{B.40}$$

B.5 The rigid Limit Interaction Term

One of the physically relevant cases is the rigid limit of an infinitely strong closing spring. Since we are looking for the interaction free energy of the system, all divergences arising from $K'\to\infty$ cancel out.

B.5.1 Entropy

For the entropy, the rigid limit is found very easily by inspection of equation (2.47):

$$\begin{aligned}
\Delta\Delta\mathcal{S}_r&=-\lim_{K'\to\infty}\frac{1}{2}\log\left(1-\frac{K'\delta K\,\langle n|\hat{K}_0^{-1}|1_N\rangle^2}{(1+K'\,\langle 1_N|\hat{K}_0^{-1}|1_N\rangle)(1+\delta K\,\langle n|\hat{K}_0^{-1}|n\rangle)}\right)\\
&=-\frac{1}{2}\log\left(1-\frac{\delta K\,\langle n|\hat{K}_0^{-1}|1_N\rangle^2}{\langle 1_N|\hat{K}_0^{-1}|1_N\rangle\,(1+\delta K\,\langle n|\hat{K}_0^{-1}|n\rangle)}\right)
\end{aligned} \tag{B.41}$$

Since $|1_N\rangle$ is the $q=0$ eigenvector in momentum space for both $\hat{K}_0$ and consequently for $\hat{K}_0^{-1}$ we can simplify this somewhat by using:

$$\langle 1_N|\hat{K}_0^{-1}|1_N\rangle=N\,\langle n|\hat{K}_0^{-1}|1_N\rangle \tag{B.42}$$

Which we will use in all calculations from here on. The rigid interaction entropy is now given by:

$$\Delta\Delta\mathcal{S}_r = -\frac{1}{2}\log\left(1 - \frac{\delta K \langle n|\hat{K}_0^{-1}|1_N\rangle}{N(1+\delta K \langle n|\hat{K}_0^{-1}|n\rangle)}\right) \tag{B.43}$$

B.5.2 Energy

First, we consider the determinant in the denominator:

$$\begin{aligned}\frac{1}{D} &= \frac{1}{\left(1+K'\langle 1_N|\hat{K}_0^{-1}|1_N\rangle\right)\left(1+\delta K\langle n|\hat{K}_0^{-1}|n\rangle\right) - K'\delta K\langle n|\hat{K}_0^{-1}|1_N\rangle^2} \\ &\to \frac{1}{K'\langle n|\hat{K}_0^{-1}|1_N\rangle\left(N(1+\delta K\langle n|\hat{K}_0^{-1}|n\rangle) - \delta K\langle n|\hat{K}_0^{-1}|1_N\rangle\right)}\end{aligned} \tag{B.44}$$

We should thus first isolate all K' terms from the terms inside the brackets in equation (2.51):

$$(i) \to \frac{K'}{2}\frac{K'\delta K\langle n|\hat{K}_0^{-1}|1_N\rangle^2}{NK'\langle n|\hat{K}_0^{-1}|1_N\rangle} = K'\langle n|\hat{K}_0^{-1}|1_N\rangle\left(\frac{\delta K}{2N}\delta L^2\right) \tag{B.45}$$

$$(ii) \to K'\langle n|\hat{K}_0^{-1}|1_N\rangle\left(\frac{(K+\delta K)^2\delta a^2}{2}\frac{\langle n|\hat{K}_0^{-1}|1_N\rangle}{1+\delta K\langle n|\hat{K}_0^{-1}|n\rangle}\right) \tag{B.46}$$

$$(iii) \to K'\langle n|\hat{K}_0^{-1}|1_N\rangle\left(\delta L(K+\delta K)\delta a\right) \tag{B.47}$$

All these terms, along with the determinant, come with a $K'\langle n|\hat{K}_0^{-1}|1_N\rangle$ term and thus cancel any divergences we might have been worried about.

$$\begin{aligned}\Delta\Delta\mathcal{E}_r = \frac{1}{N(1+\delta K\langle n|\hat{K}_0^{-1}|n\rangle) - \delta K\langle n|\hat{K}_0^{-1}|1_N\rangle}\Big[&\frac{\delta K}{2N}\delta L^2 - (K+\delta K)\delta a\delta L \\ &+ \frac{(K+\delta K)^2\delta a^2}{2}\frac{\langle n|\hat{K}_0^{-1}|1_N\rangle}{1+\delta K\langle n|\hat{K}_0^{-1}|n\rangle}\Big]\end{aligned} \tag{B.48}$$

The full rigid interaction free energy is:

$$\begin{aligned}\Delta\Delta\mathcal{F}_r = &\frac{1}{2}\log\left(1 - \frac{\delta K\langle n|\hat{K}_0^{-1}|1_N\rangle}{N(1+\delta K\langle n|\hat{K}_0^{-1}|n\rangle)}\right) \\ &+ \frac{1}{N(1+\delta K\langle n|\hat{K}_0^{-1}|n\rangle) - \delta K\langle n|\hat{K}_0^{-1}|1_N\rangle}\Big[\frac{\delta K}{2N}\delta L^2 - (K+\delta K)\delta a\delta L \\ &+ \frac{(K+\delta K)^2\delta a^2}{2}\frac{\langle n|\hat{K}_0^{-1}|1_N\rangle}{1+\delta K\langle n|\hat{K}_0^{-1}|n\rangle}\Big]\end{aligned} \tag{B.49}$$

C Supplemental Data

C.1 Other 3DNA parameters

Rise represents the physical rest distance between base pairs, lying around 3.32 Å, and all three geometries lie close to this value. Similarly, the Shift and Slide profiles display only small variations along the probe region. Although local differences between the three structures are present, they do not show the same clear separation between closed-loop and cut geometries observed for the bending parameters Tilt and Roll. We therefore do not identify these translational base-pair-step parameters as the dominant structural signature of strain in the OWL sensor.

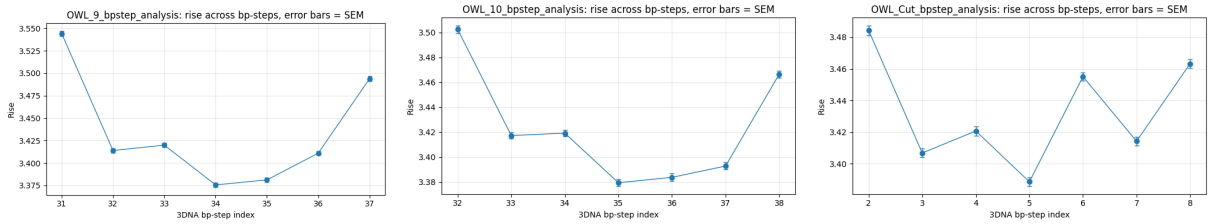

(a) OWL9 (b) OWL10 (c) OWL9-cut

Figure C.1: Comparison of rise between the three designs from figure 5.7.

Shift measures the relative displacement of neighbouring base pairs along one transverse axis of the bp reference frame. The expected value for this is around 0 Å, and all strands lie within a close range of this value.

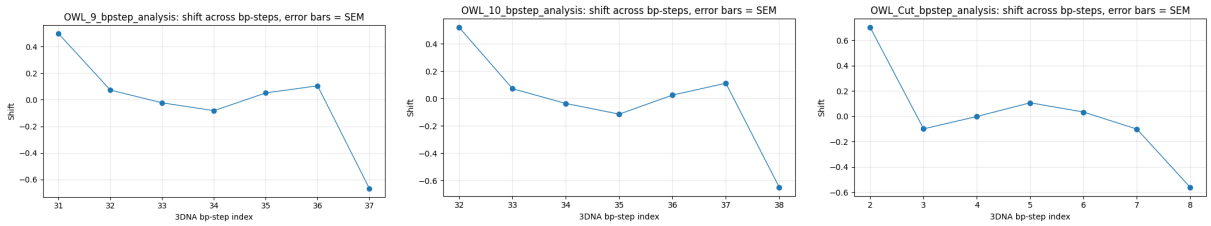

(a) OWL9 (b) OWL10 (c) OWL9-cut

Figure C.2: Comparison of shift between the three designs from figure 5.7.

Finally, the slide is the relative displacement along the other transverse axis, approximately describing whether neighbouring base pairs are displaced along the long-axis direction of the base pair. Here we expect slightly positive values around 0.23 Å. We see the same

pattern as for twist: relatively large fluctuations over the base pairs that average out to approximately the values we expect for each strand.

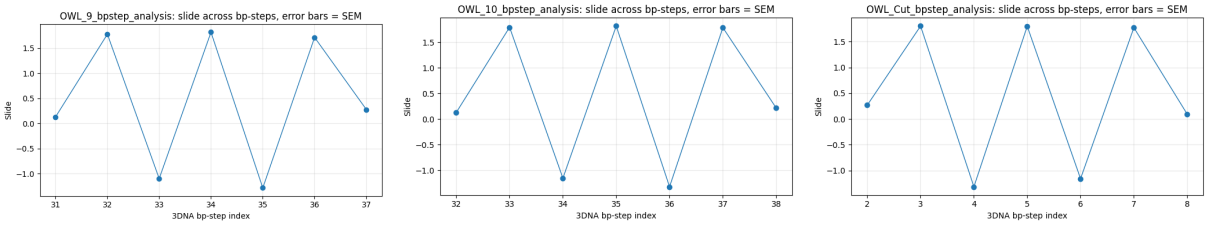

(a) OWL9 (b) OWL10 (c) OWL9-cut

Figure C.3: Comparison of slide between the three designs from figure 5.7.

DEPARTMENT OF PHYSICS AND ASTRONOMY
Celestijnenlaan 200d bus 2412
3001 LEUVEN, BELGIË
tel. + 32 16 32 71 24
fax + 32 16 32 71 24
www.kuleuven.be